UNIVERSIDADE D
COIMBRA

Natália Sofia Mota Ferreira

FATIGUE LIFE IMPROVEMENT OF AERONAUTICAL ALUMINUM ALLOYS USING PEENING TECHNIQUES

Tese no âmbito do Doutoramento em Engenharia Mecânica, Integridade Estrutural orientada pelos Professores Doutor José António Martins Ferreira e Doutor Carlos Alexandre Bento Capela e apresentada ao Departamento de Engenharia Mecânica da Faculdade de Ciências e Tecnologia da Universidade de Coimbra

Dezembro de 2022

A

"When everything seems to be going against you,
remember that the airplane takes off against the wind,
not with it."

Henry Ford

To my parents †

C

Acknowlegments

I would like to express my gratitude, in particular, to my supervisors, Professors José António Martins Ferreira and Carlos Alexandre Bento Capela, for their constant guidance and support throughout the investigation carried out. Their advice and suggestions were fundamental to this thesis project.

I would also like to extend my thanks to Dr. Joel Jesus for his help in my fatigue, tensile and hardness experiments.

I offer my thanks to Professor Marta Oliveira for her guidance in the doctoral program.

Also my thanks to my OGMA – Indústria Aeronáutica de Portugal, S.A. coworkers, in particular José Pedro Ribeiro and all the shot peening technicians, who provided me all the support throughout this process and in performing the tests.

A very special thanks to my sister Teresa and nephew Santiago for their love and constant encouragement during this difficult period and for giving me all the familiar support that I need.

And last but not least, to my dear parents, your spirit is always with me and I never feel alone. This journey that now ends has been not only my effort but also yours. God knows how proud I am to be your child.

Abstract

Shot Peening and Ultrasonic Peening are widely used in mechanical treatment of surfaces in the aeronautical, aerospace and automotive industries to improve the fatigue life of metallic components. This work aims to study the mechanical properties of the Al 7475 T7531 aluminum alloy, applying different peening processes, such as Ultrasonic Peening (USP) and Microshot Peening.

Shot Peening is a conventional technique that introduces residual compressive stresses to the surface and is widely used in the mechanical treatment of surfaces in these industries to improve the fatigue life of metallic components.

While the benefit of shot peening for steel components is well known, the use of this shot peening process for aluminum alloys can be detrimental to fatigue performance if, for example, shot peening bead size and surface roughness are not the appropriate.

Therefore, the present work aims to analyze the effects of shot peening in various aspects to fatigue life, among which are the effects on the propagation of fatigue cracks and the effects of the bead typology used in the fatigue behavior. It is also intended to understand which are the most suitable parameters for fatigue life to be benefited and, obviously, to understand the related mechanical properties.

Systematic studies on roughness, surface hardening and uniaxial fatigue testing were carried out. X-ray diffraction was performed and the surface was observed by Scanning Electron Microscopy. The microstructure was analyzed through optical microscope and microhardness was analyzed through hardness testing.

The tests were carried out on flat specimens and specimens with cylindrical geometry.

In the study with specimens with plane geometry, two thicknesses were used, 4 and 8 mm, with stress ratios of 0.05 and 0.4. For the comparative analysis of fatigue behavior between the base material, Microshot Peening and Ultrasonic Peening processes, 4 and 8 mm specimens were used.

To analyze the effect of shot peening on the propagation of fatigue cracks, 8 mm specimens were used.

In the test with cylindrical specimens, the effect of bead characteristics on fatigue life of the Al 7475-T7351 alloy was observed.

The main contributions of the work carried out include:

a) Determination and comparative analysis of the effect of Shot Peening and Ultrasonic Peening processes on fatigue life of Al 7475-T7351 alloy;
b) Comparison of the results obtained with the Shot Peening treatment and the approach of the Molski-Glinka model analytical predictions;
c) Evaluation of the Shot Peening effect on the propagation of fatigue cracks in the Al 7475-T7351 alloy;
d) Discussion of the effect of constant amplitude loads and the effect of periodic overload blocks, applied on the Al 7475-T7351 alloy;
e) Understanding the effect of the different bead dimensions used in the surface treatment of Shot Peening in the Al 7475-T7351 alloy;
f) Comparison between the different bead materials, glass and cast steel, used in Shot Peening treatment of the Al 7475-T7351 alloy.

Keywords: Shot Peening, Fatigue life improvement, Aluminum alloys, Aeronautics.

Resumo

O Shot Peening e o Ultrasonic Peening são amplamente utilizados no tratamento mecânico de superfícies nas indústrias aeronáutica, aeroespacial e automóvel para melhorar a vida à fadiga de componentes metálicos. Este trabalho visa estudar as propriedades mecânicas do Liga Al 7475-T7351, aplicando processos diferentes de peening, tais como Ultrassonic Peening (USP) e Microshot Peening.

O Shot Peening é uma técnica convencional que introduz tensões residuais de compressão à superfície e é amplamente utilizado no tratamento mecânico de superfícies nestas indústrias para melhorar a vida à fadiga de componentes metálicos.

Enquanto que o benefício do shot peening para componentes de aço seja bem conhecido, a utilização deste processo de shot peening para ligas de alumínio pode ser prejudicial ao desempenho da fadiga se por exemplo o tamanho das esferas de shot peening e a rugosidade da superfície não forem adequados.

Portanto, o presente trabalho tem como objetivo analisar os efeitos de shot peening em vários aspectos da vida de fadiga, entre os quais se destacam os efeitos na propagação de fendas de fadiga e os efeitos da tipologia das esferas utilizadas no comportamento à fadiga. Também se pretende perceber quais os parâmetros mais adequados para que a vida em fadiga seja beneficiada e obviamente as propriedades mecânicas.

Foram realizados estudos sistemáticos sobre rugosidade, endurecimento superficial e realizados testes de fadiga uniaxial. Foi realizada difracção de raios-X e observada a superfície através de Microscopia Electrónica de Varrimento. Analisada a microestrutura através de microscópio óptico e microdureza através de ensaios de dureza.

Os ensaios foram realizados em provetes com geometria plana e cilindrica.

No estudo com provetes de geometria plana, utilizaram-se 2 espessuras, 4 e 8 mm, e razões de tensão 0,05 e 0,4. Para a análise comparativa de comportamento à fadiga entre o material base, e os processos de Microshot Peening e Ultrassonic Peening utilizaram-se provetes de 4 e 8 mm.

Para a análise do efeito do shot peening na propagação de fendas de fadiga, foram utilizados os provetes de 8 mm.

No ensaio com provetes cilíndricos, foi analisado o efeito das características das esferas na vida à fadiga da liga Al 7475-T7351.

As principais contribuições do trabalho realizado são:

a) Determinação e análise comparativa do efeito dos processos de Shot Peening e Ultrassonic Peening na vida em fadiga da liga Al 7475-T7351;
b) Comparação dos resultados obtidos com o tratamento de Shot Peening e a abordagem das previsões analíticas do modelo Molski-Glinka;
c) Avaliação do efeito do Shot Peening na propagação de fendas de fadiga da liga Al 7475-7351;
d) Discussão do efeito de cargas de amplitude contante e blocos de sobrecarga periódicos, aplicados sobre a liga Al 7475-T7531;
e) Compreensão do efeito das diferentes dimensões das esferas utilizadas no tratamento superficial de Shot Peening na liga Al 7475-T7531;
f) Comparação entre os diferentes materiais, vidro e aço, utilizados nas esferas utilizadas no tratamento de shot peening na liga Al 7475-T7531;

Palavras-chave: Shot Peening, Melhoria da vida à fadiga, Ligas de alumínio, Aeronáutica

Table of Contents

List of Figures

List of Tables

Nomenclature

Abbreviations

Al	Aluminum
AMS	Aerospace Materials Specifications
ASTM	American Society of Testing and Materials
BM	Base Material
CNC	Computer Numerical Control
CSP	Controlled Shot Peening
CT	Compact Tension
FSIP	Fatigue Strenght Improvement in Percentage
JP	Jet Peening
LEMF	Linear Elastic Mechanical Fracture
LP	Laser Peening
MP	Mechanically Polished
MSP	Micro Shot Peening
OGMA	Indústria Aeronáutica de Portugal, S.A
OJP	Oil Jet Peening
SAE	Society of Automotive Engineers
SEM	Scanning Electron Microscope
S-N	Stress vs Number Cycles
SP	Shot Peening
SWT	Smit Watson Topper
TIG	Tungsten Inert Gas
UIP	Ultrasonic Impact Peening
UIT	Ultrasonic Impact Technology
USP	Ultrasonic Shot Peening

UT	Ultrasonic
WJP	Water Jet Peening
3D	Three dimensions
3PB	Three Point Bending

Symbology

a	Crack size
A	Cross section area
a_c	Critical dimension of the crack
a_i	Inicial crack depth
a_f	Final crack depth
Al	Aluminum
b	Exponent of Basquin function: fatigue strenght exponent
B	Thickness
^oC	Celsius degrees
C	Compliance
c	Exponent of Basquin function: fatigue ductility exponent
Cr	Chromium
Cu	Copper
D	Diameter
da/dN	Fatigue crack growth rate
D_p	Surface profile
E	Elasticity modulus or Young modulus
Fe	Iron
GPa	GigaPascal
Hv	Vickers toughness
Hz	Hertz
K'	Cyclic hardening coefficient
K_{cl}	Stress intensity when the crack is fully close
K_{op}	Stress intensity when the crack is fully open
K_{1c}	Critical stress intensity factor
K_f	Dynamic stress concentration factor
k_{Hz}	KiloHertz
k_g	Kilogram
K_{max}	Maximum stress intensity factor
K_{min}	Minimum stress intensity factor
K_t	Static stress concentration factor
m	Material constant (Paris law expoent)
Mg	Magnesium
Mn	Manganese

n'	Cyclic hardening exponent
Nd	Neodymium
N_f	Number of cycles to failure
N_i	Number of cycles to iniciate the crack
N_{int}	Number of intervals of periodic overload blocks
N_p	Predicted life
P	Load
P_a	Axial load amplitude
q	Notch sensitivity factor
R	Stress ratio
R_a	Roughness average
R_q	Root mean square (RMS) roughness
R_y	Maximum peak-to-valley height
R_z	Mean roughness depth
Si	Silicon
t	Time
Ti	Titanium
u	Axial grip displacement
U	Normalized load ratio parameter
w	Mesure of the width of the curve
W	Watt
wt	Weight
Y	Geometric factor
δ	Displacement
δ_0	Residual displacement
ΔK	Stress intensity factor range
ΔK_{ef}	Stress effective intensity factor range
ΔK_{th}	Stress threshold intensity factor range
$\Delta\varepsilon$	Strain amplitude
ΔS	Stress nominal factor range
σ	Stress
σ'_f	Cyclic resistance coefficient fatigue
σ_a	Stress amplitude
σ_{op}	Opening stress
σ_{cl}	Stress closure
σ_{ef}	Efective stress
σ_{f0}	Fatigue limit stress
σ_{av}	Average stress
σ_{max}	Maximum stress
σ_{min}	Minimum stress

σ_n	Nominal stress
σ_{UTS}	Tensile strength
σ_{res}	Residual stress
ε	Strain
ε_{av}	Average strain
ε_{max}	Maximum strain
ε_{min}	Minimum strain
Zn	Zinc

CHAPTER 1 – Introduction and Objectives

With the development of increasingly innovative technologies, it has been possible to improve the performance of the materials used, as well as the components manufactured, thus increasing the life of the diverse existing equipment, as well as its safety. On the other hand, it is also possible to build lighter, more resistant equipment and with fewer natural resources, which contributes to less environmental pollution. The reasons described above and the relentless pursuit of technological evolution by man, made it possible to develop techniques to improve the fatigue life of materials, such as Shot Peening.

This process and, more recently, its derivatives, Ultrasonic Peening, MicroShot Peening and Laser Peening, are increasingly used in industry in general, and in particular in branches of industry that represent a huge financial slice of the world economy.

As previously mentioned, although these techniques are being implemented in some types of industries, they are still in full development, so their improvement in the mechanical behavior of the components represents an attractive research object.

Aluminum is a material used in various industrial sectors such as the food, chemical, metallurgical and electrical industries, in structural applications, in particular in the transport industry, from automobiles to aeronautics and aerospace. The wide field of use for this material is due to the fact that it combines good mechanical strength and good corrosion resistance, with low density.

This work focuses on the behavior of aluminum alloys with a view to aeronautical applications, due to the growing need to develop adequate techniques for the maintenance and life expansion of aeronautical fleets that use this type of materials. In response to these needs, various aluminum alloys have been developed, in particular the 7000 series alloys. This series combines a very high tensile strength with good fracture toughness and corrosion resistance. Despite these characteristics, long-term fatigue strenght is relatively low, around 140 MPa for more than 5 million cycles [1, 2].

It is known that crack initiation is a phenomenon that occurs preferentially on the surface and under the influence of the present surface state. That said, by introducing residual compressive stresses near the surface, component fatigue life can be increased. One of the ways to improve this aspect is to subject components to surface treatments. Shot peening, due to its

very positive results in improving the fatigue life of mechanical components, is one of the most commonly used treatments [2]. This work aims to analyze the benefits in fatigue life strenght and fatigue crack propagation by shot peening, microshot peening and ultrasonic peening, in the Al 7475-T7351 alloy, considering the influences of thickness, stress ratio and the notch. As complementary parameters, the microstructure, microhardness and residual stresses were analyzed, in order to better understand the influence of shot peening. Using numerical models and approaches based on local stresses, life at crack initiation can be predicted and subsequently compared with the experimental results obtained.

To carry out this work, the following tasks were performed:

- Specimen preparation;
- Specimen hardness profile analysis;
- Existing residual stresses analysis;
- Experimental determination of fatigue strength curves;
- Experimental determination of fatigue crack propagation curves;
- Determination of fatigue life prediction curves;
- Result analysis and discussion.

Shot peening treatment was carried out using different parameters (material, bead size and intensity) in order to investigate lifetime consequences of fatigue in the alloy under study.

For result discussion, the evaluation was also carried out through: fatigue testing, microhardness, roughness and nanohardness measurement, residual stress induced by the processes, microstructure observation; fracture surface evaluation and obtaining of fatigue resistance curves.

The investigation results obtained were published in specialized bibliography, as indicated below:

- Ferreira, N., Jesus, J., Ferreira, J.A.M., Ferreira, Capela, C.A., Costa, J.M., Baptista, A.C., “Effect of bead characteristics on the fatigue life of shot peened Al 7475-T7351 specimens”, International Journal of Fatigue, Volume 134, May 2020.

- Ferreira, N., Jesus, J., Ferreira, J.A.M., Ferreira, Capela, C.A., Costa, J.M., "A Study of the Shot Peening Effect on the Fatigue Life Improvement of Al 7475-T7351 3PB Specimens", Mechanical Fatigue of Metals, pages 335-341, January 2019.

- Ferreira, N., Antunes, P.V., Ferreira, J.A.M., Costa, J. D. M., Capela, C.A., "Effects of Shot-Peening and Stress ratio on the Fatigue Crack Propagation of Al 7475-T7351 Specimens", Applied Sciences, March 2018.

- Ferreira, N., Ferreira, J.A.M., Antunes, P.V., Costa, J. D. M., Capela, C.A., "Fatigue crack propagation in shot peened Al 7475-T3751 alloy specimens", Procedia Engineering, volume 160, pages 254-261, December 2016.

- Ramos, R., Ferreira, N., J.A.M., Ferreira, Capela, C.A., Baptista, A.C., "Improvement in fatigue life of Al 7475-T7351 alloy specimens by applying ultrasonic and microshot peening", International Journal of Fatigue; Volume 92-Part1, pages 87-95, June 2016.

The results obtained were also presented at the following conferences:

- XVIII International Colloquium on Mechanical Fatigue of Metals – ICMFM XVIII-Gijón, Espanha; 6-8 September; 2016.

- ICMFM XIX - 19th International Colloquium on Mechanical Fatigue of Metals - ICMFM XIX – Porto, Portugal; 5-7 September; 2018.

- 1st Virtual Iberian Conference on Structural Integrity; Coimbra; Portugal; 25 - 27 March; 2020.

- 5th Iberian Conference on Structural Integrity 2022; Coimbra; Portugal; 30 March – 1 April; 2022.

- 10ª Edição SETI – Seminário Embraer de Tecnologia e Inovação; S. Paulo; Brasil; 7-10 June; 2022.

It should be noted that the author and supervisors were responsible for applying all the shot peening improvement processes used in this research study. The author was also responsible for the production of specimens at OGMA – Indústria Aeronáutica de Portugal, S.A., always under the supervision of the respective supervisors. This production of specimens included cutting raw materials, machining in CNC equipment and/or turning on CNC lathes and shot peening surface treatment. As for published articles, the author participated, namely, in writing, essays and/or result treatment. All experimental tests on specimens were carried out at the Mechanical Engineering Department of the University of Coimbra.

As detailed below, this Thesis consists of six chapters, including the articles that have been published to date:

- Chapter 1: Introduction and objectives
- Chapter 2: Literature review
- Chapter 3, 4 and 5: Published articles
- Chapter 6: Discussion, Main Conclusions, Future Works

Chapter 1 – Introduction and Objectives, includes the global presentation of this study and proposed objectives.

Chapter 2 – Literature Review, provides a summary of the fundamental concepts for the understanding of this investigation. It essentially focuses on material, mechanical properties, fatigue parameters and technological processes used in the research work.

Chapters 3, 4 and 5 – Include published articles that compose this dissertation.

Chapter 6 – Discussion, Main Conclusions, Future Works, provides a summary of the conclusions inherent to this investigation, as well as some suggestions for future works within this scope.

1.1 References

[1] – Benedetti, M., Fontanari, V., Scardi, P., Ricardo, C.L.A., Bandini, M., "Reverse bending fatigue of shot peened 7075-T651 aluminum alloy: the role of residual stress relaxation", International Journal of Fatigue, 2009, 31, p-1225-1236.

[2] – Carvalho, A.L.M., Voorwald, H.J.C., "Influence of shot peening and hard chromium electroplanting on the fatigue strenght of 7050-T7451 aluminum alloy", International Journal of Fatigue, 2007, 29, p-1282-1291.

CHAPTER 2 – Literature Review

2.1 Introduction

Aluminum is a metal of great abundance in the earth's crust, representing 8.1% of its composition. It is found, normally, combined with silicates and other oxides, as in igneous rocks, feldspars, micas and in other minerals. It is the most consumed non-ferrous metal in the world and its current production exceeds the sum of all other non-ferrous metals.

The variety of aluminum applications is related to its physicochemical characteristics, especially its low specific weight (2.7g/cm^3), when compared to other high consumption metals, such as steel (7.83g/cm^3), copper (8.93g/cm^3) or bronze (8.53g/cm^3), and for high corrosion resistance and high thermal and electrical conductivity [1].

It is a material of great application in multiple activities, with pure aluminum being more ductile than steel. However, its alloys, with small quantities of copper, manganese, silicon, magnesium and other elements, present a great amount of characteristics suitable for so many different applications. These alloys are the main material for the production of many components in the household goods industry, the automotive industry and the aeronautical industry.

2.2 Aluminum alloys

Specifications for aluminum alloy elements are defined in 3 categories:

1. Major alloying elements: define the series of elements that control the fusibility and its properties;

2. Secondary alloying elements: control solidification behavior, modify eutectic structure, promote refinement of primary phases, control grain size and shape, promote or limit phase formation and reduce oxidation;

3. Impurities: influence the fusibility and formation of insoluble phases, which sometimes limit or promote desired properties [1].

Such specifications are published through government agencies and technical associations that they reference according to nomenclature [2].

1xxx – commercially pure aluminum.

2xxx – alloys in which copper is the main binding element, in addition to other elements, such as magnesium, mainly.

3xxx – alloys in which manganese is the main binding element.

4xxx – alloys in which silicon is the main binding element.

5xxx – alloys in which magnesium is the main binding element.

6xxx – alloys in which magnesium and silicon are the main binding elements.

7xxx – alloys in which zinc is the main binding element, but that include other elements such as copper, magnesium, specified chromium and zirconium.

8xxx – alloys that include some compositions with tin and lithium, featuring different compositions.

9xxx – reserved for future use.

As for the aeronautical industry, specific alloys whose factors, strength and weight, present particularly favorable values are used. They are normally heat-treated high-strength alloys, with copper (2xxx series) or zinc (7xxx series) as the main alloying elements. They are as strong as structural steels and generally require surface protection.

2017, 2024, 2117 and 2219 alloys have high mechanical strength, high ductility, medium corrosion resistance and good cutting resistance, which makes them suitable for application in parts subject to milling and forging, and in the aeronautical industry, transport, machinery and equipment.

Al-Zn alloys, when subjected to heat treatment, have high mechanical strength, good corrosion resistance and good formability. Some examples of these alloys are 7050, 7075, 7178 and 7475 applied in parts subject to high mechanical stress in the aeronautical industry, in machinery and equipment, in plastic injection molds and structures [3].

Different types of heat treatment can be applied to these alloys, depending on material intended application:

F: as manufactured: applies to products resulting from mechanical forming (laminating, extrusion and others).

O: annealed: applies to products initially worked and afterwards annealed to obtain the lowest mechanical strength, and to cast annealed products to increase ductility and dimensional stability.

W: solubilized: unstable quenching applicable only to alloys that spontaneously age at room temperature (natural aging) after solubilization. This designation is specifically used when the natural aging period is indicated, for example when W is equal to 1 hour.

T: heat treated to produce stable quenching other than F, O or W: applies to products that are heat treated, with or without further strain, to produce stable quenching.

One or more digits always follow the letter T. A period of natural aging may occur between operations related to T quenching.

T1: high temperature formed and naturally aged.

T2: high temperature formed, cooled, cold deformed and naturally aged.

T3: solubilized, cold worked and naturally aged.

T4: solubilized and naturally aged.

T5: high temperature formed and artificially aged.

T6: solubilized and artificially aged.

T7: solubilized and stabilized.

T8: solubilized, cold deformed and artificially aged.

T9: solubilized, artificially aged and cold worked.

T10: high temperature formed, cooled, cold worked and artificially aged.

2.2.1 The Al 7475-T7351 alloy

The Al 7475-T7351 alloy is used in this study. T7351 treatment of the 7475 alloy aims to maximize corrosion resistance due to the mechanical properties and super aging of this alloy.

This is an alloy used in the form of plates and sheets in aeronautical components, where high fracture toughness is one of the fundamental project requirements. It also combines high

mechanical strength and crack propagation resistance to fatigue, whether in open air or in aggressive environments, due to its high corrosion resistance [4] [5] [6].

The Al 7475-T7351 alloy has been carefully designed from another widely used alloy, the Al 7075 alloy, in which the percentages of iron, silicon and manganese have been significantly reduced and, in addition, the conditions of heat treatment [7]. This provided the fineness of both the grain and the size of precipitates (preferred point of crack initiation), which allows a more uniform dispersing in the metallic structure. The chemical composition of these two alloys can be compared in Table 2.1.

Table 2.1 – Chemical composition of Al 7475 and Al 7075 alloys [8].

Alloy	Si	Fe	Cu	Mn	Mg	Cr	Zn	Ti	Others	Al
Al 7475	0.1	0.12	1.2-1.9	0.06	1.9-2.6	0.18-0.25	5.2-6.2	0.06	0.15	remaining
Al 7075	0.4	0.5	1.2-2	0.3	2.1-2.9	0.18-0.28	5.1-6.1	0,.0	0.15	remaining

Heat treating of the Al 7475-T7351 alloy consists of heating it up to 470°C, a process called solubilization, to obtain a single phase. Subsequent rapid cooling, or quenching, in water (to reduce crystallinity and increase hardness), with a controlled extension of 1.5 to 3%, followed by artificial aging in two phases: the first at a temperature of 121°C for 25 hours, and the second at 163°C for a period of 24 to 30 hours. Aging temperatures, appropriately conjugated with time, are chosen in order to produce a suitable precipitate size, which will, in turn, influence alloy strength and hardness [4][9].

Mechanical properties of the Al 7475-T7351 alloy can be summarized in the following Table 2.2.

Table 2.2 – Al 7475-T7351 alloy mechanical properties [8].

Thickness [mm]	Tensile strength [MPa]	Yield Strength [MPa]	Elongation [%]	K_{1c} [MPa√m] Direction LT	K_{1c} [MPa√m] Direction TL
25.43-38.10	490	414	9	55	45
50.83-63.50	476	393	8	55	45
76.25-88.90	448	365	8	55	45

For comparison purposes, Table 2.3 shows the properties recorded for the same alloy composition with another heat treatment, T651, and also for the Al alloy 7075-T7351 (with the same treatment of the alloy under study).

Table 2.3 – Mechanical properties of other aluminum alloys [8].

Alloy	Thickness [mm]	Tensile strength [MPa]	Yield Strength [MPa]	Elongation [%]	K_{1c}[MPa√m] Direction LT	K_{1c} [MPa√m] Direction TL
Al 7475 T651	25.43-38.10	538	469	9	46	41
Al 7075 T7351	6.35-101.06	476-421	393-331	7-6	32	28.6

The Al 7475-T651 alloy has, for the same thickness, higher yield strength, however it has lower K_{1c} values. Effectively, parameter K_{1c}, also known as fracture toughness, is very important in design and represents the critical value of the stress intensity factor that causes the material to fracture for a given existing crack length.

The Al 7075-T7351 alloy has similar tensile strength, but has a much lower fracture toughness value.

The subject of aeronautical component fatigue resistance has been evaluated in several studies due to its importance in aircraft integrity, high performance and cost optimization.

Verma et al [5] obtained fatigue resistance curves in specimens with a 4 mm diameter section, previously diamond polished to a finish of 1 μm. The resistance curves for R=-1, obtained in several alloys, were superimposed in Figure 2.1.

It was concluded that, in general and in comparison with other commercial aluminum alloys, the alloy chosen for this work shows excellent values of fracture toughness, tensile strength and reasonable ductility, in addition to high fatigue strength [4, 5, 8].

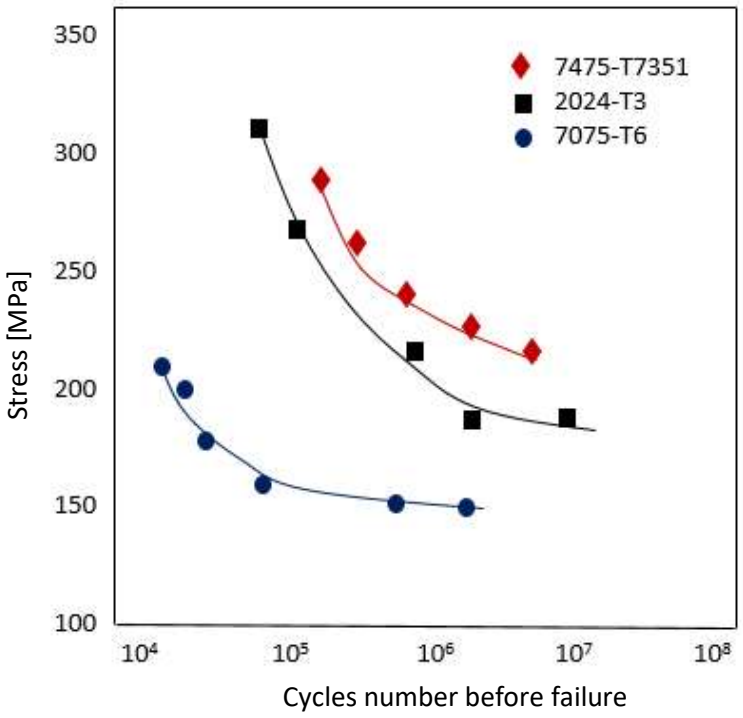

Figure 2.1 – S-N curves for different aluminum alloys**.**

From Figure 2.1 we can conclude that, for short-lived regions, Al 2024-T3 and Al 7475-T7351 alloys have similar performances, and for long lives, the Al 7475-T7351 alloy has the best fatigue resistance. This can be explained by the delay of crack initiation due to the low concentration, small size and uniform distribution of precipitates throughout the metallic matrix [7].

2.3 Fatigue

2.3.1 General considerations

Fatigue is defined as a phenomenon in which the progressive failure of materials occurs when subjected to repeated cycles of stress or strain. According to ASTM E1150 (1983) [9] it is a process of permanent, localized and progressive structural change that occurs in a material subjected to conditions that produce fluctuating stresses and strains at some point (or points), and which can culminate into cracks or complete fracture after a sufficient number of fluctuations. Also, according to Surish et al [10] fatigue is described as a failure or rupture that occurs after a component or structure has been subjected to repeated or fluctuating stress cycles, where the maximum rated stress is lower than the yield stress of the material.

The importance of fatigue studies has advanced in the last century due to the large number of failures in service that occurred in industrial equipment, with high economic and human consequences. Failure is preceded by the initiation and propagation of a crack to an unstable condition, which leads to an instantaneous failure. This phenomenon can occur after a considerable time of the material in service. As technological development has incorporated new components and equipment that are continuously subjected to dynamic stresses and vibrations, the phenomenon of fatigue has come to represent the cause of more than 90% of primary failures of metallic material mechanical components under operating conditions, such as rims and wheels of trucks, aeronautical structures upon take-off, flight and landing, among others [11]. Fatigue failure is particularly unpredictable as it happens without any warning.

The most common way of evaluating fatigue strength is the use of stress versus number of cycles to failure curves (S-N curves) [12]. This approach emerged from the first studies on the behavior of metallic materials, subjected to alternating and repetitive stresses, made by August Wöhler in the 1850s. For this reason, S-N curves are also named Wöhler curves. Normally, logarithmic scales are used and the stress used is the nominal stress (σ_a, σ_{max} or σ_{min}), without adjustment for stress concentration.

In Figure 2.2 we can see the fatigue process schematized, which can be characterized in 4 stages: nucleation of the crack(s), microscope growth of the crack(s), propagation of the crack(s) and final failure [13] [14] [15].

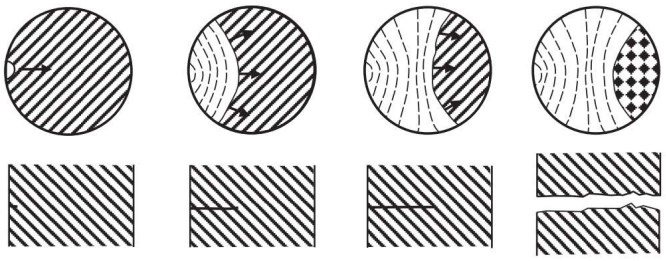

Figure 2.2 – Scheme of the four stages of fatigue process.

The nucleation of the crack is directly related to the existence of notches or other singularities, where there is a high value of stress concentration (K_t) [15]. In the absence of any surface defect, crack initiation will occur through the formation of inclusions or extrusions that are performed during cyclic loading. In microscopic growth, the orientation of the crack in the next grain is different from the previous one because the growth of the crack follows the planes where there are displacements and thus the resulting plastic strain gives rise to the formation of the crack [16]. The propagation phase begins when the crack is long enough to propagate perpendicularly to the direction of the load. It is common, for relatively low loads and ductile materials, to find stretch marks due to variation in frequency or load amplitude, each stretch mark being a fatigue cycle. Failure occurs when the crack is long enough for the cross section not to support the applied load, as the material's toughness value has been reached.

Fatigue life (N_f) can be expressed as the sum of two life segments, the number of cycles required to initiate the crack (N_i) added to the number of crack propagation cycles (N_p) [15] [17].

$$N_f = N_i + N_p \tag{2.1}$$

Fatigue in a material only appears if the applied stress varies with time. Stress cycles can be constant stress amplitude or a variable stress amplitude, described by a sinusoidal wave, square wave or trapezoidal wave. In Figure 2.3, a constant stress cycle with a sinusoidal wave can be observed.

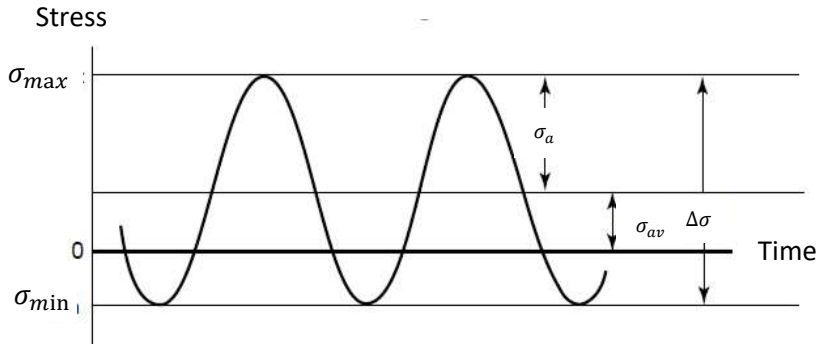

Figure 2.3 – Representation of a fatigue load with constant amplitude [18].

Being σ_{max} and σ_{min} the maximun stress and minimum stress respectively, the nominal stress, σ_{av} can be given by:

$$\sigma_{av} = \frac{\sigma_{max} + \sigma_{mín}}{2} \tag{2.2}$$

The stress amplitude σ_a is half of the apllied stress ($\Delta\sigma$),

$$\sigma_a = \frac{\sigma_{max} - \sigma_{mín}}{2} \tag{2.3}$$

Finally, the stress ratio R is obtained by:

$$R = \frac{\sigma_{mín}}{\sigma_{max}} \tag{2.4}$$

2.3.2 Fatigue resistance curves

Many engineering components are subjected to forces that vary in service, such as a rotating shaft, a bicycle pedal, the thermal expansion and contraction of machine components, the fuselage of aircraft, etc. A material subjected to repeated stress cycles undergoes microstructure modifications designated by the general term fatigue damage or simply fatigue. This damage is not taken by a detectable macroscopic change and failure can occur at low stress levels, often below the elastic limit, but whose repetition constitutes a hazard. Fatigue is caused by localized plasticities that appear at points of stress concentration where locally stress is greater than the yield point stress.

The resistance of materials to fatigue is generally evaluated through the so-called basic S-N curves of the material (Figure 2.4). In these curves, the ordinate axis represents the stress cycle amplitude and the abcissa axis represents the number of cycles until failure, N.

The basic S-N curve is generally obtained in standardized specimens of the material, small in size, highly polished and with a negligible stress concentration, in order to assess the fatigue resistance, without the influence of these variables.

The ordinate of the S-N curve constitutes the fatigue strength, which must always be specified for the corresponding number of cycles. The S-N curve shows that the fatigue strength, considered with the amplitude σ_a of the stress cycle applied to the specimen, decreases with the increase in the number of cycles until failure. For certain materials such as mild steel, there appears to be a stress below which fatigue failure does not occur (the material would last indefinitely without breaking). In other materials, this limit stress, called basic fatigue limit stress, σ_{f0} defined in Figure 2.4, does not exist or cannot be defined in good time.

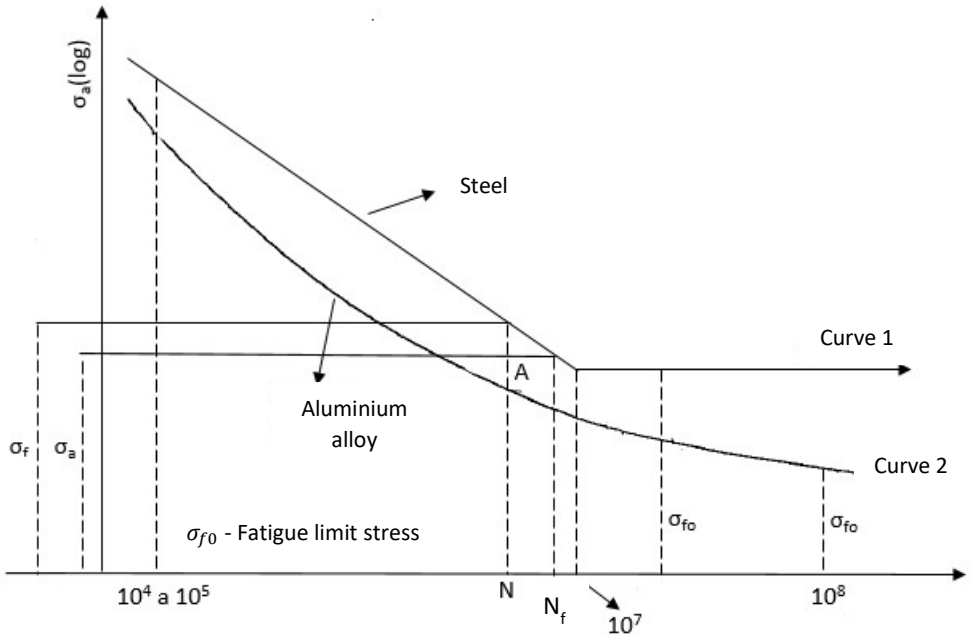

Figure 2.4 – Schematic representation of the S-N curves and fatigue limit stress [19].

In materials that do not present fatigue limit stress in the assymptote condition of the S-N curve (curve 2 of Figure 2.4), a fatigue limit stress is also defined, which is equal to the fatigue strength for 10^8 or $5x10^8$ cycles.

The S-N curves were obtained from the statistical treatment results of fatigue testing and, therefore, represented a certain probability of material fatigue curve.

Upon the design phase, the designer can choose the S-N curve corresponding to the failure probability that he/she has defined. High failure probability reduces design reliability and safety, but leads to higher allowable stresses. By setting a low failure probability, reliability and safety are increased, but lower allowable stresses are estimated. The S-N curve equation generally has the form:

$$\log \sigma_a = \log C - c \log N_f \tag{2.5}$$

or

$$\sigma_a N_f^c = C \tag{2.6}$$

Where σ_a is the stress amplitude, N_f is the number of cycles until failure, c and C are material constants and test conditions.

Basic S-N curves are generally obtained for rotated cycles and for bending (rotative or flat) or tensile-compression stresses. The frequency of load application does not normally affect the results of fatigue tests, at least in the frequency range between $^1/_{60}$ and 300 Hz.

Equations 2.5 and 2.6, defined for a given failure probability, allow the designer to calculate the fatigue strength for a given specified duration. In order to have a theoretically infinite duration, only the fatigue limit stress is used, which constitutes the basis for the calculation of the allowable stress in the case under study.

The S-N curve in Figure 2.4 only shows the zone of time greater than 10^5 cycles, commonly known as long-term fatigue or fatigue with a high number of cycles. In this zone, the nominal stresses are normally elastic (less than the yield stress of the material) and the failure occurs without visible plastic deformation.

In the zone below 10^4 – 10^5 cycles, the stresses already enter the plastic domain and the elastic S-N curve can no longer characterize the material fatigue resistance. At this level, the extension amplitude of the stress cycle applied to the part should be analyzed. At this point, there is plastic fatigue, oligocyclic fatigue, low cycle fatigue or fatigue at a low number of cycles.

Low cycle fatigue has specific behavior laws that were studied in the specialized texts and fatigue, cited in the reference list. This type of fatigue can occur in applications such as pressure vessels, pipelines, turbine blades, ovens, nuclear power plant reservoirs, rolling mill rolls, oil exploration platforms, etc.

Fatigue strength depends on many parameters, the most important of which are:

- Surface finish
- Residual stresses
- Size
- Environment
- Medium stress
- Stress concentration
- Temperature
- Material and heat treatment

A brief analysis of the influence of such parameters is presented below.

2.3.2.1 Surface finish influence

Surface finish is a fundamental parameter in fatigue resistance. A part with poor surface finish will present a high number of surface defects that constitute areas of easy fatigue crack nucleation, and consequently, low fatigue resistance. It can be said that the worse the surface finish, the lower the fatigue strength. The mirror-polished finish of the specimens used to determine the basic S-N curve provides maximum fatigue strength and serves as a fatigue strength standard.

2.3.2.2 Residual stress influence

The existence of residual stresses varies the fatigue strength of the part. Residual compressive stresses are beneficial because they cause the closure of the cracks or microcracks that appear at the beginning of the fatigue process, thus delaying the appearance of failure. Residual tensile stresses are harmful and can be induced on part surface either by severe polishing or by certain types of electrolytic coating, such as chrome plating, cadmium plating and nickel plating.

There are several techniques used to introduce compressive residual stresses to the surface that have produced a significant increase in fatigue strength. The most commonly used mechanical treatments are shot peening, surface hammering, shot blasting, and surface rolling.

Heat treatments that produce residual compressive stresses are carburizing, nitriding, carbonitriding and induction quenching.

2.3.2.3 Size influence (geometric effect)

Part size influences fatigue strength and essentially depends on three effects:

- stress gradient in cross section;
- volume of material;
- part surface area.

In this way, larger parts will have lower fatigue strength, because both the volume of material subjected to higher stress and the surface area are greater. Regarding the first factor, this is particularly important in parts that have tension gradients in cross section caused by bending or torsional stresses or by notches. In this case, for the same maximum stress, the greater the stress gradient, which decreases with increasing cross section, the greater the fatigue strength, because the volume of the material subjected to higher stress in the most extreme fibers of the section decreases.

A larger surface area of the part increases the probability of surface defects, which also contributes to the reduction of fatigue resistance with the increase of part dimensions.

2.3.2.4 Environment influence

Fatigue resistance significantly depends on the environment surrounding the part. In environments considered relatively inert, such as dry air, fatigue resistance is generally maximum. In corrosive environments or with high percentages of water vapor (humid air), fatigue resistance is low, constituting the phenomenon of fatigue with corrosion, which can be defined as the application of dynamic loads to a part placed in a corrosive environment.

Salt solutions, including seawater, are environments that cause high reductions in fatigue strength. Reductions of more than 100% are observed in certain types of steel. The fatigue limit stress, which would normally be obtained if the part were tested in air, does not exist in most cases if the material is susceptible to fatigue with corrosion in salt solutions. The S-N curve is then continuously decreasing and the fatigue strength becomes negligible for very high duration values (greater than 10^8 cycles).

Unlike fatigue in inert environments, corrosion fatigue resistance increases with load frequency due to the shorter contact time of the corrosive medium with the part surface that occurs at higher frequencies.

The effect of size is also manifested in corrosion fatigue in a manner similar to that observed in air, i.e., corrosion fatigue resistance increases with part dimension. This aspect is the result of the longer path to failure that the crack has to travel in long pieces exposed to corrosive environments, in which the fatigue duration is primarily defined by the crack propagation period (shortest initiation period).

To obtain a fatigue resistance similar to that obtained in air in a part exposed to a corrosive environment, part surface must be properly protected from the environmental chemical attack. For this purpose, several types of coating or protection techniques are used, for example, cathodic protection.

Figure 2.5 schematically illustrates the effect of fatigue with corrosion, with a divergence between the curves in air and in a corrosive environment, which, for the reasons mentioned above, increases with part life.

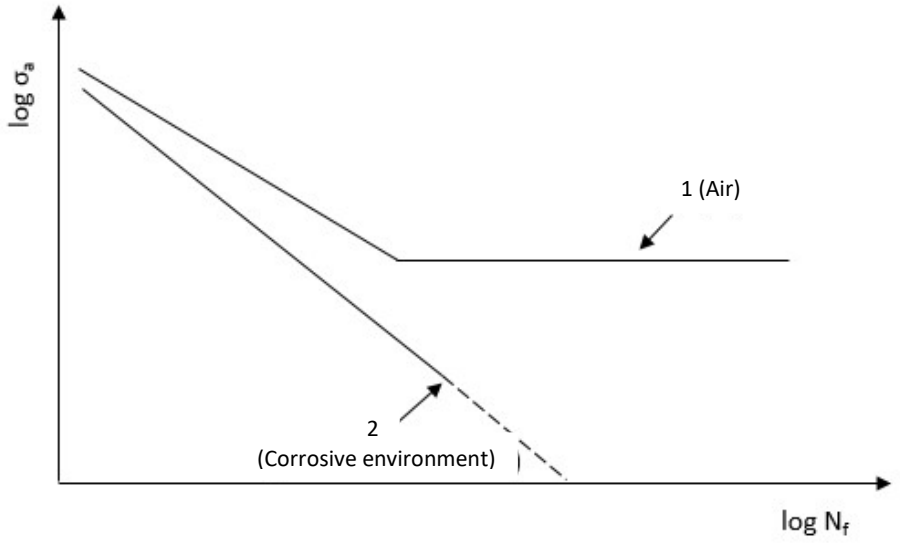

Figure 2.5 – Schematic representation of the environment effect in fatigue resistance [19].

As it becomes clear, the design of parts subjected to fatigue with corrosion requires special care, namely in regard to:

- choosing the material that has the maximum resistance to corrosion fatigue in the specified environment and in the absence of coating;

- choosing the most suitable coating to guarantee maximum resistance to corrosion fatigue and that does not crack or lose adhesion due to repeated action of dynamic loads (prevents part direct contact with the environment);

- choose the most convenient part shape, in order to prevent or reduce stress concentration zones, as much as possible.

Generally, corrosion fatigue design is considered by means of a reduction coefficient in relation to fatigue in air, which assumes that part is in direct contact with environment. This procedure is used even if part is coated, unless there is an S-N curve obtained from the same material, environment and type of coating as the one used in service.

2.3.2.5 Medium stress influence

For the reasons explained above, medium compressive stresses or cycles with predominant compressive stresses are the most favorable from the point of view of fatigue strength. Fatigue strength or fatigue limit stress amplitude increases with decreasing cycle mean stress if it is tensile. Up to close to yield strength, if the medium stress is compressive, fatigue strength increases with the value of medium stress.

The effect of medium stress on fatigue strength is quantified in several calculation equations, the best known being the Goodman equation (Equation 2.7):

$$\sigma_a = \sigma_{f0}\left(1 - \frac{\sigma_{av}}{\sigma_{UTS}}\right) \tag{2.7}$$

where σ_a is the stress amplitude (where for a non-zero medium stress), σ_{av} is the medium stress, σ_{f0} is the fatigue limit stress for σ_{av}= 0 and σ_{UTS} is the tensile strenght.

2.3.2.6 Stress concentration influence

Stress concentration is one of the most important parameters of fatigue strength. The introduction of geometric discontinuities, such as holes, notches, weld seams and changes in diameter, among others, causes an increase in static or monotonous stresses, and so does dynamic stresses applied to a component, regardless of the material.

The theoretical or static stress concentration factor, K_t is defined by the ratio that exists between the maximum local stress σ_{max}, and the nominal stress σ_n, (Equation 2.8).

$$K_t = \frac{\sigma_{max}}{\sigma_n} \tag{2.8}$$

The relationship between notched and not notched fatigue strength limits is designated as the dynamic stress concentration factor, K_f. Theoretically, K_f would be expected to be equal to the static stress concentration factor, K_t. Tests, however, show that K_f is often less than K_t. To quantify this phenomenon, the notch sensitivity index q is commonly used (Equation 2.9), which diversify between 0 and 1. When a material is very sensitive to the presence of notches, K_f=K_t is obtained, that is, the notch sensitivity factor is equal to 1. Metals with uniform and fine grain are sensitive to the presence of notch, so the notch sensitivity is high. On the other hand, K_f=1 for a material that has little notch sensitivity, so the presence of the notch does not affect component life, as it is the case with cast iron, where lamellar graphite acts as a microscopic notch, facilitating nucleation of cracks and significantly reducing the effect of macroscopic notches. Notch sensitivity is a complex parameter that depends on notch geometry (radius), loading nature (tensile/compression, bending and torsion) and material strength, which, in turn, depends on its hardness. Very small notch radi, approaching internal (microscopic) material imperfections, lead to a notch sensitivity index close to zero. Therefore, the difference between K_t and K_f increases the smaller the notch radius and the greater the material strength [20]. A hard and fragile material has a high notch sensitivity, so a softer, more ductile material has a lower notch sensitivity. That said, the change from a soft and more ductile material to a hard and fragile material in a given application, increases fatigue strength, but not as much as it would be supposed given the notch sensitivity phenomenon:

$$q = \frac{K_f - 1}{K_t - 1} \tag{2.9}$$

Imperfections (scratches and others) on component surface that are greater than the microscopic material imperfections, as well as high material roughness, are factors that reduce fatigue strength. This effect is more pronounced in very hard and resistant materials compared to less hard and more ductile materials. Thus, smooth or polished surfaces are recommended for materials that are more resistant.

In a local approach, the dynamic or fatigue stress concentration factor, K_f, can be defined as the quotient between the effective stress, σ_{ef} from the fatigue strength point of view (Equation 2.10), and the nominal stress, σ_n:

$$K_f = \frac{\sigma_{ef}}{\sigma_n} \tag{2.10}$$

In general, it can be said that the theoretical or static stress concentration factor, K_t, is responsible for the amplification of the stresses that will initiate fatigue cracks, and the dynamic or fatigue stress concentration factor is responsible for the stress amplification, which ensures that the crack will continue to propagate beyond the critical distance.

2.3.2.7 Temperature Influence

Temperature influences fatigue strength in different ways, depending on whether it is below or much above room temperature. In the first case, the results indicate that fatigue strength increases when temperature drops. In the second case, creep phenomenon and low fatigue strength may arise with increasing temperature.

For example, in heat-resistant alloy steels, creep is the main cause of failure at temperatures above 700°C.

Contrary to what was considered in the previous paragraph, thermal fatigue is a failure mode, caused by thermal stresses, due only to temperature variations and in conditions in which stresses are not produced by mechanical means. Thermal fatigue analysis requires knowing, in addition to mechanical fatigue variables, the temperature variations that occur in the part and the thermal expansion characteristics of the specified material.

For design purposes and outside the fatigue-creep interaction region, the temperature effect is considered by means of a reduction coefficient applied to the fatigue limit stress value, at ambient temperature.

2.3.2.8 Material and heat treatment influence

As expected, fatigue strength depends on the material metallurgical structure, that is, on the mechanical properties obtained in the conventional tensile test.

It is important for the designer or user to note that fatigue strength can be changed by the microstructure of material modifications.

In general, and in particular in aluminum alloys, it seems that fatigue strength increases with material tensile strength, with the exception of carbons and untreated alloys that from 1400 MPa of tensile strength the fatigue limit stress does not change.

2.3.2.9 Microstructure effect

Any change in the microstruture or surface condition has the potential of altering the S-N curve, especially at long fatigue lives. In metals, resistance to fatigue is generally enhanced by reducing the size of inclusions and voids, by small grain size, and by a dense network of dislocations. However, special processing aimed at improvements due to microstructure may not be successful unless it can be accomplished without substancially decreasing the ductility. In this material, a higher degree of cold work by drawing increases the dislocation density and hence the fatigue strength. Larger grain sizes are obtained by more thorough annealing, thus lowering the fatigue strength.

Microstructures of materials often vary with direction, such as the elongation of grains and inclusions in the rolling direction of metal plates. Fatigue resistance may be lower in directions where the stress is normal to the long direction of such an elongated or layered grain structure. Similar effects are especially pronounced in fibrous composite materials, where the properties and structure are highly dependent on direction. Fatigue resistance is higher where larger numbers of fibers are parallel to the applied stress, and especially low for stresses normal to the plane of a laminated structure [21, 22].

2.3.3 Fatigue crack propagation

The fatigue strength of a part is quite difficult to predict through an analytical expression obtained from a theoretical analysis. The main problem arises in determining the number of crack initiation cycles, since the number of cracking or crack propagation cycles can be calculated directly from the integration of the crack propagation law of the material that proves to be the most appropriate for the material and service conditions.

The integration of the crack propagation law, which uses the LEMF parameters, will thus provide a reliable prediction of the fatigue strength of the part. In cases where the crack initiation period is reduced, as in welded joints and in areas of high stress concentration, this method will even give an approximate prediction of fatigue strength.

It is known that, in the crack, the nominal stresses are normally lower than the yield stress of the material. Given that the stress intensity factor controls the field of stresses and strains at the crack tip for static loads, it is logical to assume that this parameter will also control the crack propagation velocity, in the case of periodic stresses. The crack growth rate, da/dN is thus a function of the stress intensity factor in the load cycle, that is,

$$\frac{da}{dN} = f\ (\Delta K, R) \tag{2.11}$$

where $\Delta K = K_{max} - K_{min}$ with $K_{max} = Y\sigma_{max}\sqrt{\pi a}$ and $K_{min} = Y\sigma_{min}\sqrt{\pi a}$, being σ_{max} and σ_{min} the maximum and minimum stresses of stress cycle.

The fatigue cracking characterized by the LEMF is, therefore, a process of slow growth of a crack (or defect), for values of the stress intensity factor below the critical value K_{1c} (K_c) of unstable failure. This cracking process is the subcritical defect growth and covers the period of crack growth from a given initial dimension, a_i, to a critical dimension a_c.

The $da/dN - \Delta K$ diagram, which is usually obtained in tests, has the progress indicated in Figure 2.6. In this diagram three propagation regimes identifies, designated as regimes I, II and III.

The Paris diagram (Figure 2.6) also represents the variation of the crack growth ratio as a function of the stress intensity factor ΔK:

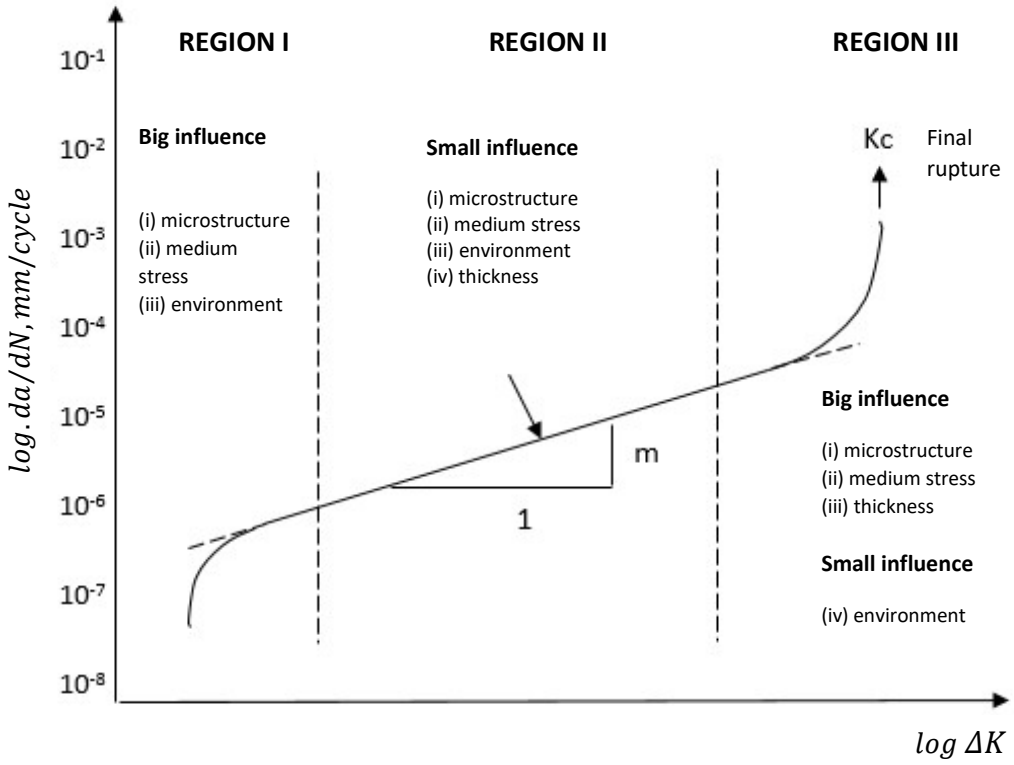

Figure 2.6 – Paris Diagram. Three regions that identify the variation of the crack growth rate as a function of the stress intensity factor, ΔK [23].

2.3.3.1 Main parameters of $da/dN - \Delta K$ curves

The three regions identified above depend on several parameters.

In region I, the propagation speed strongly depends on the stress intensity factor, there being a value ΔK, that is the propagation threshold, ΔK_{th}, of stress intensity factor, below which the crack propagation is or is not or the propagation speed is less than 10^{-7} mm/cycle.

In region II, the propagation velocity varies less sharply with ΔK.

In region III, in fragile or high-strength materials, an acceleration of crack propagation is verified, when K_{max} approaches the tenacity K_c, corresponding to the unstable fracture.

Several analytical expressions describe the function $da/dN, \Delta K$. For the purpose of approximate prediction of fatigue duration, the most commonly used equation is the so-called Law of Paris:

$$\frac{da}{dN} = C(\Delta K)^m \tag{2.12}$$

Where in C and m are material constants that depend on the material, medium stress, frequency, environment, etc. The Paris law is only strictly valid in region II but remains the most commonly used, due to predicting the results with a certain margin of safety and presenting a great mathematical simplicity

The propagation threshold ΔK_{th} is an important parameter because it relates the stress level with the dimension of a defect in the part, so that it does not propagate by fatigue. Thus, for a given defect of a dimension the range of minimum stress $\Delta\sigma_{th}$ that would cause the propagation of this defect by fatigue, will be given by the equation

$$\Delta\sigma_{th} = \frac{\Delta K_{th}}{Y\sqrt{\pi a}} \tag{2.13}$$

The ΔK_{th} value depends on the same parameters that affect the $da/dN, \Delta K$ diagram. ΔK_{th} can be determined experimentally, carrying out tests that have the drawback of being quite time consuming in order to obtain very low crack propagation speeds.

2.3.3.2 Crack closure concept

The concept of crack closure it was introduced by Elber [24] to explain certain anomalies in the behavior of an unloaded crack, observed experimentally during the analysis of variations in the compliance of thin specimens of 2024-T3 alloy. While in the ideal situation of the application of MFLE a crack subjected to a tensile load closes, i.e. the crack faces contact, when the load is completely removed, a fatigue crack can close during unloading, even before it is reached the zero tension. Also during the load process, the gap can only open after the charge has reached a certain value. Thus, the propagation velocity is not only be influenced by the conditions existing in front of the crack tip, but also by the nature of the contact between the crack faces behind its tip. Elber's work provided a certain understanding of the dependence of propagation velocity on factors such as loading history, crack length, stress state, among others, as the conditions existing in the crack edge wake are the result of these parameters.

Elber determined the remote loads for which the two faces of the slit closed and opened completely, respectively, during loading and unloading. This determination was carried out by measuring the evolution of displacement during a load cycle, between two points P and P' located above and below the crack plane and approximately 2 mm behind its tip (see Figure 2.7). Figure 2.7 schematically shows the voltage-displacement record obtained during discharge.

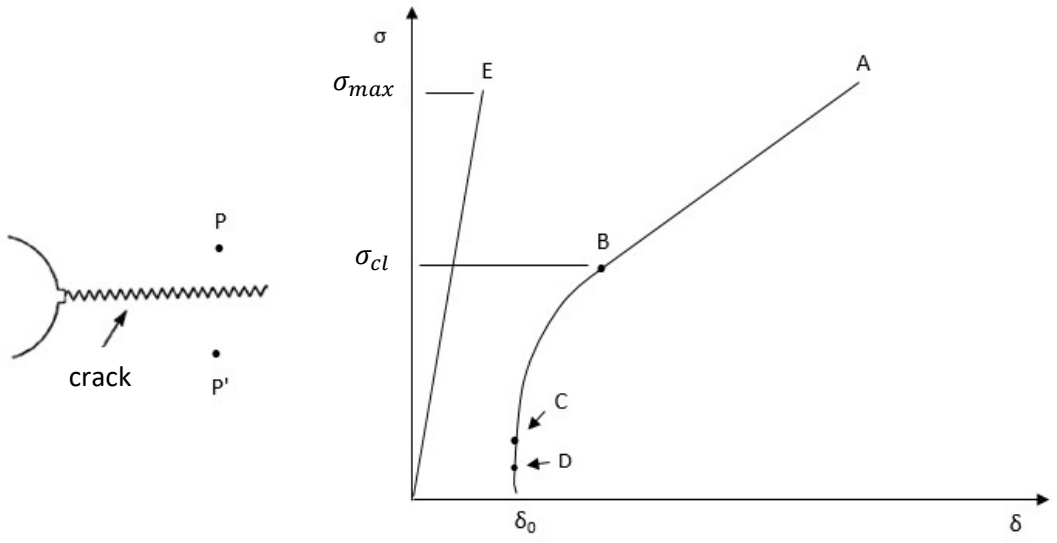

Figure 2.7 – Schematic representation of the applied stress *versus* the displacement between P and P′ points measured by a displacement transducer [24].

Basically, three regions can be distinguished. In the region between A and B, the crack is completely open, the linear behavior and compliance being equal to that measured in an identical specimen with a thin notch (saw-cut) with a length equal to that of the fatigue crack. Between B and C, the crack closes with variation in compliance due to the change in geometry. In the final stage of the discharge below point C, the crack closed completely, the behavior being once again linear and the slope of CD equal to that observed in a similar specimen without a crack and represented in Figure 2.7 by the line E. The stress corresponding to point B, where the contact between crack faces starts, is the closing stress, σ_{cl}. With zero remote load, δ_0 is the residual displacement produced by the plastic trail of the crack, that is, by the plasticized region on both sides of the crack.

During loading, the $\sigma - \delta$ curve is very similar to the one seen in Figure 2.7. However, due to the plastic deformations produced in each cycle and the contact between the crack faces during its closing, the loading and unloading curves are not coincident completely, generally observing a certain hysteresis. The remote stress at which the full opening of the crack occurs is called the opening stress σ_{op}. As already mentioned, during the contact between the crack faces, a certain plastic crushing occurs between the crack surfaces in the area close to its extremity, so the stresses

σ_{cl}e σ_{op} differ slightly. However, in practical terms, is assumed in generally that the remote closing-to-opening stresses of the crack are identical.

Elber considered that propagation can only occur during the part of the load cycle in which the crack is fully open, because while closed it can transmit compressive stresses between the two faces and, therefore, the remaining part of the cycle is relatively inefficient. Thus, he defined the driving force of crack propagation in fatigue through an effective range of the stress intensity factor, ΔK_{ef}, given by

$$\Delta K_{ef} = K_{max} - K_{op} \tag{2.14}$$

where K_{op} is the stress intensity factor for which the crack is fully open, that is, the value of K corresponding to K corresponding to σ_{op}. Figure 2.8 illustrates the definition of the ΔK_{ef} parameter, schematizing the effect of crack closure by comparing the evolution of K with the displacement of the crack opening during the load cycle. Thus, crack closure produces a protective effect at the crack end, as it reduces the driving force of propagation.

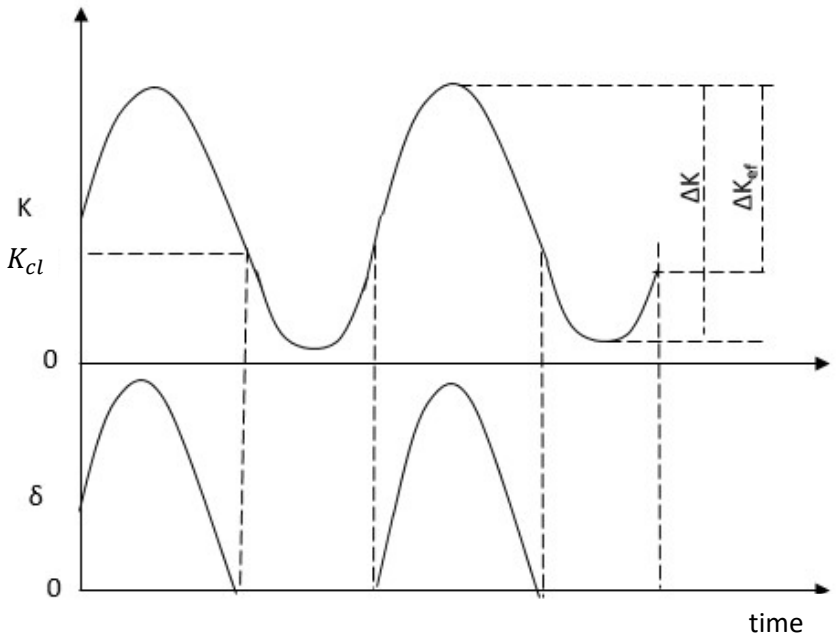

Figure 2.8 – Variation of the crack opening displacement *versu*s load showing the $\boldsymbol{\Delta K_{ef}}$ definition [25].

The ΔK_{ef} and ΔK parameters can be related to each other through the following expression

$$\Delta K_{ef} = U\,\Delta K \tag{2.15}$$

Being U the normalized parameter of the stress ratio, U, definited by Elber [25] as

$$U = \frac{K_{max} - K_{op}}{K_{max} - K_{min}} \tag{2.16}$$

2.3.4 Fatigue life prediction

Aeronautical components and structures are often subject to random multi-axial loads, in which cyclic loads are applied with different frequencies, and/or phase differences, in different directions [26]. Cyclic multiaxial stresses in regions with notch occur both for multiaxial cyclic loading and for uniaxial loading, and this is because the geometric constraint of the notch causes multiaxial stresses to occur at the root of the notch, even though the component is in a state of uniaxial tension [27].

As already mentioned, the fatigue process under multiaxial loads is quite complex, therefore, it is very important to accurately predict the behavior of components with this type of loading. Thus, in order to develop a universal model of multiaxial damage, several efforts have been developed. However, to date, it has not been successfully achieved. That said, the life of notched components could be analyzed through several models, which are divided into three categories: stress-based models; energy-based models and strain-based models.

Next, the first 2 models are briefly presented and the model based on deformations is presented in more detail, as this is what will be used in this study.

2.3.4.1 Models based on stresses

Stress-based models are based on empirical relationships between applied stress and the number of cycles to failure (S-N curves). The presence of geometric discontinuities causes stress concentration, which, in turn, causes local stresses in the notch region, and in its vicinity, higher than the nominal stress.

Even though this is a good approach for determining the fatigue strength reduction factor, the most reliable is the experimental approach. However, it is relatively expensive and time consuming. In order to overcome this obstacle, alternative approaches have been proposed, which

are grouped into different methods, such as: effective stress method, Fracture Mechanics method, and stress field strength method. The method based on effective voltage is the one that has been mostly used. This assumes that fatigue damage is not only controlled by the maximum local stress at the root of the notch, but also by the average of the local stresses evaluated along a small line, area or volume around the root of the notch. It is thus concluded that fatigue failure occurs when the average stress, at a critical distance from the notch root, is equal to or greater than the fatigue strength of a smooth component [27].

2.3.4.2 Models based on energy

The energy supplied in a cyclic loading is stored in the material and emitted as heat, which in turn is generally divided into a reversible and an irreversible part, the latter being represented by the hysteresis circuit. When deformation is controlled, the area of the hysteresis loop is practically constant throughout the life of the material and represents the plastic deformation energy absorbed per cycle. This cyclic hysteresis loop can be used as a damage parameter to assess fatigue failure for the entire fatigue life spectrum.

2.3.4.3 Models based on local deformation

Cyclic strains with the presence of average strain result in an average component of acting stress. This stress component, in most cases, causes a “relaxation” of the material with the continuous application of deformation cycles. The relaxation induced in the material is a result of the presence of plastic deformation and, therefore, the rate of relaxation will depend on the magnitude of the amplitude of plastic deformation present [28]. Figure 2.9 illustrates this relaxation phenomenon due to the presence of mean strains.

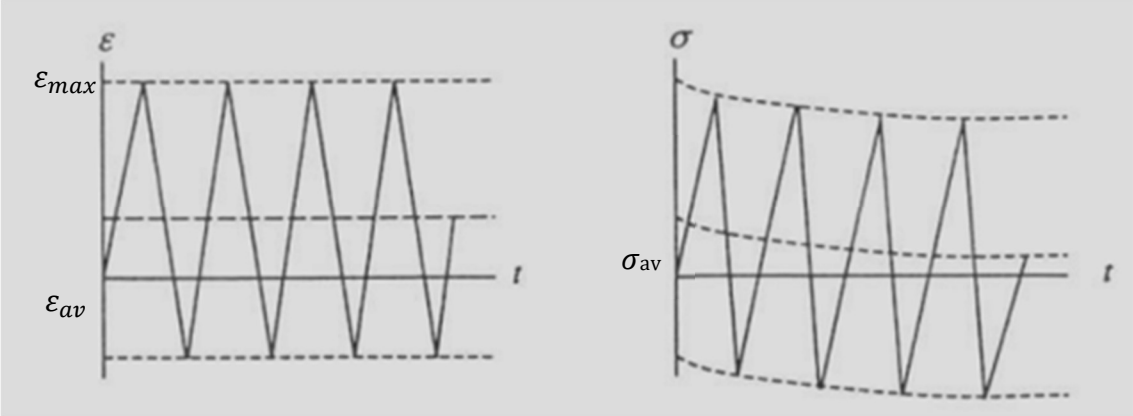

Figure 2.9 – Material relaxation during the cyclic application of strain in the presence of medium strain [28].

Relaxation due to medium stress is different from the cyclic softening phenomenon and can occur in any material. Since higher mean relaxation stresses occur at larger strain amplitudes, due to large plastic strains, the effect of mean stress on fatigue life will be smaller in low-cycle fatigue regions and greater in high-cycle fatigue [29]. Different types of models that consider the effect of mean stress on fatigue life prediction are available in the literature.

Models based on deformation are related to the plasticity existing at the notch root. This modeling assumes that notched and smooth specimens have the same life, and accumulate the same damage, if their stress-strain histories are similar at their crack initiation locations. There are different ways to determine the stress-strain fields, namely analytical methods, methods based on the finite element method or experimental methods Regardless of the method chosen, it is imperative to know precisely the stress-strain history at the root of the notch.

The analytical methods based on local deformation used in this study were as follows:

- Morrow's method;
- SWT method (Smith, Watson and Topper).

2.3.4.3.1 Morrow's method or local deformation model

Morrow's method has a formulation as shown in Eq. (2.17).

By this method, both the terms elastic and plastic consider situations where the average stress exists (eq. 2.17):

$$\frac{\Delta\varepsilon}{2} = \varepsilon_{av} = \frac{\sigma_f' - \sigma_{av}}{E}\left(2N_f\right)^b + \varepsilon_f'\left(\frac{\sigma_f' - \sigma_{av}}{\sigma_f'}\right)^{b/c}\left(2N_f\right)^c \quad (2.17)$$

where, $\frac{\Delta\varepsilon}{2}$ is the total strain amplitude, σ_f' is the fatigue strenght coefficient, σ_{av}, is the mean stress, E, is the elastic modulus, N_f, is the number cycles to failure, b is the failure local, ε_f' is the fatigue ductility coefficient and c is the fatigue ductility exponent [30].

On the other hand, Morrow also describes an equation where he disregards the presence of the average stress in the plastic component of the deformation.

Morrow [31] suggested that the elastic term of the total strain-life equation (eq. 2.18), can be modified by subtracting the mean stress, σ_{av}, from the fatigue strenght coefficient, σ_f', to account for the mean stress effect as:

$$\frac{\Delta\varepsilon}{2} = \varepsilon_{av} = \frac{\sigma_f' - \sigma_{av}}{E}\left(2N_f\right)^b + \varepsilon_f'\left(2N_f\right)^{bc} \quad (2.18)$$

The medium stress σ_{av} is the stress acting at the critical point of the part, usually at the root of the notch, thus being different from the average rated stress.

The Morrow model predicts that mean stresses have larger effects at longer fatigue lives, where the elastic strain amplitude dominates the total strain amplitude. The model also predicts that the mean stress has much smaller effects at low fatigue lives, where the plastic strain is significant. The model predictions are consistent with experimental observations that the mean stresses have significant influences at high cycle fatigue than low cycle fatigue [31].

2.3.4.3.2 SWT – Smith, Watson and Topper

The SWT – Smith, Watson and Topper model for life deformation can be evaluated in Equation 2.19:

$$\frac{\Delta\varepsilon}{2} = \varepsilon_{av} = \frac{\left(\sigma_f'\right)^2}{\sigma_{max}\,E}\left(2N_f\right)^{2b} + \frac{\sigma_f'\varepsilon_f'}{\sigma_{max}\,E}\left(2N_f\right)^{b+c} \quad (2.19)$$

This equation assumes that for different magnitudes of strain ε_{av} and different values of mean stress σ_{av}, the product $\sigma_{max}\varepsilon_{av}$ remains constant for a given lifetime. If σ_{max} is zero, the above equation predicts infinite life, which indicates that stress must be present to populate fatigue fracture. The SWT method has been shown to be more efficient in the correlation of situations with the existence of average stresses for different types of materials and, therefore, this method has been more effective for general cases. Similar to the stress-life (S-N) method, in

addition to the presence of average stress, other factors can influence the strain-life behavior of the material.

Smith, Watson and Topper (SWT) suggested that the function of the maximum tensile stress, σ_{max} and the strain amplitude, ε_{av} should control the influence of mean stress in the fatigue life analysis, equation 2.20:

$$\sigma_{max}\,\varepsilon_{av} = \sigma_{max}\,\frac{\Delta\varepsilon}{2} = \frac{\left(\sigma_f'\right)^2}{E}\left(2N_f\right)^{2b} + \sigma_f'\varepsilon_f'\left(2N_f\right)^{b+c} \tag{2.20}$$

where, $\sigma_{max} = \sigma_{av} + \sigma_a$ is the maximum stress of a given cycle.

The SWT model can be classified as the stress- strain or energy type of damage parameter. The SWT model assumes that the damage parameter, $\sigma_{max}\,\varepsilon_{av}$ remains constant for diferent values of the product of the maximum stress, σ_{max} and the strain amplitude, ε_{av} at a given life. The SWT model shows good predictions to account for the mean stress effects under tensile mean stress conditions at low and long fatigue lives [32, 33, 34, 35, 36]. However, it shows non-conservative predictions for large compressive mean stresses [37] and predicts zero fatigue damage for compression-compression loadings where the maximum stress is $\sigma_{max} \leq 0$. A theorethical limitation of the SWT model can easily show that the damage function, $\sigma_{max}\,\varepsilon_{av}$ is not defined if $\sigma_{max} \leq 0$.

2.3.4.4 Life prediction of fatigue crack propagation

The prediction of fatigue crack propagation life is generally performed using the criteria of Linear Elastic Fracture Mechanics. Through them, propagation laws are obtained, normally based on experimental results, which try to mathematically represent the evolution of the fatigue crack propagation velocity. Thus, the determination of the number of cycles spent in the propagation of a defect, from the initial dimension a_i to the final dimension a_f, boils down to the integration, between these limits, of the corresponding propagation law.

It is possible to determine critical loads, critical defect dimensions and inspection intervals, based on the capability of non-destructive inspection techniques or if the initial dimension of a crack is known, in order to be able to estimate the residual life of that component.

The crack dimension increases with the number of cycles and with the voltage level [38]. This relationship is usually expressed through a relationship of the type da/dN *versus* the

amplitude of the stress intensity factor, ΔK. The crack propagation speed, da/dN, is a function of several parameters, such as the stress intensity factor, ΔK, the stress ratio, R, the temperature, the environment, the rolling direction, the thickness component and the stress cycle.

The prediction of the fatigue life of a component in which it is assumed that there will be crack propagation is made by integrating the da/dN - ΔK curves. For example, integrating the Paris law, for constant stress amplitude, comes:

$$N_f = \frac{1}{C(\Delta\sigma)^m}\ x\ I \tag{2.21}$$

where I is the propagation integral given by the equation:

$$I = \int_{a_i}^{a_f} \frac{da}{(Y\sqrt{\pi a})^m} \tag{2.22}$$

In the 2.22 equation a_i e a_f are, respectively, the initial and final dimensions of the crack considered in the part.

To determine the number of cycles spent in the propagation of fatigue cracks, i tis necessary to know a set of data and parameters:

1. The crack propagation law of the material obtained experimentally under the same service conditions as the structure (metallurgical state, thickness, environment, medium stress, frequency, temperature, etc.) or, through results obtained by other researchers;
2. The equation of stress intensity factor is valid for the structure geometry and crack location;
3. The size of the initial crack or defect that can correspond to the size of a defect or crack that has been detected in service of the structure. Another hypothesis is to consider that in the structure there are always defects with a dimension equal to the values of the detection limits of the non-destructive inspection technique that is being used;
4. The nominal applied stress that is used in the stress intensity factor definition equation;
5. The distribution of stresses in the neighborhood of the crack (stress concentration effect);
6. The non-propagation threshold values, ΔK_{th} and K_{1c} under the conditions (1);

Once these parameters are defined, the crack propagation law is integrated.

2.4 Fatigue improvement techniques

2.4.1 Introduction

A significant percentage of aeronautical structures currently in service (central fuselage supports, connecting joints, fuel tank support structures and wings) have already exceeded their design life. However, they are not being replaced by new structures not only due to the high costs involved in the manufacture of such structures, but also as a consequence of the time delay that would be required for the new construction, during which it would not be in service. Thus, there are additional losses of an economic nature, or other, in this subject area of aeronautics where costs regarding all processes are too high.

However, on the other hand, keeping aged structures in service, without risk of loss of structural integrity, gives rise to additional maintenance costs, which can be classified into three different types:

i) Inspection costs, to check the existence of cracks or other defects in the structure, especially in the welded joints;

ii) Condition control costs, to assess the evolution, over time, of loads or stresses in the structure, and compare these values with the initial design parameters, (if these are available);

iii) Repair costs in the damaged areas, to rehabilitate the structure, so that the repaired welds can accept an extension of life with sufficient safety.

Miki et al [39] published a database of fatigue failure repair cases, which is available on the Internet.

Nowadays, due to economic constraints, there is a tendency to use structures to the maximum of their life potential. To achieve this objective, must be carried out, inspection, condition control and repair. Life extension of fatigue-aged structures may be possible without jeopardizing structural integrity, if are introduced rehabilitation methods such as surface treatment methods.

Rehabilitation is of the structure achieved when local treatment or repair provides greater fatigue strength in the identified area, at least equal to the fatigue strength of the original undamaged detail. If the treatment is properly applied, the rehabilitation of the detail can be

guaranteed, and the nature of the improvement methods can even produce, after repair, a higher fatigue strength and residual life than the initial detail, if this has not been initially subject to no ameliorating treatment.

Improvement techniques to rehabilitate can be used structures damaged by fatigue. The damaged structure can be treated locally and very often with the structure in service. If the treatment is successfully applied, the damage can be quickly removed and after the treatment, the initial mechanical properties of the structure can be recovered or even improved, also achieving a significant life extension period. This procedure avoids much more costly repairs, which would be the case if the structure had to be removed, rebuilt and put into service.

All fatigue improvement techniques are based on simple principles, which aim to increase the time to crack appearance, reintroducing a significant crack initiation period, and/or hamper its propagation [40]. These principles are:

- Reduction of the stress concentration factor;
- Reduction in the number of defects likely to give rise to a crack (roughness reduction);
- Creation of a local state of compressive stresses.

The fatigue improvement techniques, which are based on the modification and introduction of residual stresses, can be classified into two methods [41, 42]:

- Mechanical methods;
- Thermal methods.

These two methods can still be reclassified, according to Table 2.4.

Table 2.4 – Reclassification of the two fatigue improvement methods.

Mechanical methods	Impact methods	Shot blasting (*shot peening*)
		Hammering
		Impact with explosives
		Impact with ultrasound
	Overload methods	Initial overload
		Local compression
Thermal methods	Relaxation of thermal stresses	
	Local heating	
	Gunnerts method	

Given the great variety of these processes, we will present the surface improvement treatment processes and essentially the peening processes studied here in this work

2.4.2 Mechanical methods based on the introduction of residual stresses

2.4.2.1 Shot peening

The shot peening process consists of bombarding small beads (made of steel, ceramics, glass or other materials) into a target component (through an air jet or centrifugal force) at a speed between 20-100m/s in order to plastically deform the surface to create residual compressive stresses [43, 44]. The process schematization can be represented in Figure 2.10 [45].

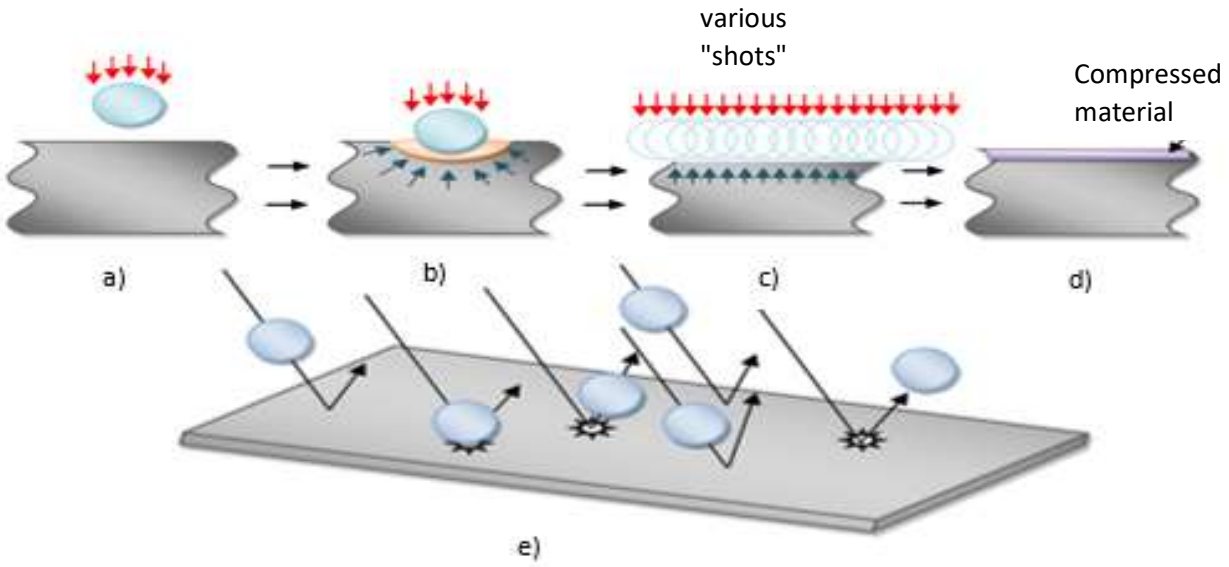

Figure 2.10 - Step-by-step schematic view of the shot peening process: a) Movement of the beads at high speed; b) Plastic deformation after impact, creating residual stresses; c) and d) Replication of the various "shots" in a target object; e) Creation of several small indentations [45].

Within this process, there may be several conditioning factors that will alter the distribution of residual stresses created. These differences may be due to the characteristics of the projectiles (diameter, hardness, density), the hardness of the workpiece or the process used (incidence angle, shooting speed, coverage, magnitude and depth) [43]. This method will have to be carefully controlled as the treated part will present a new roughness profile that will result in a new coefficient of surface stress concentration (K_t) which may have a more harmful than beneficial effect on material fatigue [43, 16], mainly in materials of low hardness.

2.4.2.1.1 Beads type

The particles used in the shot peening process can have different sizes as well as different materials. This selection is based on the material to be bombarded as hardness, intensity, iron contamination (in non-ferrous materials) and permissible surface roughness will be determined. The projectiles must have at least a hardness similar to the material to be shot so that in this way it is possible to induce plastic deformation [46].

Steel beads are the most commonly used, as in addition to being the most economical material, they have consistency, great durability and can be recycled. Beads from carbon steel cut

wire have the same characteristics as steel beads, but their manufacturing process results in more refined size control. Glass or ceramic particles are lighter and smaller than steel and are used where low intensities are required and where iron contamination is a design criterion. Basting by these beads, due to their smaller radius, results in a relatively smooth surface when compared to steel projectiles [47].

2.4.2.1.2 Coverage

An appropriate process is obtained when the processed surface has a total shot peening coverage, that is, the entire observed area must include spherical cutouts from the projected material [43]. The 100% coverage appears only on the theoretical plane, because as the piece is shot, the coverage increases, as well as a phenomenon known as overlap. Figure 2.11 shows a phenomenon that occurs when a surface is shot by more than one bead. In this way, an overlap of material can occur and there is the possibility of the formation of folds that affect the roughness and the consequent decrease in the fatigue life [43] [48].

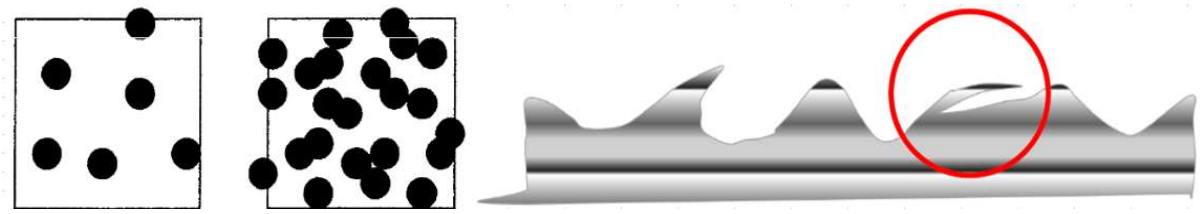

Figure 2.11 – (left) Process of gradual coverage of shot blast areas from individual "shots" to their overlapping [48]. (right) Shaping due to the peening excess [48].

2.4.2.1.3 Intensity

In 1944, John O. Almen proposed a model that allows the evaluation of the intensity of residual stresses introduced by the shot peening process [46]. This evaluation model is influenced by the beads size, hardness, shape, impact angle, exposure time, speed, etc., that is, all factors that influence the shot peening process, as the preliminary intensity measurement can be made with all the characteristics in which the shot blasting will be developed. Almen suggested bending and deforming a SAE 1070 spring steel plate with three different thicknesses that correspond to three intensities. By evaluating the arc height, it is possible to define the intensity of the method. Almen strips classified as "N", "A", "C" which only change in thickness. The N strip is 0.79mm thick, the A strip is 1.29mm and the C strip is 2.39mm where the greater the desired intensity, the

greater the chosen thickness [46] [47] [49]. The major disadvantage of this method has to do with the fact that this method uses all the variables (incidence angle, speed, hardness, beads size and shape, etc.) possible in a single method, not specifying the parameters individually [50]. In Figure 2.12 a representation of the evaluation process by Almen [49].

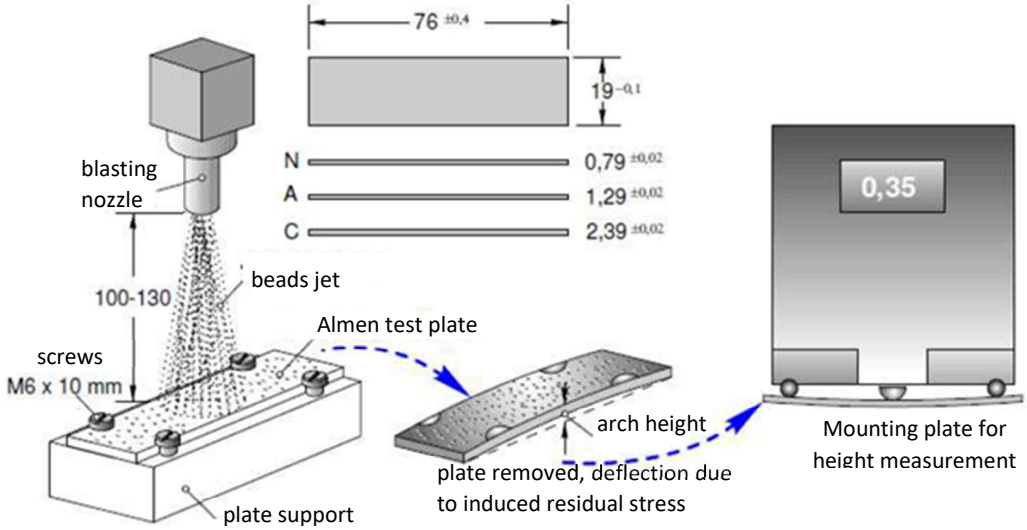

Figure 2.12 – Step-by-step scheme of the intensity evaluation process. [47].

Despite all the variables involved in the process, the time that a component is exposed to the shot peening treatment is one of the most critical factors involved in the process [47]. As can be seen in Figure 2.13, saturation occurs when twice the time of T, i.e., $2T$ does not provide an increase greater than or equal to 10% of the arc height.

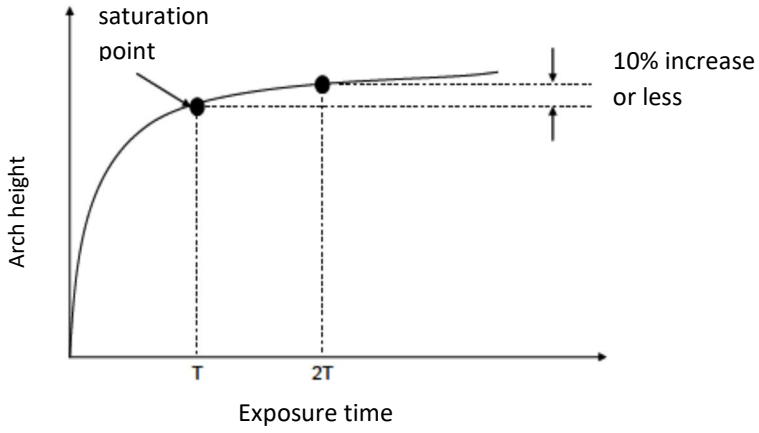

Figure 2.13 – Saturation point of the shot peening method calibration.

2.4.2.1.4 Shot peening effect on fatigue strength

Gao, Y. K. [51] surface treated alloy 7050-T7451 through shot peening, changing the material and the average diameter of the beads. In this study, which you can see in Figure 2.14, he analyzed which beads produce the highest residual compressive stresses from the surface to 275μm depth. With the exception of the GB150 glass beads (which show their maximum on the surface), all the others obtain similar behavior. They reached their maximum (-375MPa) between 30 and 100 μm depth and then the values rise to zero [51].

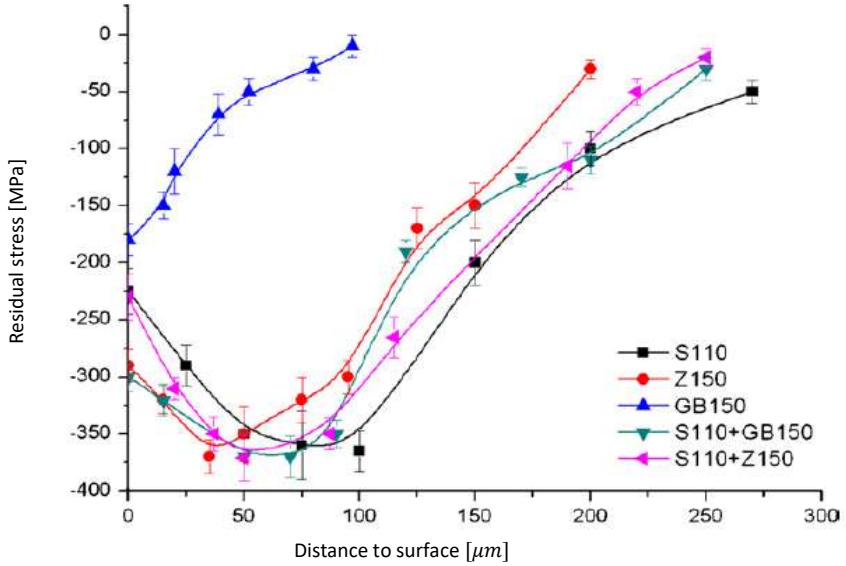

Figure 2.14 – Residual compressive stresses introduced by shot peening [51].

Subsequently, he carried out fatigue tests in rotational bending with R= -1 and obtained results that are directly related to the values of residual stresses. Table 2.5 shows the percentage of improvement in fatigue life resistance in relation to the base material specimens.

Table 2.5 – Improved fatigue strength compared to base material specimens.

Superficial treatment	Fatigue limit stress [MPa]	Improved fatigue strength to one million cycles [%]
Machined base material	185	0
GB150	190	2.7
S110	223	20.5
Z150	248	34.1
S110 + Z150	245	32.4
S110 + GB150	250	35

Table 2.6 presents an excerpt from a table where Gao studied the roughness introduced by the different processes and the associated stress concentrations.

Table 2.6 – Analysis of introduced roughness and associated stress concentrations [51].

Superficial treatment	R_a $[mm]$	K_t
Machined base material	0.87	-
GB150	1.29	1,09
S110	4.15	1,14
Z150	2.42	1,04
S110 + Z150	2.81	1,08
S110 + GB150	2.06	1,04

To link the residual stress graph and the fatigue limit and roughness tables, it can be stated that the compressive residual stresses have a positive effect on the fatigue limit stress, while the roughness has a negative effect.

2.4.2.2 Ultrasonic peening

o The mechanical surface treatment using ultrasound began to be developed around the 40s and 50s of the 20th century, and emerged from another technique already known, the Hammer Peening. Throughout the development of Ultrasonic Peening, this process has known several names such as: Ultrasonic Treatment (UT), Ultrasonic Impact Technique/Technology/Treatment (UIT) and Ultrasonic Impact Peening (UIP).

2.4.2.2.1 Ultrasonic Impact technology (UIT)

During the second half of the 20th century, this method was progressively improved, mainly by the Russian and Ukrainian scientific communities, and is currently a technique commercialized by the company Applied Ultrasonics. It is a widely known technique that stands out from other surface deformation techniques, as it is economically profitable, and allows the adjustment of operating parameters; it is simple and safe.

The Ultrasonic Impact Technology technique reconciles ultrasonic oscillation and high frequency impacts from strikers or stops on the part or weld bead to be treated, and these impacts cause plastic deformation of the surface layers of the material. In this way, it is intended that the relaxation of residual tensile stresses and the introduction of compressive stresses occur, the reduction of the stress concentration of the weld seams, and the improvement of the mechanical properties of the material, which leads, in short, to improving fatigue life behavior and corrosion resistance [52, 53, 54].

The equipment used by this technique can be seen in Figure 2.15:

Figure 2.15 – Ultrasonic Impact Technology (Esonix®UIT) equipment [55].

Modern equipment basically consists of a portable computer, a generator and a hand tool. A computer program is installed on the portable computer that allows monitoring the quality of the UIT process. The ultrasonic generator, with a total consumption of 250W, varies the frequency of the input alternating current (50-60 Hz) to the operating frequency (20-27 KHz). Hence the explanation for the name that this technique adopts, since it works for frequencies equal to or higher for which the division between human audible sound and ultrasound is made, 20 KHz. Finally, the hand tool, with an approximate weight of 3 kg, is internally constituted by a piezoelectric transducer, which converts the alternating electrical energy into mechanical energy through the piezoelectric effect. The working heads are attached to the end of the hand tool, which in turn support the strikers, which have axial freedom of movement, as they are not connected to the transducer. The diameter of these strikers varies between 3 and 5 mm, and a head can contain more than one striker, depending on the industrial application in focus. The final end of the transducer oscillates with an amplitude between 20 to 40 μm at the aforementioned operating frequency and strikes the striker at different stages of the oscillation cycle. The striker, in turn, oscillates in a small amplitude of 0.01 to 0.1 mm, periodically and at a lower frequency than the transducer. Strikers strike the material to be treated, causing plastic deformation and introducing compressive residual stresses [55, 56]. Figure 2.16 shows the different possibilities of work heads.

Figure 2.16 – Work heads used by UIT [57].

UIT can be applied to a wide range of materials such as medium strength carbon steel, high strength steel, high carbon steel, titanium alloys, aluminum alloys and bronze [58].

Togasaki et al [59] tested the improvements introduced by the UIT in a Web-Gusset weld bead in SM570Q steel with a tensile strength of 608 MPa, yield strength of 514 MPa and an elongation of 34%. The system used for surface treatment was an Applied Ultrasonic ESONIX®UIT trademarked device. The strikers had a radius of curvature of 3 mm and an operating range of 30 μm.

First, the fatigue tests were carried out at controlled temperature, at a test frequency between 4 and 9 Hz and a stress ratio of 0.1. The tests were concluded for 10 million cycles. The aim was to compare two sets of identical specimens, one untreated by UIT and the other treated. The S-N curves obtained can be seen in Figure 2.17.

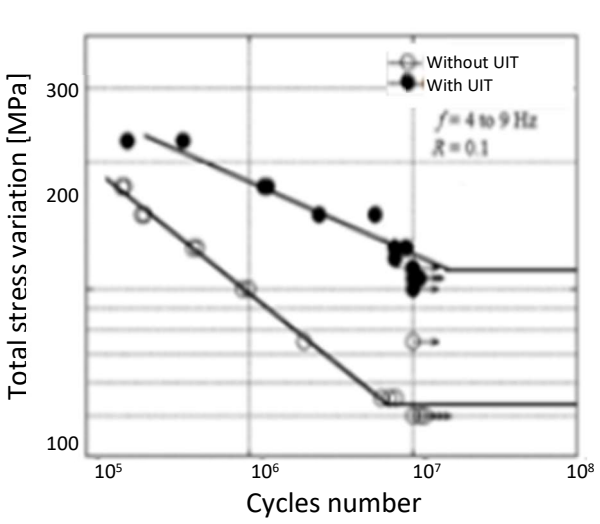

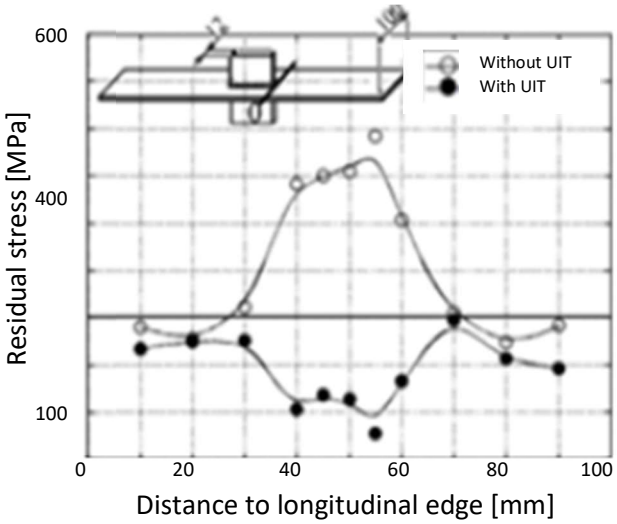

Figure 2.17 – (left) UIT effect on fatigue life;

Figure 2.18 – (right) Distribution of residual stresses before and after application of the UIT at weld bead.

Ensure that, the fatigue life of the weld bead improved very significantly with the application of the UIT, and, specifically, the fatigue limit stress increased from 53 MPa in the untreated specimens to 111 MPa in the treated specimens. Residual stresses were analyzed too using the X-ray diffraction method. The authors compared the residual stresses before and after application of the treatment at the weld bead area (Figure 2.18).

As can be seen in Figure 2.18, residual stresses above 400 MPa before treatment in the weld bead area, and after the application of the UIT, these stresses dropped to -100 MPa, representing a decrease of approximately 500 MPa. The authors also used 3D laser microscopy technology to determine the geometry of the beads before and after the UIT treatment and, later, to determine the change in the stress concentration factor K_t. They concluded that the stress concentration factor after the application of the UIT decreased around 40% in relation to the original. The authors also studied the grain size from the impact surface of the treatment to a depth of 25 μm of the specimens with and without UIT (Figure 2.19). Electron diffraction technology was used and they concluded that there was a grain refinement after the application of UIT.

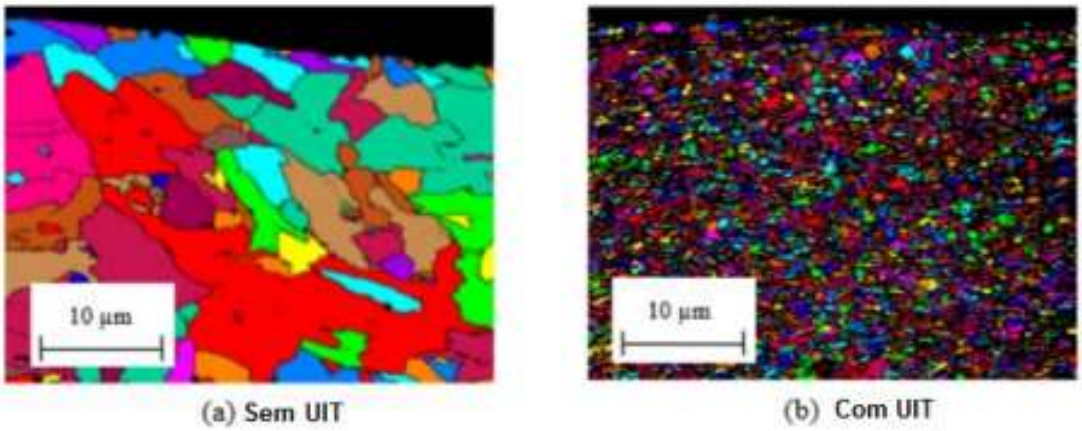

Figure 2.19 – Specimens grain size. a) Without UIT, a) With UIT.

Finally, they also analyzed the hardness as a function of the distance from the surface. A nanoindenter used with the application of a maximum load of 2000 mN, which corresponds to the $Hv_{0,2}$ hardness test. The results obtained can be seen in Figure 2.20.

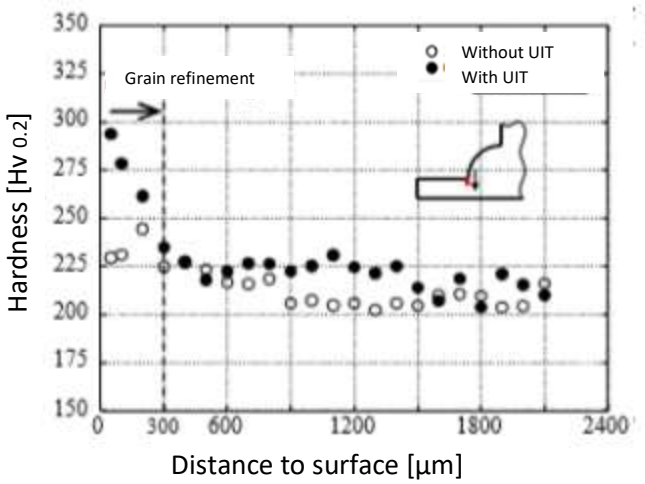

Figure 2.20 - Vickers hardness distribution.

They concluded that the surface hardness increased by about 30% with the application of UIT, precisely in the area of refined grain, and that the hardness returned to common values when the grain was no longer refined.

Statnikov et al [60] studied this and other plastic deformation treatments. The S-N curves were obtained by fatigue tests (4-point bending, using the CDM-10 hydro-pulsator machine, R=0.1; 7 Hz, test temperature varying between 20 and 28ºC) performed on Weldox 420 steel. The results obtained can be seen in Figure 2.21.

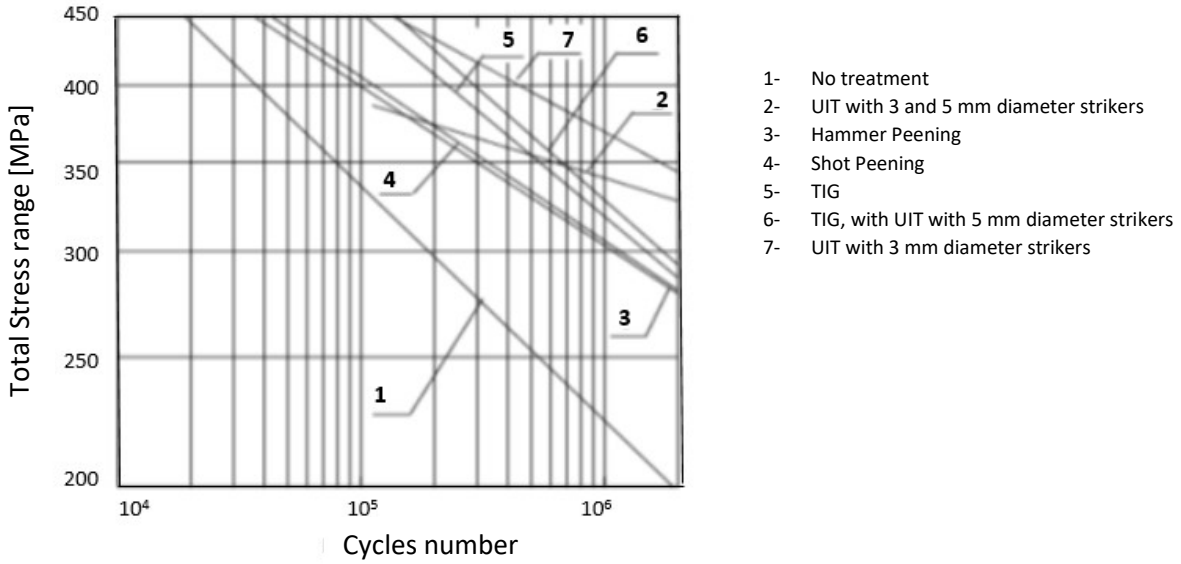

Figure 2.21 – S-N curves for different superficial treatments.

It can be concluded that all the treatments used improve the fatigue life behavior of the weld seams. However, naturally, some exhibit better and others worse results. It appears, therefore, that Hammer Peening and Shot Peening introduce the same improvement. Next, with approximately the same slope as the regression line are the TIG results. It is noted that in the TIG treatment, with subsequent UIT it is still possible to slightly improve the results. Finally, regarding the UIT process, it is possible to verify a possible optimization of the parameters, since the results obtained by the process when using 3 mm diameter strikers are superior to the results when using 3 and 5 mm strikers. That is, from this it appears that the decrease in the diameter of the strikers leads to an increase in the UIT effectiveness.

Yang et al [61] studied the influence of UIT on a Friction Stir Welding welded joint in 7075-T651 aluminum alloy. The UIT generator operated at a frequency of 19,8 kHz and the strikers had an operating amplitude of 30 μm, which worked at a speed of 1,5-2m/min. The stress ratio used in the fatigue tests was R= 0,5. These authors concluded that the UIT could increase the fatigue limit stress by about 52%. Through SEM analysis of the fracture surface, zones of plastic deformation of the surface were identified up to a depth of about 300 μm, being below this value, in the superficial sublayers, the crack initiation site. On the other hand, through metallographic analysis, it was found that the grains on the surface were deformed and refined (Figure 2.22), an effect that is not felt up to a depth of 300 μm. The surface microhardness also increased significantly. For the determination of residual stresses, the X-ray diffraction method was used, having obtained a residual stress at the surface of -100 MPa, and a maximum of -217,3 MPa for a depth of 300 μm. The change from compressive to tensile stress took place at 700 μm depth.

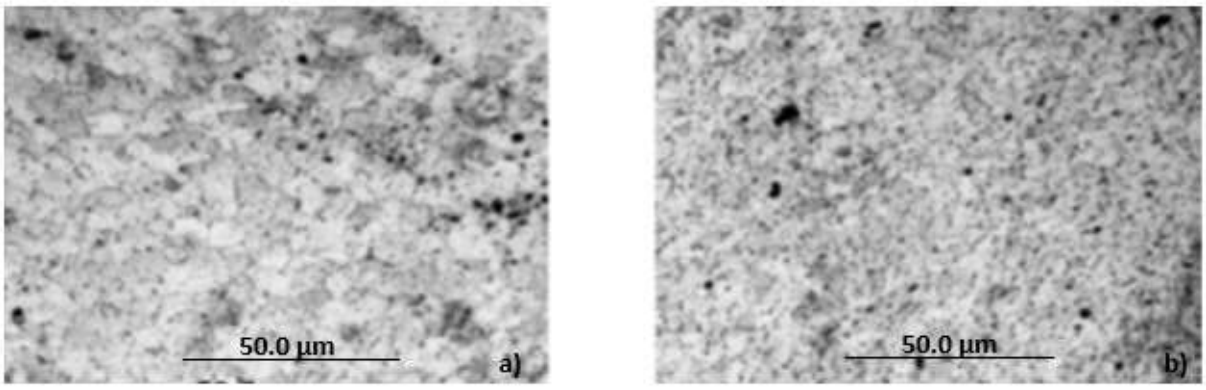

Figure 2.22 – Micrographs of Al 7075-T651 alloy microstructure: a) Before; b) After Ultrasonic Peening.

Other authors [62, 63] also obtained relevant improvements to fatigue by using the UIT technique. They also concluded that the process can be used in structures or welded joints, where fatigue failure is more likely to occur, since there is only a short period for crack initiation. The process is able to close already initiated microscopic cracks and prolong the fatigue life of the structural element [64, 65, 66].

Grain refinement was also observed in the UIT application zone in Q345 steel [67].

2.4.2.2.2 Ultrasonic Peening (USP) variant

The "Ultrasonic Peening" is a cold surface treatment technique developed by SONATS (Stressonic® technology), which improves mechanical strength, fatigue life and corrosion resistance. It has great industrial applicability, such as in compressors, gears and reservoirs. As the name of the technique suggests, the process can be understood as a combination of "Ultrasonic Impact Technology" with "Shot Penning" or "Microshot Peening".

The induction of plastic deformation, and the consequent introduction of residual stresses, is also achieved by striking beads (from 1 to 2 mm in diameter) as in Shot Penning, but, while in Shot Peening the beads are accelerated by an airflow at a given pressure, in Ultrasonic Peening or USP the beads are accelerated by a vibrating surface at a frequency similar to that of Ultrasonic Impact Technology. The central unit where the generator is contained produces an electrical signal with an ultrasonic frequency. The emitter converts the electrical signal into mechanical displacement, and the intensifier and sonotrode amplify it. The amplitude and frequency of the

sonotrode give the steel beads a random displacement throughout the volume of the chamber and on the part to be treated (the chamber is therefore open), which gives it a uniform surface treatment with low roughness (less than in the conventional shot peening). The equipment is represented in Figure 2.23.

The chambers can be designed specifically for each type of components to be treated. The process is entirely controlled by a computer and can even be automated. This treatment eliminates the use of compressed air, reduces the cycle time, the number of beads and the total energy consumed [68].

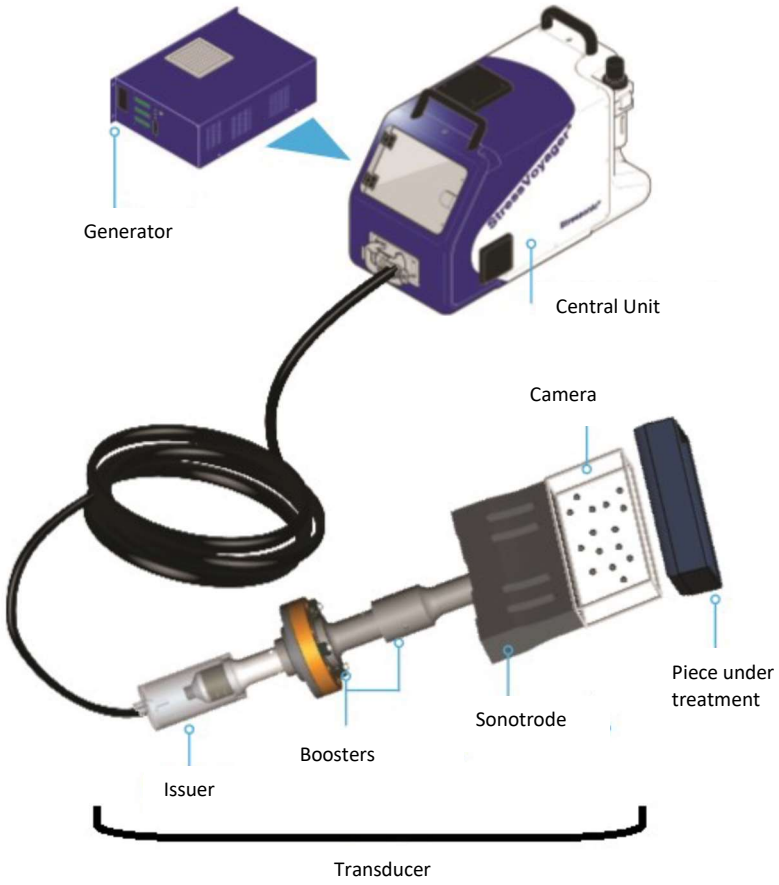

Figure 2.23 – Scheme of Ultrasonic Peening process (USP) [68].

Sanada et al [69] found, by optimizing certain parameters, an improvement in the fatigue life of specimens made of a magnesium alloy AZ61 treated by USP. The most significant improvements were noticed when using 1 and 2 mm diameter beads and 300% coverage. On the other hand, Xing et al [70] verified the existence of compressive residual stresses in a soft steel

with a maximum value at the surface of -309 MPa, with a gradual decrease of compressive stresses until a depth of 250 μm, where the residual stresses have positive values [68].

2.4.2.3 Microshot peening (MSP)

A The "Microshot Peening" technique consists of projecting steel, glass or ceramic beads against the surface of the material to be treated with the aim of creating plastic deformation and, consequently, introducing residual stresses. The impact of the beads on the material produces indentations (some level of roughness) on the surface of the material, and, below this, compressive stresses are created. This process is easy to perform, safe and repeatable, and it can be automated using a CNC[1] machine [69]. The beads diameter can diversify between 0.03 and 0.5 mm [70]. The depth of the residual stresses depends on the intensity of the process, the relative hardness of the material of the spheres and the material to be treated, and the diameter of the beads themselves.

Thus, the main operating parameters are: beads hardness and size, process intensity, exposure time, coverage, air pressure, impact angle and nozzle characteristics [72].

All parameters mentioned must be carefully selected to obtain the maximum possible improvement in the strength of the material. Markovina et al [71, 73] also reported the possible harmful effect of "overpenning", i.e., coverage greater than 100%, when the material treatment parameters are poorly matched (covering effect).

Lundberg et al [74] studied 12 different combinations of the Microshot Peening process. To change bead diameter (S170, S330 and S550, all with the same Rockwell class C hardness, equal to 56), for two types of materials to be treated (both cast irons: gray iron and compacted graphite iron, the first one with worse mechanical properties than the second one), and for 2 different intensities (adjusting the Almen target type as the increase in beads density). The studied combinations are referred to in Table 2.7.

[1] CNC machine – Computer Numerical Control Machine.

Table 2.7 - Lundberg et al tests parameters [74].

Bead diameter (mm)		0.43 (S170)	0.84 (S330)	1.40 (S 550)
Almen Intensity	Low	0.17 mmA	0.30 mmA	0.17 mmC
	High	0.37 mmA	0.16 mmC	0.29 mmC
Coverage (%)		300	300	300

In a study only focused on residual stresses, they concluded that: all possibilities introduced compressive residual stresses; the highest residual stresses were achieved when using the smallest beads (S170), low intensity (0,17 mmA) and 100% coverage; the lowest residual stresses were achieved when using the largest beads (S550), high intensity (0.29 mmC) and 300% coverage; for the same size of beads and cover, the greater the intensity of the process, the greater the value and dimension of the zone of compressive residual stresses; for low intensity, increasing the size of the beads increased the penetration depth of residual stresses more significantly than their value in the subsurface layer.

Gao and Wu [75] studied the effect of applying Microshot Peening precisely on the alloy studied in this dissertation, Al7475-T7351, in a semicircular notch with a radius of 3.2 mm and a 5mm specimen thickness. The treatment was produced by a pneumatic machine at an intensity of Almen 0.20 mm (type A), 100% coverage and a 0.25 MPa air pressure. Steel S110 beads were used in this study.

Residual stresses were measured by X-ray diffraction and their evolution can be seen in diagram in Figure 2.24.

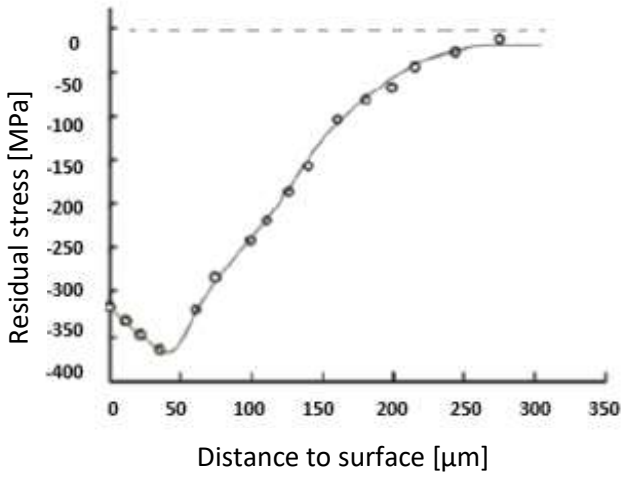

Figure 2.24 - Residual stresses induced by Microshot Peening [75].

The residual stress at the surface has a value of -308 MPa and the maximum compressive stress occurs at a depth of 45 µm. From that point, the value gradually decreases until it becomes practically zero at a depth of 300 µm.

2.4.2.4 Laser peening (LP)

In the "Laser Peening" (LP) process, the material to be treated can be (or not) [76] coated with an ablative layer (which aims to increase the absorption of a laser beam that is emitted against the surface) and is involved by a transparent layer, usually water. When a pulse lasting a few nanoseconds strikes the material, the resulting energy is so intense that the material vaporizes and plasma is generated. This plasma, which is confined by the transparent layer, cannot expand due to the inertia of the layer, and instead exerts a great pressure on the material. If the pressure exerted by the plasma is greater than the yield stress of the material, this will result in a plastic deformation of the microstructure at depth. Schematized process by Figure 2.25.

Laser Peening (LP) can be used in various applications in aerospace (crankshafts, gears), medical (orthopedic implants and surgical tools) [77].

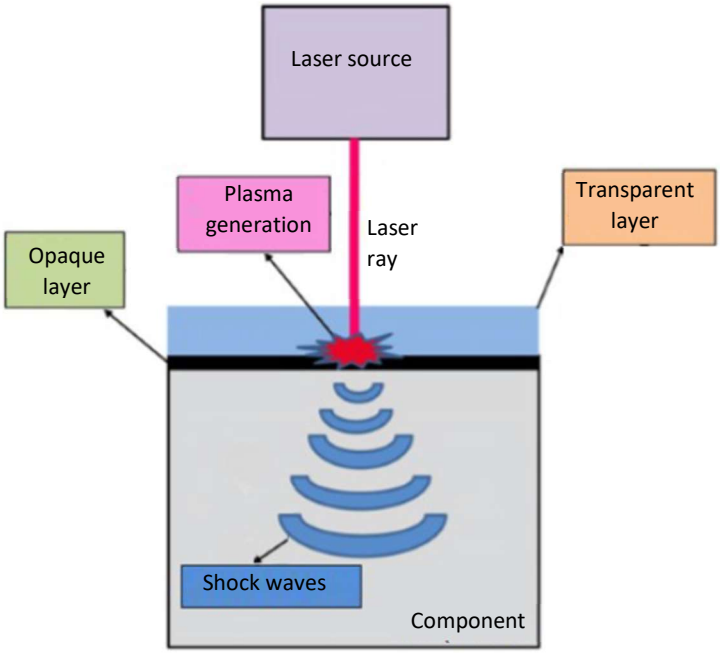

Figure 2.25 - Laser peening process scheme [77].

Sathyajith and Kalainathan [78] studied the effect of a low energy beam, Nd: YAG of 300mJ/pulse, for an Aluminum 6061-T6 alloy and for two different densities (22 and 32 pulses/mm^2). They found that for a R_a and an R_q, 1.9 and 3.2 µm, respectively, the maximum pulse density; the greater the pulse density, the greater the roughness obtained. They also verified that increasing the number of pulses per mm^2 does not increase the value of the induced residual stresses (-216.5 MPa, maximum value at the surface), due to the harmful thermal effect on the surface. They also verified that the hardness value increases for great depths the greater the beam pulse density (maximum difference at the surface of 8 Hv; $Hv_{0,05}$ test for 10s).

Gao [79] compared the effects produced by the "Laser Peening (LP)" and "Shot Peening (SP)" processes regarding the introduced compressive residual stresses, roughness, fatigue life and fracture surface in 7050-T7451 aluminum alloy, in specimens with circular shape. It used the Nd: glass laser with an intensity of 2x109 W/cm^2, duration per pulse of 50ns, 50J/pulse at a frequency of 0.54 Hz and Almen intensity of 0.08 mmC. Four total times of application of the process were used: 120s, 240, 360s and 480s. Gao found that the highest and deepest residual stresses are obtained for the times of 240s and 360s, up to a depth of 2 mm, a depth that is about

10 times greater than that recorded in his best SP test (Double "Shot Peening": S110+GB150[2]). The value of residual stresses at the surface of the two processes are practically similar. For a roughness evaluation length of 2 mm, the highest values obtained for the "Laser Peening" process were for LP-360s with R_a and R_z equal to 1,24 and 5,92 μm, respectively. The lowest SP roughness values were obtained for low intensities with the use of glass beads. All SP roughness values are higher than those obtained by LP.

The fatigue tests were of the rotational bending type. The greatest improvement obtained for the SP was recorded for the S110+GB150 with an improvement factor over the untreated specimens of 3,667. The greatest improvement noted for the LP was registered for the time of 240s with a factor of 6,608 also in relation to the untreated specimens. The roughness and residual stress values explain the different fatigue performance of the two processes.

Finally, the authors observed that the fracture of the treated specimens occurred in the subsurface layer, below the region of compressive stresses introduced for the two surface treatments, while, for the untreated specimens, the fracture occurred on the surface.

2.4.2.5 Jet Peening (JP)

The "Jet Penning" technique consists of the impact of a large flow of drops or jet of water ("Water Jet Peening", WJP, Figure 2.28) or oil ("Oil Jet Peening", OJP) on the surface of the material to be treated, in order to cause plastic deformation and consequent introduction of compressive stresses on the surface, as in the before mentioned techniques. In the case of Water Jet Peening, if the treatment parameters are not optimized correctly there may be erosion or surface damage, thus impairing fatigue resistance. The fundamental parameters of the process are: velocity of impact of the treatment fluid, distance from the nozzle, number of passes and fluid pressure.

[2] Double Shot Peening is a variant of Shot Peening in which two types of beads are used to treat the material. In this case, first type S110 (steel; 0.28mm diameter) was issued and later the glass beads GB150 (0.15mm diameter). Very briefly, the first type of beads is used with a high intensity to create a deep surface layer with compressive stresses, and the second type of beads is used at a lower intensity to also increase the value of compressive stresses, but mainly to modify the topography of the surface, namely to improve the roughness.

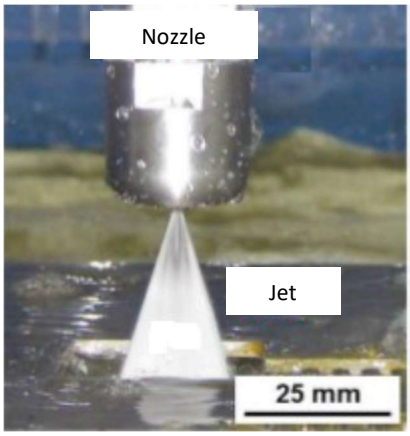

Figure 2.26 - Water Jet peening process scheme..

Boud et al [80] studied the effects of changing parameters in the WJP in a 7475 aluminum alloy, in the form of a 3 mm thick sheet. The authors varied the water impact speed between 3000mm/min and 5000mm/min, the distance to the nozzle from 10 to 25 mm, the number of passes from 1 to 4, and the water pressure from 345 to 275 MPa. The roughness R_a that the different treatments imposed on the surface varied between 5.5 and 6.5 μm. The treatment that stood out in terms of maximum imposed compressive stresses (-125 MPa) was performed with the parameters of maximum fluid velocity, shorter distance from the nozzle to the treated material, higher number of passes and lower pressure. This treatment, with these specific characteristics, also had the lowest rates of material removed. The fatigue tests performed did not cover life spans that were too wide for it to be possible to say with certainty that the WJP is beneficial in improving fatigue life.

Authors Grinspan and Gnanamoorthy reported [52], on the other hand, the low magnitudes and low depths reached by the residual stresses induced by WJP, as well as the localized erosion caused in the material to be treated (the aforementioned material removal). Thus, the authors refer that increasing the viscosity of the used fluid reduces the erosion caused by it and favors a smoother surface after treatment. Thus, the authors analyzed the residual stresses and hardness changes imposed on two types of aluminum (Al 6063-T6 and Al 6061-T4) using VG68 anti-wear oil as the treatment fluid. The researchers concluded that the maximum value of residual stresses decreased with increasing distance from the nozzle to the treated material and that the stresses were higher the greater the yield stress of the material. The maximum compressive stress recorded was -107.13 MPa at a depth of 40 μm for Al 6063-T6. The increase in hardness of the treated

surface, for the two aluminum, increased between 34 and 44% in relation to the untreated material. In a second part of the study [54], the authors conclude that the elastic limit stress of the material influences the roughness that the treatment is able to impose on the material. The Al 6061-T4, with lower yield stress, recorded a R_a of 6 and 7 μm, if the nozzle was at a distance of 25 or 40 mm, respectively, from the treated material, and a R_z of 45 and 40 μm, for the same distances. Al 6063-T6, with a higher yield strength, always kept its roughness values practically unchanged. In addition, erosion pits were recorded only on the surface of Al 6061-T4. They also concluded that the diameter and depth of the indentations and the roughness increase with the distance from the nozzle to the treated material.

2.5 References

[1] – American Society for Metals, ASM Handbook, "*Introduction to aluminum and aluminum alloys*", www.asmhandbook.com, consulted on 25 November 2020.

[2] – Davis, J., American Society for Metals Speciality Handbook, "*Aluminum and aluminum alloys*"; OH, EUA, p-784; 1993.

[3] – Associação Brasileira de Alumínio, ABAL, "*Fundamentos do alumínio e suas aplicações*"; p-81; São Paulo; 2004.

[4] – Kaufman, J. G., "*Introduction to Aluminum Alloys and Tempers*", p. 39-76, "ASM International"; 2000.

[5] – B. B. Verma, J. D. Atkinson, and M. Kumar,"*Study of fatigue behaviour of 7475 aluminium alloy*", Bull. Mater. Sci, vol. 24, no. 2, p. 231–236; 2001.

[6] – Unknown (1998), MIL-HDBK-5H,"*Military Handbook-Metallic materials and elements*" acessed on the 10th Jully 2020.

[7] – Ramos, R., "*Melhoria da Vida à Fadiga em Ligas Aeronáuticas de Alumínio por Ultrasonic Peening e Microshot Peening*" Tese de Mestrado em Engenharia Mecânica da Faculdade de Ciências e Tecnologia da Universidade de Coimbra; 2015.

[8] – ALCOA, "*Alcoa Mill Products, 7475 Aluminium Alloy Plate and Sheet*", acessed on the 15 November 2020 at http:// www.alcoa.com/ mill_products/ catalog/ pdf/ alloy7475techplatesheet.pdf.

[9] – Barroso, E., "*Efeito da Pré-deformação e Shot Peening na Tenacidade à Fratura e Propagação de Trinca por Fadiga da Liga de Alumínio 7475-T7351, de Aplicação Aeronáutica*" Universidade Federal de Ouro Preto; 2004.

[10] – Surish, S., "*Fatigue of Metals*", 2nd edition, Cambridge University Press, Inglaterra; 1998.

[11] – Schütz, W., "*A history of fatigue*", Engineering Fracture Mechanics, vol.54, nº2, p-263-300, 1996.

[12] – Garcia, A., Spim, J.A., Santos, C.A., "*Ensaios de Materiais*", LTC – Livros Técnicos e Científicos Editora S.A; 2000.

[13] – Kamal, M. e Rahman, M.M., "*Advances in fatigue life modeling: A review*", Renewable and Sustainable Energy Reviews 82 (2018), p-940-949; 2018.

[14] – ASM International; "*Elements of Matallurgy and Engineering Alloys*", acesso em 27 de Novembro de 2020, www.asminternational.org; 2018.

[15] – Azeez, A. A., "*Fatigue Failure na testing Methods*", Tese de Bacharelato em Engenharia Mecânica e Tecnologias de Produção pela Universidade de Ciências Aplicadas de Hamk; 2013.

[16] – Kulazi, A.J., "*Comportamento à fadiga do aço DP600 processado por jacto de água*", Dissertação para obtenção do grau de Mestre em Engenharia Mecânica no Instituto Superior Técnico de Lisboa; 2007.

[17] – Sangid, M.D., "*The physis of fatigue crack initiation*", International Journal of Fatigue 57, p-58-72; 2013.

[18] – Meyers, M.A e e Chawla K.K., "*Mechanical Behavior of Materials*", 2ªedição, Cambridge University Press; 2007.

[19] – Branco, C.M., Capítulo 14 em "*Mecânica dos Materiais*", Ed. Fundação Calouste Gulbenkian, Lisboa; 1985.

[20] – Lee C., Lee W., Kim J., Choi D., Yeon Y., Jung S., "*Lap point properties of FSWed dissimilar formed 5052 Al and 6061 Al alloys with diferente thisckness*", Journal of Materials Science, p-3296-3304; 2008.

[21] – Dowling N.E, "*Mechanical Behaviour of Materials*", Engineering Methods of Deformation, Fracture and Fatigue, Pearson; 2013.

[22] – Sinclair, G. M. and Craig W.J., "*Influence of grain size on work hardening and aftigue characteristics of alfa brass*", Trans. of the Am. Soc. For Metals, vol. 44, pag. 929-948, 1952.

[23] – Randon J.C., Rosa L.G., "*Fatigue threshold behaviour, Part I: modelling of FCG near threshold*", Proc. Of NATO ASI on Advances in Fatigue Science and Technology, NATO ASI Series, Series E, vol. 159, p- 129-139.

[24] – Elber W., "*Fatigue crack closure under cyclic tension*", Engineering Fracture Mechanics, Vol.2, p 37-45, 1970.

[25] – Elber W., "*The significance of fatigue crack closure*", Damage Tolerance in Aircraft Structures, ASTM STP 486, American Society for Testing and Materials, p- 230-242.

[26] – Wang C.H., Brown M.W., "*A path-independent parameter for fatigue under proportional and non-proportional loading*", Fatigue & Fracture of Engineering Materials and Structures, p-1285-1298, 1993.

[27] – Fatemi A., Shamsaei N., "*Multiaxial fatigue: An overview and some approximation models for life estimation*", International Journal of Fatigue, p- 948-958, 2011.

[28] – Fatemi, A. "*Cyclic Deformation & Strain-Life Approach*", University of Toledo, Slide, 2006.

[29] – Ferreira, A.L. J., "*Efeito da Presença de Tensão Média sobre a vida do aço ASTM A743 – CA6NM*", Universidade de Brasília, 2009.

[30] – De Jesus, J., Ferreira, J.M., Borrego, L., Costa, J.D., Capela, C., "*Fatigue Failure from Inner Surfaces of Additive Manufactured Ti-6Al-4V Components*", Materials 2021 Journal, 2021.

[31] – Ince, A., "*A generalized mean stress correction model based on distortional strain energy*", Journal of Fatigue, 2017, p-273-282.

[32] – Li, J., Wang, X., Li, R.-T., Qiu, Y.-Y., "*Multiaxial fatigue life prediction for metals by means of an improved strain energy density-based critical plane criterion*", European Journal of Mechanics, 2021.

[33] - Kujawski, D., "*An interpretation and modification of the SWT function*", Fatigue and Fracture of Engineering Materials and Structures, 2021.

[34] - Himmiche, S., Mortazavi, S.N.S., Ince, A., "*Comparative Study of Neural Network–Based Models for Fatigue Crack Growth Predictions of Short Cracks*", Journal of Peridynamics and Nonlocal Modeling, 2021.

[35] - Albinmousa, J., Topper, T., "*Application of cyclic plasticity to fatigue modeling*", Cyclic Plasticity of Metals: Modeling Fundamentals and Applications, 2021.

[36] - Bang, D.J., Ince, A., "*A short and long crack growth model based on 2-parameter driving force and crack growth thresholds*", International Journal of Fatigue, 2020.

[37] - Mortazavi, S.N.S., Ince, A., "*An artificial neural network modeling approach for short and long fatigue crack propagation*", Computational Materials Science, 2020.

[38] – Radaj, D., "*Design and Analysis of Fatigue Resistant Welded Structures*", Abington Publishing, 1990.

[39] – Miki, G., Goto, G., Ito, Y., "*Database of Repair Case for Fatigue Failure on Internet*", IIW-DOC-XIII-1887-01, 2001.

[40] – Maddox, S.J., "*Fatigue Strength of Welded Structures*", Abington Publishing, Cambridge, UK, 1991.

[41] – Lieurade, H.P., Huther, I., "*Fatigue Strength Improvement Solutions for Welded Structures and Components*", IIW-DOC-XIII-1904-01, 2001.

[42] – Tomkings, A.B., "*A Review of alternative Techniques for Improving Properties of Weldments*", Research, Development and testing for industry – Worldwide, November, 1993.

[43] – Totten, G., Howes, M. e Inoue, T., "*Handbook of residual stress and deformation of steel*", ASM International, 2002.

[44] – Franchim, A. S., Campos, V. S., Travessa, D. N, C. M. N., "*Analitycal modelling for residual stresses produced by shot peening*", Materials and Design 30, p-1556-1560, 2009.

[45] – Ramjith, J., "*Experimental investigation into the comparison between shot peening and laser shoot peening on Al 6056-T4 Aluminium alloy*", Tese de Mestrado em Engenharia pela universidade de Witwaterrand, Johannesburg, 2014.

[46] – Bhuvaraghan, B., Srinivasan, M., Maffeo, B., "*Optimization of the fatigue strength of materials due to shot peening*", International Journal of Structural Changes in Solids – Mechanics and Applications, 2010.

[47] – Becker, A., "*The effect of laser shock peening and shot peening on the fatigue performance of aluminium alloy 7075*", Tese de Mestrado em Engenharia Mecânica pela Universidade de Cape Town, 2017.

[48] – Krk, D. e Abyaneh, M. Y., "*Theoretical Basis of Shot Peening Coverage Control*", The Shot Peener, Volume 9, Issue 2, 2002.

[49] – Rocha, C., "*Desempenho em fadiga de arames submetidos ao processo de shot peening*", Dissertação de mestrado em Engenharia Mecânica pela Universidade Federal do Rio Grande do Sul, 2010.

[50] – Braga, A., "*Análise de ligas de alumínio conformadas por jateamento com granalhas – caracterização e previsão de deformação*", Dissertação para obtenção de grau de Mestre em Engenharia Mecânica pela Universidade de São Paulo, 2001.

[51] – Gao, Y. K., "*Improvement of fatigue property in 7075-T7451 aluminium alloy by laser peening and shot peening*", Materials Science and Engineering A528 (2011), p-3823-3838, 2011.

[52] – S. Grinspan, R. Gnanamoorthy, *"Surface modification by oil jet peening in Al alloys, Al 6063-T6 and Al 6061-T4: Residual stress and Hardness"*, Applied Surface Science, vol. 253, no. 2, p. 989-996, 2006.

[53] – S. Grinspan and R. Gnanamoorthy, *"Surface modification by oil jet peening in Al alloys, Al 6063-T6 and Al 6061-T4. Part 2: Surface morphology, erosion, and mass loss",* Applied Surface Science, vol. 253, no. 2, pp. 997–1005, 2006.

[54] – Mahr Gmbh, "*Perthometer Surface Texture Parameters*", 1999.

[55] – Y. Kudryavtsev, J. Kleiman, G. Prokopenko, V. Knysh, L. Gimbrede, *"Effect of Ultrasonic Peening on Microhardness and Residual Stress in Materials and Welded Elements"*, International Institute of Welding, IIW Document XIII-2010-04.

[56] – L. L. Martinez, "*Life of FPSO's structural details using ultrasonic peening*", Procedia Engineering, vol. 10, pp. 1059–1068, 2011.

[57] – Y. Kudryavtsev, J. Kleiman, "*Fatigue of Welded Elements: Residual Stresses and Improvement treatments"*, 2004.

[58] – E. Statnikov, "*Physics and Mechanism of Ultrasonic Impact Treatment, International Institute of Welding*", IIW Document XIII-2004-04.

[59] – Y. Togasaki, H. Tsuji, T. Honda, T. Sasaki, and A. Yamaguchi, *"Effect of UIT on Fatigue Life in Web-Gusset Welded Joints",* vol. 4, no. 3, pp. 391–400, 2010.

[60] – E. S. Statnikov, V. O. Muktepavel, A. Blomqvist *"Comparison of Ultrasonic Impact Treatment (UIT) and other Fatigue Life Improvement Methods"*, Welding in the World, vol. 46, no. 3-4, pp. 20–32, 2002.

[61] – Q. Yang, D. Wang, S. Wu, and S. Li, *"Research on the Effect of Ultrasonic Impact Peening on the Fatigue Property of 7075-T651 Aluminum Alloy"* Advanced Materials Research, vol. 295–297, pp. 1896–1900, 2011.

[62] – S. Roy, J. W. Fisher, *"Improving Fatigue Strength of Welded Joints by Ultrasonic Impact Treatment.*

[63] – P. Schaumann and C. Keindorf, "*Enhancing fatigue strength by Ultrasonic Impact Treatment for welded joints of offshore structures*", Third International Conference on Steel and Composite Strutures, p 921-926, Manchester, UK.

[64] – Y. Kudryavtsev, J. Kleiman, A. Lugovskoy, G. Prokopenko, *"Fatigue Life Improvement of Tubular Welded Joints by Ultrasonic Peening"*, International Institute of Welding, IIW Document XIII-2117-06.

[65] – H. Günther, U. Kuhlmann, A. Durr, *"Rehabilitation of Welded Joints by Ultrasonic Impact Treatment (UIT) Ultra Sonic Impact Treatment (UIT)"*, IABSE Symposium, Lisboa, pp. 1–7, 2005.

[66] – G. P. Tilly, P. A. Jackson, S. J. M. Dic, *"Fatigue strengthening of welds in light rail structures"* no. September, Institution of Civil Engineers, Bridge Engineering 163 Issue BE3, pp. 147–152, 2010.

[67] – D. Yin, D. Wang, H. Jing, L. Huo, *"The effects of ultrasonic peening treatment on the ultra-long life fatigue behavior of welded joints"*, Materials and Design, vol. 31, no. 7, pp. 3299–3307, 2010.

[68] – SONATS, acessed on the 15 Jully 2015 at http://www.sonats-et.com/page_17-peening-solutions.html.

[69] – K. Sanada, T. Kakiuchi, Y. Uematsu, K. Hattori, Y. Watanabe, *"Effect of ultrasonic shot peening treatment on fatigue behavior of AZ61 magnesium alloy*", Recent Advances in Structural Integrity Analysis: Proceedings of the International Congress, Sydney, 9-12 Dezembro, p.104-108, 2014.

[70] – Y. M. Xing, J. Lu, *"An experimental study of residual stress induced by ultrasonic shot peening"*, Journal of Materials Processing Technology, vol. 152, no. 1, pp. 56–61, 2004.

[71] – Markovina R., Blagojevic B., Ban D., *"Investigation of Influential Parameters on Shotpeening of Aluminum Alloys"*, 12th International Research/Expert Conference, Istanbul, 26-30 Agosto, pp. 245–248, 2008.

[72] – H. Kumar, S. Singh, P. Kumar, *"Modified Shot Peening Processes - a Review"*, International Journal of Engineering Sciences and Emerging Technologies, vol. 5, no. 1, pp. 3–16, 2013.

[73] – F. Petit-Renaud, *"Optimization of the Shot Peening Parameters",* USF Impact Finishers (Shot Peening Division) and USF Vacu-Blast International, Slough, UK.

[74] – M. Lundberg, R. L. Peng, M. Ahmad, T. Vuoristo, D. Bäckström, S. Johansson, *"Influence of Shot Peening Parameters on Residual Stresses in Flake and Vermicular Cast Irons,* Material Science Forum, vol. 768–769, pp. 534–541, 2013.

[75] – Y. K. Gao, X. R. Wu, "*Experimental investigation and fatigue life prediction for 7475-T7351 aluminum alloy with and without shot peening-induced residual stresses*", Acta Materialia, vol. 59, no. 9, p. 3737–3747, 2011.

[76] – S. Sathyajith, S. Kalainathan, S. Swaroop, *"Laser peening without coating on aluminum alloy Al-6061-T6 using low energy Nd: YAG laser",* Optics and Laser Technologies, vol. 45, no. 1, pp. 389–394, 2013.

[77] – A. Vasu, R. V Grandhi, *"Effects of curved geometry on residual stress in laser peening"*, *Surface and Coating Technology*, vol. 218, pp. 71–79, 2013.

[78] – S. Sathyajith and S. Kalainathan, *"Effect of laser shot peening on precipitation hardened aluminum alloy 6061-T6 using low energy laser", Optics and Lasers in Engineering*, vol. 50, pp. 345–348, 2012.

[79] – Y. K. Gao, *"Improvement of fatigue property in 7050-T7451 aluminum alloy by laser peening and shot peening"*, Materials Science and Engineering A, vol. 528, p. 3823–3828, 2011.

[80] – F. Boud, L. F. Loo, P. K. Kinnell, *"The impact of plain waterjet machining on the surface integrity of aluminium 7475",* Procedia CIRP 13, vol. 13, pp. 382–386, 2014.

CHAPTER 3 – Improvement in fatigue life of Al 7475 T7351 alloy specimens by applying ultrassonic and microshot peening

Published in: International Journal of Fatigue 92, 2016, 87-95

R. Ramos[a], N. Ferreira[b], J.A.M. Ferreira[a], C. Capela[a,b], A.C. Batista[c]

[a] CEMUC, Department of Mechanical Enginnering, University of Coimbra, Rua Luís Reis Santos, 3030-788, Coimbra, Portugal

[b] ESTG, Department of Mechanical Enginnering, Instituto Politécnico de Leiria, Morro do Lena- Alto Vieiro, 2400-901 Leiria, Portugal

[c] CFisUC, Department of Physics, University of Coimbra, 3004-516 Coimbra, Portugal

Abstract

Shot peening and ultrasonic peening are widely used mechanical surface treatment in the automotive and aerospace industries to improve the fatigue life of metallic components. This work aims to further improve the mechanical properties of the Al 7475-T7351 alloy by applying three different peening processes: Ultrasonic Peening (USP) and Microshot Peening with two different beads size (MSP).

A systematic study was carried out on the roughness, surface hardening, residual stress profiles and fatigue life. Uniaxial fatigue tests were conducted. Residual stresses were evaluated by X Ray diffraction, and the fracture surface was observed and analyzed by Scanning Electron Microscope. The microstructures of the specimens were observed by optic microscope. Microhardness and roughness were also measured. All of the surface treatments enhanced the specimens fatigue lives, despite having created different superficial conditions. In addition, the experimental results and analytic predictions according to the Molski-Glinka approach were compared, and in general, agree well.

Keywords: Aluminium Alloys, Ultrasonic Peening, Microshot Peening, Fatigue Life Enhancement.

3.1 Introduction

Aluminium and its alloys are widely used in the aerospace and aeronautical industries due to the high strength-to-weight ratio, good mechanical properties and low densities at relatively good prices. The alloy in study, Al 7475-T7351, is an improved version of another available high strength aerospace aluminium alloys such as 7050 and 7075 alloys [1- 4]. Strengthened aluminium alloys, despite its high tensile strength, have a relatively low fatigue resistance: the fatigue endurance. Since the majority of fatigue cracks initiate on the surface, the conditioning of the surface to resist crack initiation and earlier crack growth is an attractive method of improving fatigue performance. It is well known that tensile residual stresses incorporated in the material and in welded joints decrease tensile load capacity and fatigue strength as well. Thus, several mechanical processes are being studied in order to reduce or even introduce compressive residual stresses on the material surface and deeper layers [5-11]. Shot peening is a widely used mechanical surface treatment to improve the fatigue life of metallic components. The indentation of each impact produces local plastic deformation (increase in hardness) whose expansion is constrained by the adjacent deeper material, given rise to a field of surface compressive stresses. Positive effect of shot peening was proven by many works of researchers [12-14], commonly accredited to the introduction of compression residual stresses in the subsurface layers of the material. The optimum fatigue strength improvement corresponds to a certain Almen intensity, which depends on the properties of the peened alloy. In this work, two different peening processes were used: Ultrasonic Peening and Microshot Peening. Both of them employ and bombard beads, in this case, made of steel, into the material surface in order to induce plastic deformation and increase the material density. This leads to the increase of hardness and strength of the material.

In the case of Microshot Peening, the beads are bombarded into the material surface by a nozzle, and the main process parameters are the beads diameter, process intensity, exposure time, coverage, air pressure, impact angle and nozzle characteristics and all of them can be optimized [15-18]. Like in steels, literature shows that the major part of this improvement can be attributed to the compressive residual stresses in the surface region, which very often overcompensates the worsening of surface morphology [19-23].

In some cases, the shot peening treatment can produce also microstructural transformations. The shot peening in aluminium alloys causes the work hardening that will be responsible for

enhanced resistance to crack initiation, but on the other side, it causes lower crack growth resistance due to material embrittlement. Like this, peening of aluminium alloys, with steel shot used for high-strength steel and titanium alloys, is quite detrimental to fatigue performance. Luo et al. [24] using rough peened surface of 7075-T6 aluminium specimens obtained only an increase of 7% in fatigue life, while, on the contrary, Sharp et al. [20] peening with lighter materials such as glass or ceramic beads decreased the surface roughness and improved significantly the fatigue strength. Benedetti et al. [25] studied the effect of the influence of the peening intensity on the reverse bending fatigue behavior of Al 7075-T651 and discussed accounting for the effects of surface modifications (roughness and strain hardening) and of residual stresses and it relaxation. No significant residual stress relaxation was observed in samples tested to a load levels approaching the high cycle. Summarizing, the parameters of controlled shot peening (CSP) in terms of fatigue damage, are: the surface roughening that accelerates the nucleation and early propagation of cracks, the strain hardening that retards the propagation of cracks, and the residual stress profile that provides crack closure stress reducing the driving force for crack propagation [23].

The Ultrasonic Peening is a technique developed by the company SONATS (Stressonic® technology equipment) and derived from conventional shot peening. The material to be treated is in contact with a chamber that contains the beads inside. These beads are excited by a sonotrode at a frequency of 20 kHz. This process provides a low intensity and multidirectional treatment with low roughness [26-27]. USP produces a number of beneficial effects in metals and alloys. Foremost among these is increasing the resistance of materials to surface-related failures, such as fatigue and stress corrosion cracking. The results of fatigue testing showed that USP is one of the most efficient techniques for increasing the fatigue life of welded elements as compared to such existing improvement treatments as grinding, TIG-dressing, shot peening, hammer peening, etc. Until now, techniques such as shot peening and ultrasonic peening treatment have been studied and applied particularly for fatigue designs of welded structures in order to improvement of its fatigue performances by means induced compressive residual stress [28-31].

The understanding of the improvement in fatigue strength due to surface peening, allowing the effectiveness of the in-service process on components, needs to be better studied in order to allow the development of less conservative designs based on more accurate fatigue life and prediction models. The objective of this paper is to evaluate the shot peening (using two different

bead diameter) and ultrasonic peening influence on the fatigue strength of aluminium 7475-T7351 alloy.

3.2 Materials and Experimental Procedures

3.2.1 Base Material and Specimens

In this research, the 7475-T7351 aluminium alloy was used. This alloy has an optimized precipitate dispersion due to its chemical composition and temper conditions. The alloy was heat treated at 470°C, then water quenching and controlled stretching from 1.5 to 3% followed by artificial aging in two phases: first at 121°C for 25h and second at 163°C in the range of 24–30 h. The chemical composition and the principal mechanical properties of Al 7475-T7351 are given by ALCOA Company and are listed in Table 3.1 and 3.2, respectively.

Table 3.1 – Chemical composition of Al 7475-T T7351 aluminium alloy (wt%), (according to ALCOA).

Si	Fe	Cu	Mn	Mg	Cr	Zn	Ti	Other
0,1	0.12	1.2-1.9	0.06	1.9-2.6	0.18-0.25	5.2-6.2	0.06	0.15

Table 3.2 – Mechanical properties of Al 7475-T T7351 aluminium alloy (according to ALCOA).

Young's modulus [GPa]	71.7
Tensile strength, σ_{uts} [MPa]	490
Yield strength, σ_{ys} [MPa]	414
Elongation, ε_r [%]	9

Specimens were machined with 4mm and 8mm thickness. All the specimens have the same configuration and dimensions, which is shown in Fig. 3.1a), and only differ in thickness. Loading direction coincides with the rolling direction L. The surface treated specimens were peened along a contour with 12 mm width as shows Fig.3.1b).

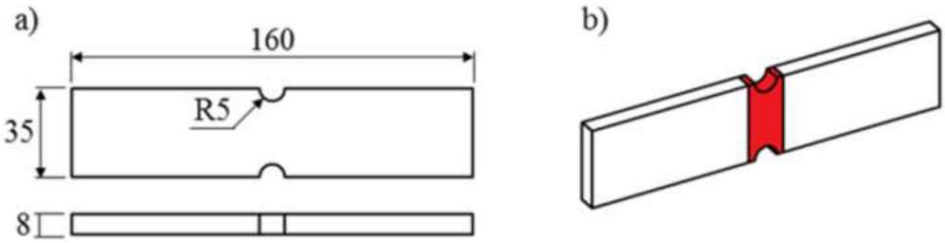

Figure 3.1 – a) Geometry of the 4mm and 8mm thick specimen; b) Schematic view.

3.2.2 Surface Treatments Conditions

In this investigation, three different peening processes were studied: Ultrasonic Peening (USP) and Microshot Peening with two different bead sizes (MSP1 and MSP2). A reference batch of ground and polished specimens was also tested. MSP with two different bead sizes were used in order to relate surface roughness and fatigue strength improvement. Then, the specimens were divided into four series: one series was ground and polished with no further surface treatment, other two series were shot peened in contour region illustrated in Fig. 3.1b), and finally, one series with the region illustrated in Fig. 3.1b) ultrasonic peened after ground and polished. Shot peening was done in OGMA – Indústria Aeronáutica de Portugal S.A., in a SURFATEC machine, using an Almen strip type A. Table 3.3 summarizes the processing parameters. The batch of surface USP specimens was manufactured by SONATS ultrasonic peening technology in Carquefou, France, using an Almen intensity of F20A. Table 3.4 summarizes the processing parameters.

Table 3.3 – Microshot peening processing parameters.

Treatment	Diameter of bead [mm]	Material	Pressure [bar]	Coverage [%]	Almen Intensity [mmA]	Impact Angle
MSP1	0.43	Steel	2.2	200	0.0074	90°
MSP2	0.28	Steel	2.4	200	0.0077	90°

Table 3.4 – Ultrasonic peening processing parameters.

Treatment	Diameter of bead [mm]	Material	Sonotrode Frequency [kHz]	Impact Angle
USP	From 1 to 2	Steel	20	Multidirection

3.2.3 Fatigue Testing

Fatigue tests were carried out in an Instron servo-hydraulic machine, applying a sinusoidal load wave, using a frequency of 20–30 Hz, depending upon the stress level, and stress ratio of R= 0 and R=-1. The load amplitude and mean load, required as input data for fatigue tests, were calculated taking into account the values of the nominal stresses, calculated at holed sections, according to the Eq. (3.1):

$$\sigma_a = \frac{P_a}{WxB} \tag{3.1}$$

where σ_a is the stress amplitude, P_a is the axial load amplitude, B is the thickness and W the width of the specimen in holed section.

Fatigue results were plotted as S–N curves, presenting the stress amplitude against the number of cycles to failure. Table 3.5 summarizes the fatigue tests conditions performed into the present work.

Table 3.5 – Parameters of fatigue test series.

Group	Treatment	Thickness [mm]	Stress ratio R
1	Base material	4	0
2	Base material	8	0
3	Base material	8	-1
4	USP	4	0
5	USP	8	0
6	USP	8	-1
7	MSP1	8	-1
8	MSP2	8	-1

3.2.4 Microstructure, Roughness, Hardness, Residual Stresses Testing and Fracture Analysis

One specimen of each type of treated sample (USP, MSP1 and MSP2) was cut through the minimal cross section. Afterwards, the cut surfaces were gradually polished with smaller granulometry silicon carbide papers, and at the end diamond particles with a 1 μm diameter were used until it became a mirror-like surface. Then, those surfaces were etched with Keller reagent (2,5% HNO_3; 1,5% HCl; 1% HF; 95% H_2O [volume]). The optical microscope Leica DM 4000 M LED was used to photograph the etched surfaces.

The roughness evaluation was carried out according to DIN EN ISO 4288 standard using the Surftest SJ-500 Mitutoyo surface roughness measuring system. The parameters evaluated for each superficial treatment were: roughness average R_a, root mean square (RMS) roughness R_q and mean roughness depth R_z.

Vickers hardness testing was performed according to ASTM E384-99 in the surfaces photographed before using a Struers Duramin 1 microhardness tester with a 0.1 Kg load for 15 seconds. As shown in Fig. 3.2, the following measurement lines/surfaces were made: longitudinal surface, longitudinal mean line, notch surface and transversal mean line. All these parameters are constituted by various indentations (or punctual values of microhardness) which were spaced 0.5 mm from each other. Then, the averages of those parameters were calculated. Longitudinal and notch surface measurements were collected along a line 0,05 mm from the plate surface as suggested by cited standard.

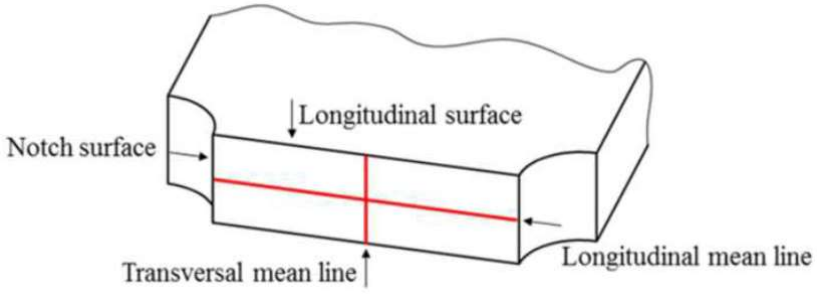

Figure 3.2 – Schematic view of the hardness measurement.

Residual stress analysis was performed by X-ray diffraction using a Proto iXRD equipment. Lattice deformations of the {222} diffraction planes were measured using Cr-Kα X-ray radiation.

The stress was evaluated with an elliptical regression of sin2ψ data and the X-ray elastic constants values of 18.56×10-6 MPa-1 for (1/2) ·S_2 and -4.79×10-6 MPa-1 for S_1. For the analyzed material and considering the radiation used, the average penetration depth of the X-rays was about 11 μm. Measurements were made for all studied treatments at 4 points along the surface of one specimen. Such points were: one point for each longitudinal surface and one point for each notch surface in the central position, as shows in Fig 3.3. The analysis of the in-depth evolution of the residual stresses in the longitudinal surface was performed by X-Ray diffraction, after successive layer removal by electro polishing.

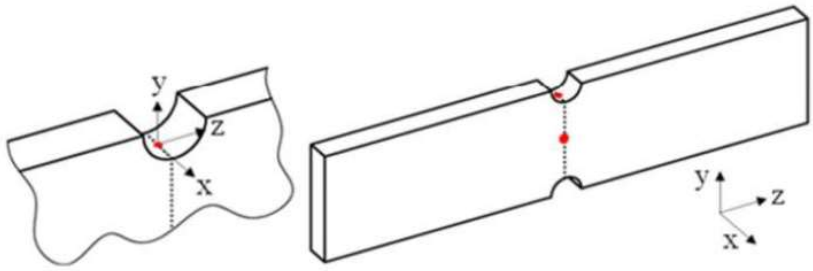

Figure 3.3 – Schematic view of the residual stresses measurement sites.

Finally, the fracture surface analysis was performed with a scanning electron microscope (Philips XL30).

3.3 Results

3.3.1 Microstructure

The microstructure after USP is presented in Fig. 3.4 and shows good surface finish. The upper layer of the longitudinal surface, until approximately 50 μm, suggests that the grain is compressed and that the phenomenon of grain refinement is not perfectly clear. In the deeper layers below the surface (from 250 μm), the microstructure consists of grains elongated in the rolling direction, and it can be considered the base material microstructure. On the other hand, the surface finish of the specimen treated by MSP1 (Fig. 3.5) is worse than USP and a slight grain refinement can be seen close to the surface. Severe defects acquired by the specimens' fillet were noticed. The specimen treated by MSP2 (the smallest sphere used) displays a very similar

appearance as MSP1, while MSP2 shows a slight worse one. The deformation lines due to plastic deformation are the most accentuated.

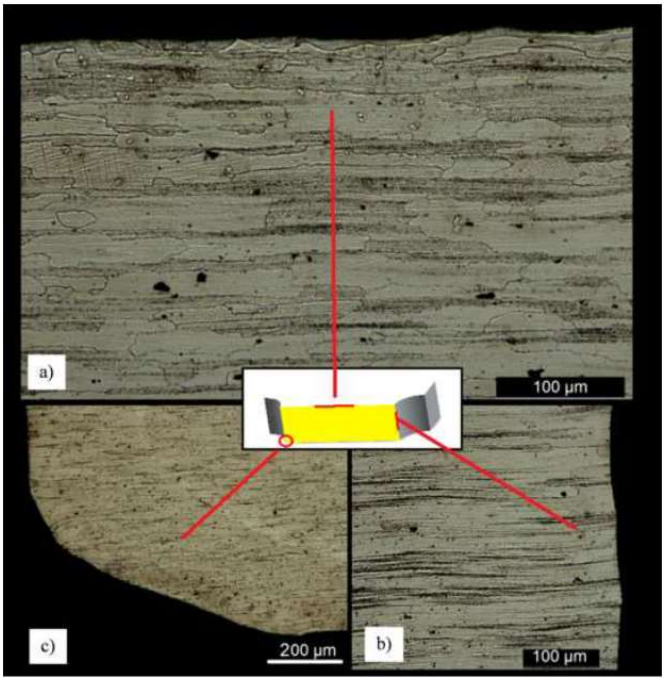

Figure 3.4 – Microstructure on a USP specimen: a) Longitudinal surface; b) Notch surface; c) Fillet.

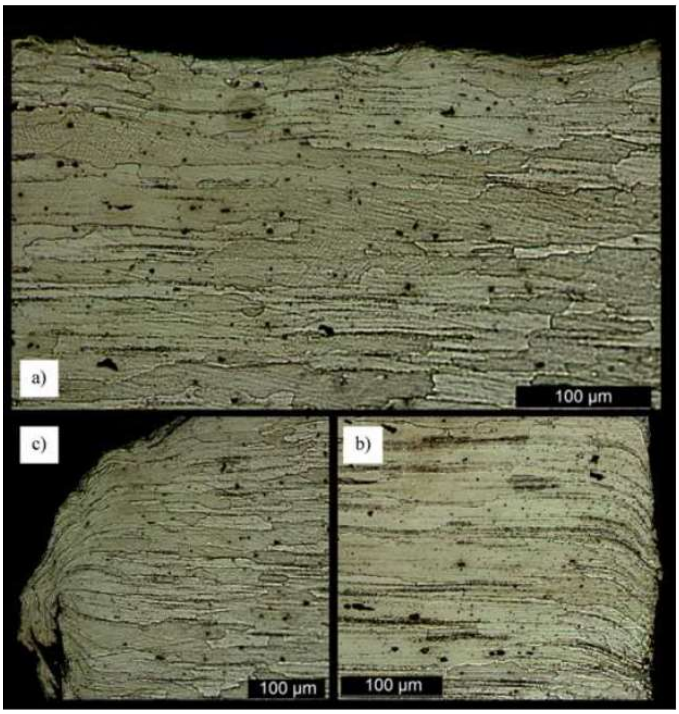

Figure 3.5 – Microstructure on a MSP1 specimen: a) Longitudinal surface; b) Notch surface; c) Fillet.

3.3.2 Roughness

As noticed in 3.1, the roughness values created by the superficial treatments follow the same trend demonstrated in Table 3.6: USP produces the lowest values of surface roughness, whereas MSP2 produces the highest values. In fact, this can be mainly explained by the diameter of the bead used in each treatment. This is because, if the contact area of the bead increases, impact intensity reduces and therefore roughness reduces as well.

Table 3.6 – Roughness values of all treatments.

Treatment	R_a ± standard deviation [µm]	R_q ± standard deviation [µm]	R_z ± standard deviation [µm]
Base Material	1.22±0.02	1.50±0.02	7.74±0.13
USP	2.46±0.15	3.05±0.19	14.80±0.96
MSP1	3.70±0.17	4.60±0.01	23.50±2.00
MSP2	4.01±0.32	5.01±0.36	26.41±2.01

3.3.3 Hardness

Hardness results of all treatments according to Fig.3.2 are shown in Table 3.7. This table shows that all treatments, in longitudinal and notch surface, slightly increased the hardness in comparison with the Base Material (BM) due to the cold work and the ensuing plastic deformation induced by the beads impacts. More precisely, the longitudinal surface displays a higher value than notch surface for all treatments. That could be related to the shape of the treated material: flat shapes seem to be more treatable than curved shapes due to the beads impacts.

Table 3.7 – Hardness values of all treatments.

BM Hardness [$Hv_{0.1}$] 156,84±3,96			
	USP	**MSP1**	**MSP2**
Longitudinal Surface	161.02±5.97	166.63±4.77	163.86±7.20
Notch surface	159.20±4.61	162.13±6.31	161.73±3.36
Longitudinal Mean Line	157.54±3.67	157.68±4.29	156.72±5.23
Transversal Mean Line	157.56±5.91	160.13±4.90	156.81±5.31

It is worthwhile to notice that, in both surfaces, the hardness imposed by the treatments appears in the same order: USP exhibits the less improvement, whereas MSP1 has the better one. MSP2 displays intermediate values.

3.3.4 Residual Stresses

The residual stresses measurements were carried out as explained in Fig. 3.3. Indepth distributions of residual stresses in the longitudinal surface are shown in Fig.3.6.

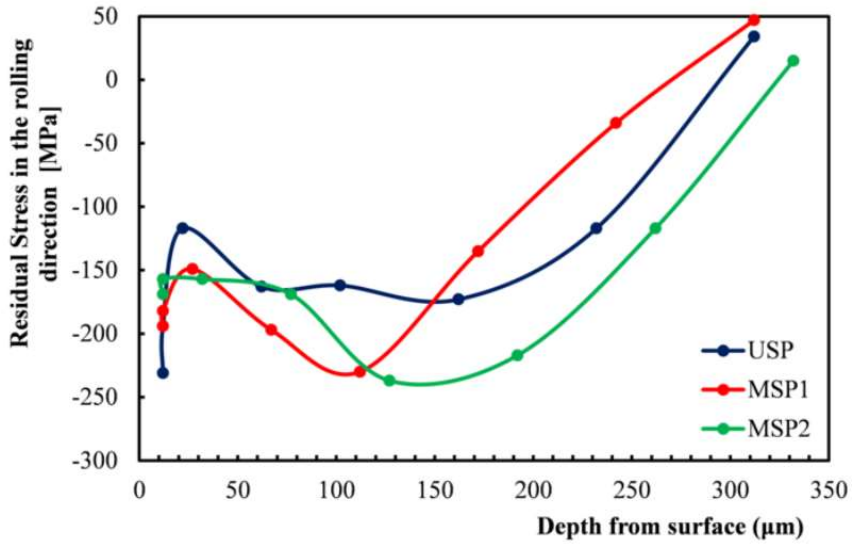

Figure 3.6 – In-depth residual stress distribuitions in the longitudinal.

All surface treatments increased the residual stress on the surface layer (which is the first measurable layer by X-Ray diffraction at a depth of 11 µm from the plate surface, due to X-Ray penetration. As displayed in Table 3.8, USP treatment shows the higher residual stress on the surface layer with an average of -253 MPa, followed by MSP1 with a value of -174 MPa, and finally, MSP2 with -164 MPa. Thus, higher values of compressive residual stresses on the surface layer and lower values of roughness are produced by higher values of bead diameters.

Table 3.8 – Residual stress values on the surface.

Treatment	Surface	Real measurement depth [μm]	Residual stress [MPa]	Average [MPa]
USP	notch 1	11	-273	**-253**
	notch 2	11	-313	
	face 2	11	-231	
	face 1	11	-194	
MSP1	notch 1	11	-167	**-174**
	notch 2	11	-153	
	face 2	11	-194	
	face 1	11	-182	
MSP2	notch 1	11	-172	**-164**
	notch 2	11	-159	
	face 2	11	-169	
	face 1	11	-157	

USP treatment shows a minimum compressive stress of -117 MPa at 20 μm, which can be explained by the formation of a very thin compressed layer on the surface. It can also be concluded from Fig. 3.8 that the depth where the maximum of compressive residual stress is obtained varies according to bead diameter: larger diameters (USP) produce their maximum on the surface, intermediate diameters (MSP1) produce their maximum on the subsurface layer (from 50 μm to 100 μm). Finally, MSP2 exhibits the deeper and higher maximum compressive residual stress (from 130 μm).

3.3.5 Fatigue Tests Results

The Fig. 3.7 compares the S-N curves for USP series with different thicknesses (4 and 8 mm) tested at R=0. Despite similar behaviors, the 8 mm USP series is plotted slightly above the 4 mm series in the high-cycle region ($N>10^6$). The fatigue strength improvement in percentage (FSIP) was calculated by Eq. (3.2):

$$FSIP = \left(\frac{\sigma_{modified}}{\sigma_{baseline}} - 1\right) \text{x } 100\% \quad (3.2)$$

where $\sigma_{modified}$ and $\sigma_{baseline}$ are the stresses associated to a given fatigue life of one testing batch and the reference S-N curve, respectively.

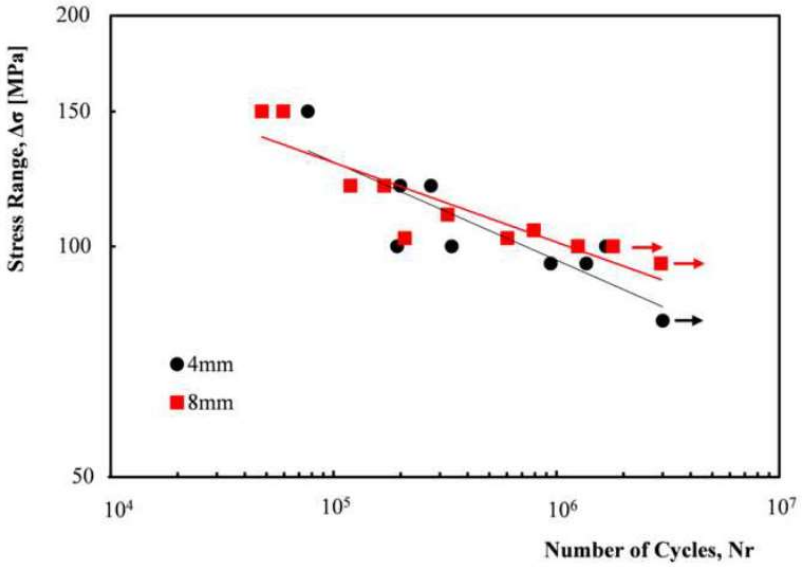

Figure 3.7 – S-N Curves on USP; 4 and 8 mm thickness, R=0.

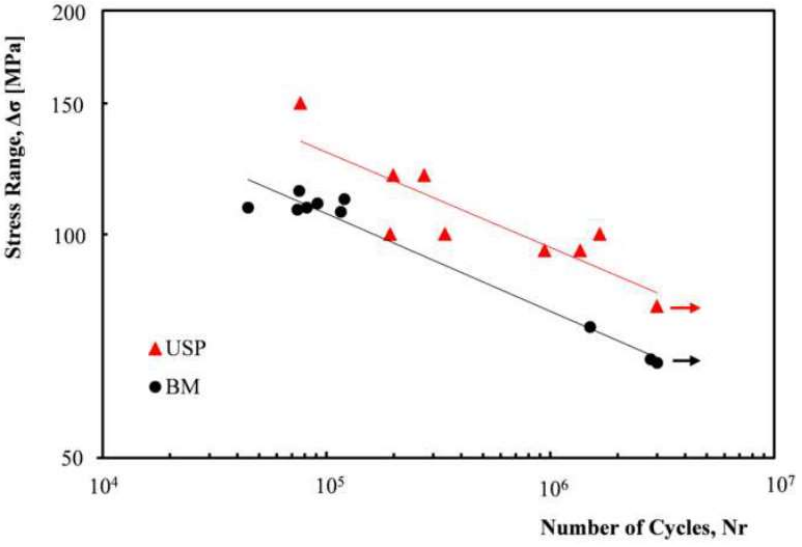

Figure 3.8 – S-N Curves on BM and USP; 4 mm thickness, R=0.

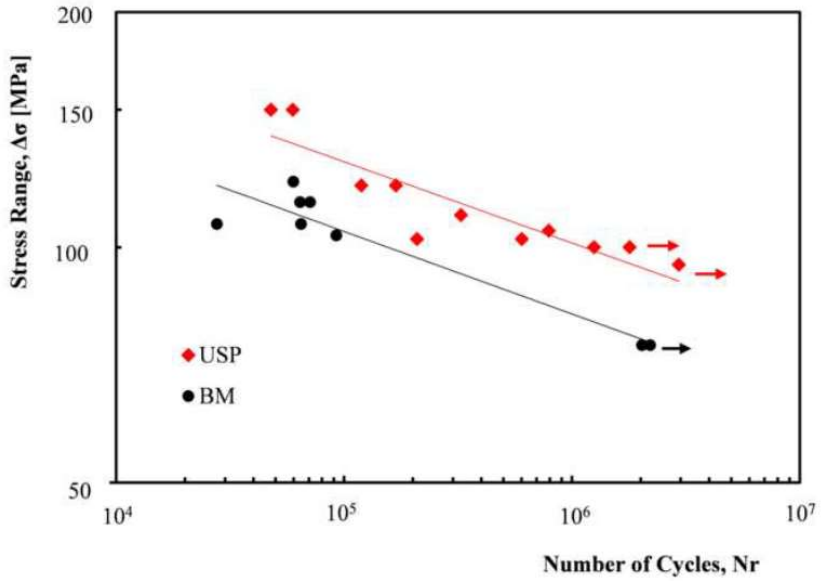

Figure 3.9 – S-N Curves on BM and USP; 8 mm thickness, R=0.

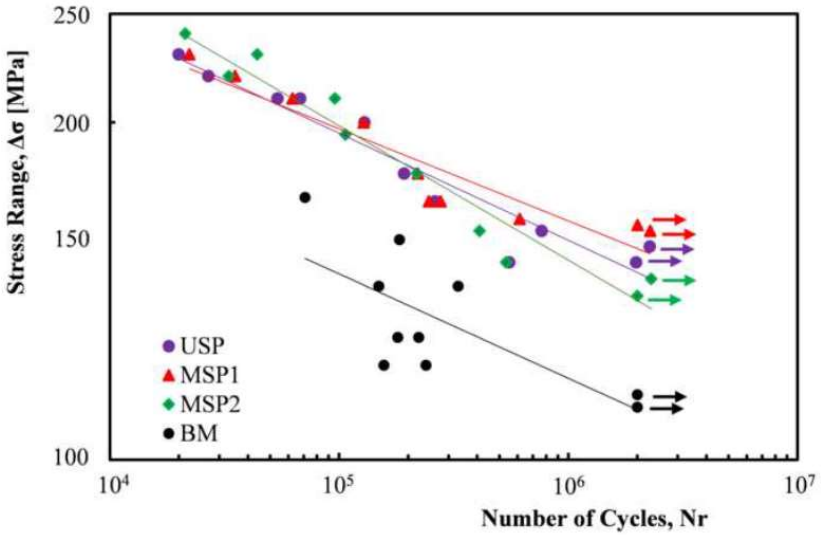

Figure 3.10 – S-N Curves; 8 mm thickness, R=-1.

The S-N curves were fitted using the Basquin´s law, Eq. (3.3):

$$\sigma_a = \sigma'_f \, \mathrm{x} \, \left(N_f\right)^b \tag{3.3}$$

Series of 8 mm thickness, as indicated in Table 3.9, shows a performance about 7% higher than the 4 mm series, which can be associated with a larger propagation region. Moreover, the m

value (obtained from the exponent of the Basquin function [b= -1/m]) for 8 mm is higher than for the 4 mm series, which implies that the crack initiation had been retarded.

Table 3.9 – Analysis of the S-N Curves of USP, 4 and 8mm thickness.

	σ'_f **[MPa]**	**b**	**Improvement [%]** (in relation to 4mm USP for $2x10^6$ cycles)
4 mm	562.51	-0.128	-
8 mm	425.79	-0.104	7.2

For specimens of 4 mm and 8 mm thickness treated by USP, with R=0, USP series are plotted above BM (Fig. 3.8 and 3.9), and the FSIP ranges from 21.4% to 23.9 % (Table 3.10).

Table 3.10 – Analysis of the S-N Curves of USP, 4 and 8mm thickness.

		σ'_f **[MPa]**	**b**	**Improvement [%]** (in relation to BM for 10^6 cycles)
4 mm	BM	483.02	-0.131	-
	USP	562.51	-0.128	21.4
8 mm	BM	353.52	-0.106	-
	USP	425.79	-0.104	23.9

Table 3.11 – Analysis of the S-N Curves of all treatments, 8mm thickness.

	σ'_f **[MPa]**	**b**	**Improvement [%]** (in relation to BM for 10^5 cycles)	**Improvement [%]** (in relation to MSP2 for $2x10^6$ cycles)
BM	428.27	-0.093	-	-
USP	586.58	-0.095	34	6.8
MSP1	508.45	-0.082	35	11.8
MSP2	789.04	-0.12	35	-

For the fatigue tests at R=-1, all superficial treatments increased approximately 35% of fatigue strength for 100000 cycles in relation to BM (Fig. 3.10). Furthermore, the treatments show slightly different behaviors in different regions of fatigue life. As demonstrated in Table 3.11, MSP2 induces a performance 6.5% better than MSP1 in the low-cycle region ($N=2x10^4$cycles), whereas, in the high-cycle region, MSP1 induces a performance 11.8% better than MSP2. In both regions, USP assumes an intermediate performance between MSP1 and MSP2.

3.3.6 Fracture Surfaces

The fracture surface analysis showed that the crack initiated on the specimens surface, in all treatments and specimens, and propagated through the cross section. It was observed that the crack growth occurred under two types. In the first one, under low nominal stress range (Fig. 3.11a)), the micro cracks initiated along the surface plate in distinct points; they micro nucleated (stage I), and then gradually joined at a certain depth where the crack started to propagate (stage II). In the other case, under high nominal stress range, due to the low number of cycles, the cracks propagated from the surface plate, as shown in Fig 3.11b). In both cases, the propagation zone displays large radial striations, which characterizes the ductile fracture with plastic deformation.

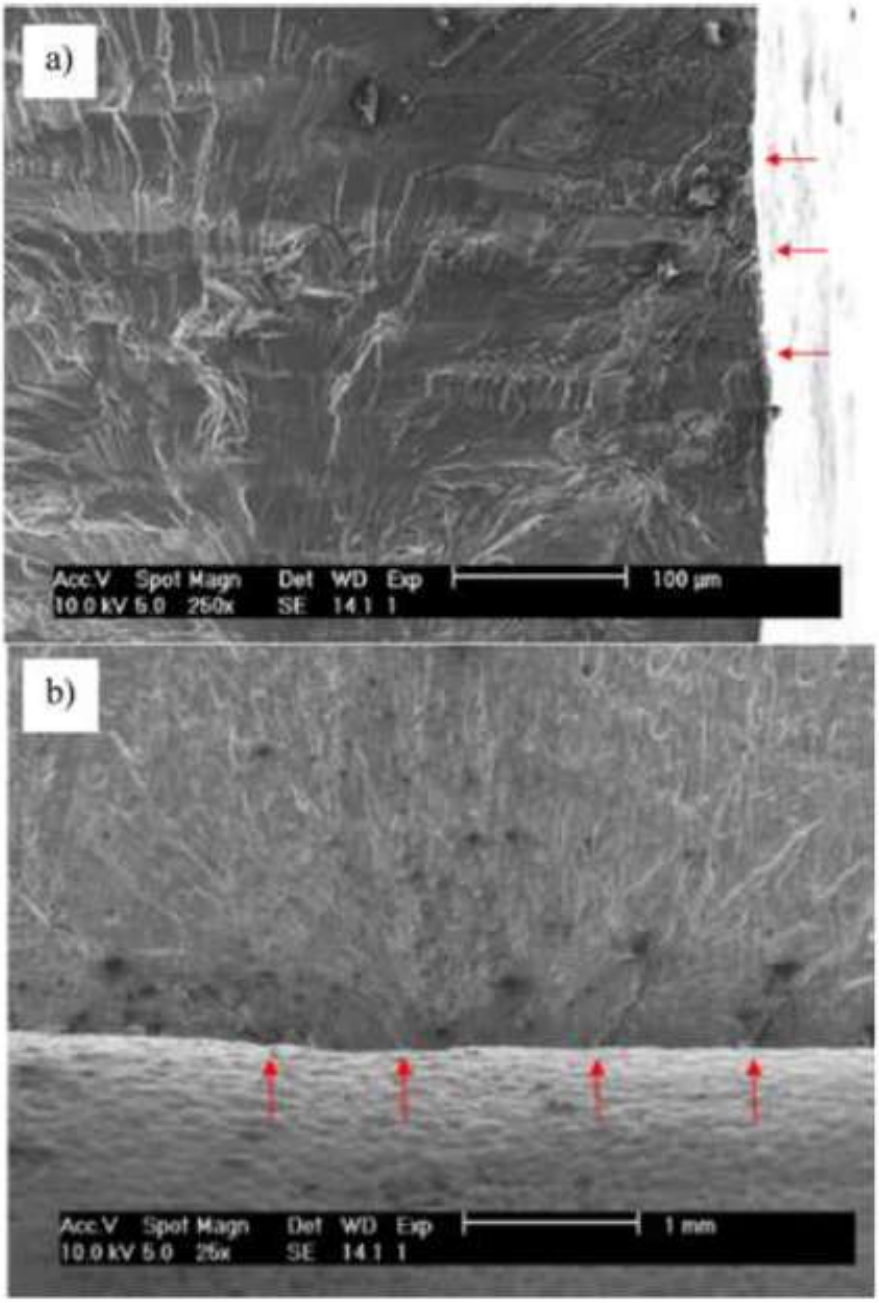

Figure 3.11 – SEM images of fracture surfaces, USP treatment: a) Crack growth under low nominal stress range; b) Crack growth under high nominal stress range.

3.4 Results Discussion

Taking into account Fig. 3.6, the order of the higher and deeper values of compressive stresses induced by the treatments (in ascending order: MSP1, USP, MSP2) is inversely

correlated to the performance order in the high-cycle region shown in Fig. 3.10. Thus, this fact suggests that, in the high-cycle region, higher and deeper compressive stresses are not so relevant and that the process zone is the surface where fatigue cracks nucleate and grow. Thereby, MSP2 exhibits the lowest performance in this region because it has the highest value of roughness and the lowest compressive stress on the surface. Although USP displays the better surface finish and the highest compressive residual stress, USP has a very low value of residual stress on the subsurface layer, whereas this is where MSP1 possesses the highest microhardness and compressive residual stress, which prevent the cracks growth.

In addition to this, analytic predictions according to the Molski-Glinka approach (Eq. (3.4)) were made. The main objective of the whole process consists in the comparison of the experimental life obtained in the fatigue tests with the predicted life. This predicted life can be calculated in tree steps, as follows: first, to the same nominal stress range ΔS previously used on the fatigue tests (which led to the specimens failure), the maximum local stress σ_{max} was calculated using the Molski-Glinka function (Eq. (3.4)). Second, these different values of σ_{max} (to each experimental ΔS) can be introduced in Eq. (3.5), the Ramberg-Osgood function, in order to deduce a certain elongation range, $\Delta\varepsilon$.

$$\Delta S = 2\sqrt{\left\{\frac{2E}{K_t^2}\left[\frac{{\sigma_{max}}^2}{2E} + \frac{\sigma_{max}}{(n'+1)}\left(\frac{\sigma_{max}}{K'}\right)^{\frac{1}{n'}}\right]\right\}} \tag{3.4}$$

where n' is the cyclic hardening exponent and assumes the value of 0.08 [32]; K_t, the stress concentration factor, which was calculated using the Peterson's analytic expression for a tension strip with opposite semicircular edge notches and has the value of 2.1648.

$$\frac{\Delta\varepsilon}{2} = \frac{\sigma_{max}}{E} + \left(\frac{\sigma_{max}}{K'}\right)^{\frac{1}{n'}} \tag{3.5}$$

The parameter K' is the cyclic hardening coefficient and can be deduced by Eq. (3.6):

$$K' = \frac{\sigma'_f}{(\varepsilon'_f)^{n'}} = 875.6 \text{ MPa} \tag{3.6}$$

where σ'_f and ε'_f are the fatigue strength coefficient (983 MPa) and the fatigue ductility coefficient (4.246), respectively. These two values are securely assumed from the Al 7475-T761

alloy, which is an alloy with the same chemical composition of the alloy here in study, and the temper only differs residually [33].

Lastly, using these values and according to the Morrow function (Eq. (3.7)), it is possible to calculate the predicted life, N_p.

$$\frac{\Delta\varepsilon}{2} = \frac{\sigma'_f - \sigma_{Res.\ Stress}}{E}\left(2N_p\right)^b + \varepsilon'_f\left(2N_p\right)^c \tag{3.7}$$

where b and c are the fatigue strength exponent and the fatigue ductility exponent, respectively, and can be calculated by Eq. (3.8) and (3.9):

$$b = -\frac{n'}{1-5n'} = 0{,}1333 \tag{3.8}$$

$$c = -\frac{b}{n'} = 1{,}6663 \tag{3.9}$$

Moreover, the averages of each residual stress profile shown in Fig. 3.6 were also measured until the depth of 150 μm. This depth value was assumed from the typical values of the characteristic distance of the pre-fracture (process) zone, d^*, found by Ostash *et al* [34] for aluminium alloys. Afterwards, these obtained residual stress values of each treatment were applied in Eq. (3.7) as $\sigma_{Res.\ Stress}$.

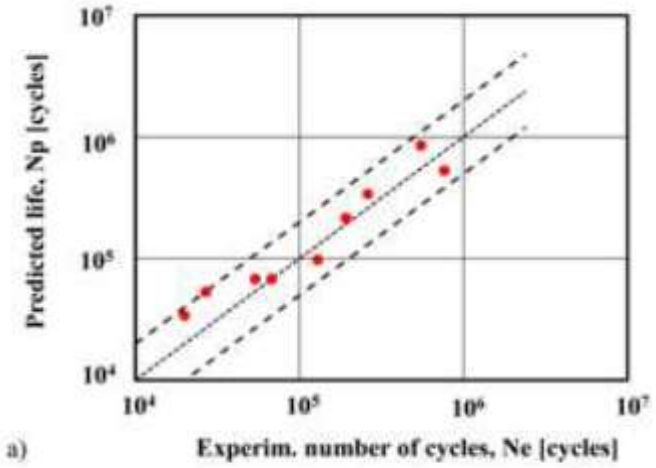

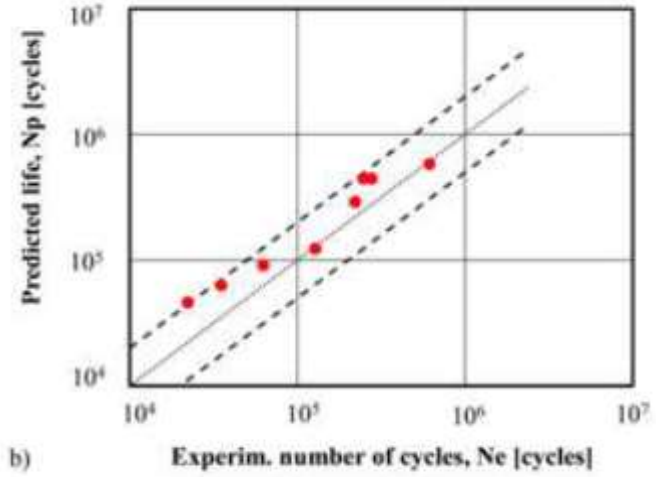

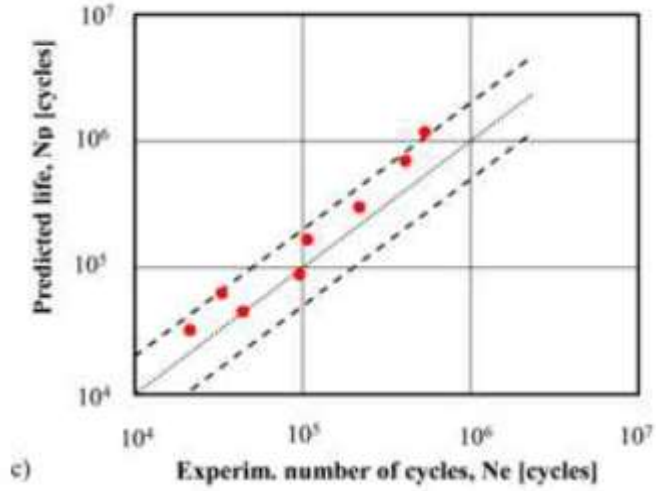

Figure 3.12 – Comparison between predicted fatigue lives: a) USP, R=-1; b) MSP1, R=-1; c) MSP2, R=-1.

Figs 3.12a), b) and c) present, for each treatment, the comparisons between predicted fatigue lives, N_p, obtained with the above-mentioned method with experimental lives, N_e. Experimental fatigue lives were monitored until the specimen's failure. In order to have a criterion of prediction exactness, two straight lines N_p=2N_f and N_p=0.5N_f were also plotted and used as limits. In general, for all treatments, the predictions agree well to the experimental results since the points are mainly between the two straight lines.

In Fig 3.13, the overlapping of the USP SEM images with the USP residual stresses profile is shown, which indicates that micro cracks grow slowly (stage I) until the depth where the residual stress is near zero, and then, with unfavorable residual stresses, the propagation (macrocracks) starts (stage II).

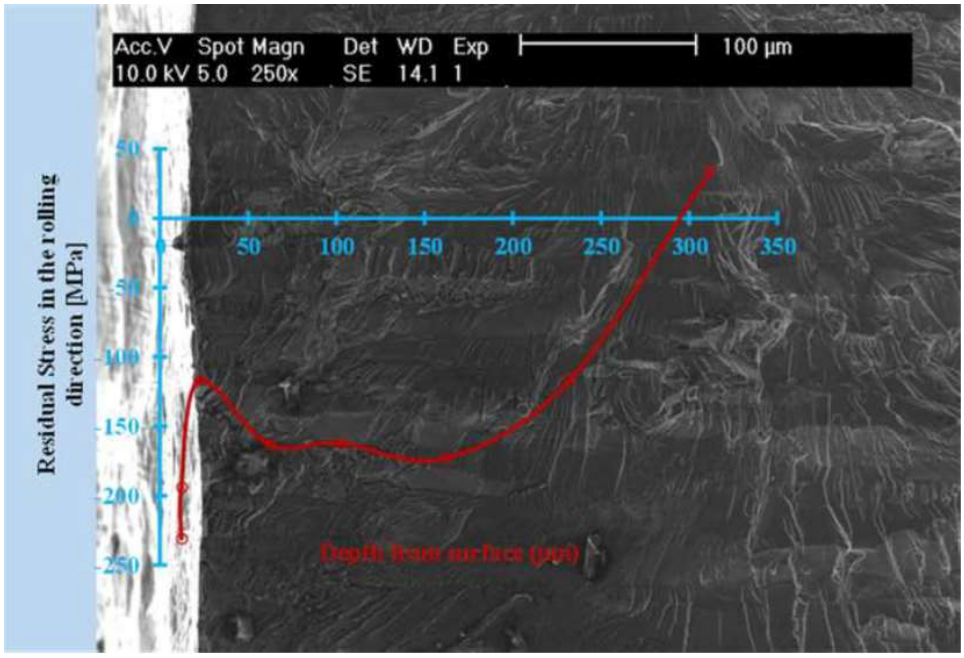

Figure 3.13 – Overlapping of the USP SEM images with the USP residual stresses profile.

.

3.5 Conclusions

This work was focused in the study of the effect of the shot peening and ultrasonic peening on the fatigue strength of the aluminium 7475-T7351 alloy. The main conclusions are:

- USP promotes better surface finish and lower roughness values than MSP. All three surface peening operations slightly increased the Base Material surface hardness, in ascending order: USP, MSP2 and MSP1;
- All he three surface peening were able to improve fatigue life. For 4 mm and 8 mm thickness USP specimens, the improvement on fatigue strength at R=0, to one million of cycles, was ranged from 21.4% to 23.9 %. For the test at R=-1, higher fatigue life enhancement was attained. For 10^5 cycles, all treatments increased fatigue strength in about 35% in comparison with BM;
- Micro nucleation was observed in general cases and particularly for low nominal stress;
- Analytic predictions according to the Molski-Glinka approach related well to the experimental results.

3.6 Acknowledgements

The authors would like to acknowledge OGMA-Indústria Aeronáutica de Portugal, Alverca, Portugal, and also Dr. Ana Guimarães and Engr. João Miranda for the cooperation in the supply of materials and samples used in this project and shot peening processing.

3.7 References

[1] – A. Heinz, A. Haszler, C. Keidel, S. Moldenhauer, R. Benedictus, and W. Miller, "*Recent development in aluminium alloys for aerospace applications*", Mater. Sci. Eng. A, vol. 280, no. 1, pp. 102–107, 2000.

[2] – B. B. Verma, J. D. Atkinson, and M. Kumar, "*Study of fatigue behaviour of 7475 aluminium alloy*", Bull. Mater. Sci., vol. 24, no. 2, pp. 231–236, 2001.

[3] – C. Y. Kim, J. M. Choi, and J. H. Song, "*Fatigue crack growth and closure behavior under random loadings in 7475-T7351 aluminum alloy*", Int. J. Fatigue, vol. 47, pp. 196–204, 2013.

[4] – K. Alrubaie, E. Barroso, and L. Godefroid, "*Fatigue crack growth analysis of pre-strained 7475–T7351 aluminum alloy*", Int. J. Fatigue, vol. 28, no. 8, pp. 934–942, 2006.

[5] – A. Abdullah, M. Malaki, and A. Eskandari, "*Strength enhancement of the welded structures by ultrasonic peening*", Mater. Des., vol. 38, pp. 7–18, 2012.

[6] – E. S. Statnikov and V. N. Vityazev, "*Physics and mechanism of ultrasonic impact*", Ultrasonics, vol. 44, pp. 533–538, 2006.

[7] – Y. Togasaki, H. Tsuji, T. Honda, T. Sasaki, and A. Yamaguchi, "*Effect of UIT on Fatigue Life in Web-Gusset Welded Joints*", Journal of Solid Mechanical and Material Engineering, vol. 4, no. 3, pp. 391–400, 2010.

[8] – S. Sathyajith, S. Kalainathan, and S. Swaroop, "*Laser peening without coating on aluminum alloy Al-6061-T6 using low energy Nd: YAG laser*", Opt. Laser Technol., vol. 45, no. 1, pp. 389–394, 2013.

[9] – F. Boud, L. F. Loo, and P. K. Kinnell, "*The impact of plain waterjet machining on the surface integrity of aluminium 7475*", Procedia CIRP, vol. 13, pp. 382–386, 2014.

[10] – A. S. Grinspan and R. Gnanamoorthy, "*Surface modification by oil jet peening in Al alloys, Al 6063-T6 and Al 6061-T4: Residual stress and Hardness*," Appl. Surf. Sci., vol. 253, no. 2, pp. 997–1005, 2006.

[11] – A. S. Grinspan and R. Gnanamoorthy, "*Surface modification by oil jet peening in Al alloys, Al 6063-T6 and Al 6061-T4. Part 2: Surface morphology, erosion, and mass loss*", Appl. Surf. Sci., vol. 253, no. 2, pp. 997–1005, 2006.

[12] – K. Miková, S. Bagherifard, O. Bokůvka, M. Guagliano, L. Trško, "*Fatigue behavior of X70 microalloyed steel after severe shot peening*", Int. J. Fatigue. 55 (2013) 33-42.

[13] – S. Bagherifard, M. Guagliano, "*Fatigue behavior of a low alloy steel with nanostructured surface obtained by severe shot peening*", Eng. Fract. Mech. 81 (2012) 56-68.

[14] – P. Zhang, J. Lindemann, L. Leyens, "*Shot peening on the high-strength magnesium alloy AZ80 - effect of peening media*", J. Mater. Process. Technol. 210 (2010) 445-450.

[15] – D. Ban, R. Markovina, B. Blagojevic, "*Investigation of Influential Parameters on Shotpeening of Aluminum Alloys*", 12th International Research/Expert Conference, Istanbul, 26-30 August, pp. 245–248, 2008.

[16] – H. Kumar, S. Singh, and P. Kumar, "*Modified Shot Peening Processes – A Review*", Int. J. Eng. Sci. Emerg. Technol., vol. 5, no. 1, pp. 12–19, 2013.

[17] – F. Petit-Renaud, "*Optimization of the Shot Peening Parameters*," Int. Conf. Shot Peen., 2002.

[18] – M. Lundberg, R. L. Peng, M. Ahmad, T. Vuoristo, D. Bäckström, and S. Johansson, "*Influence of Shot Peening Parameters on Residual Stresses in Flake and Vermicular Cast Irons*," Mater. Sci. Forum, vol. 768–769, pp. 534–541, 2013.

[19] – Mutoh Y, Fair GH, Noble B, Waterhouse RB., "*The effect of residual stresses induced by shot peening on fatigue crack propagation in two high strength aluminium alloys*", Fatigue Fract Eng Mater Struct 1987;10(4):261–72.

[20] – Sharp PK, Clayton JQ, Clark G., "*The fatigue resistance of peened 7050-T7451 aluminium alloy-repair and retreatment of a component surface*", Fatigue Fract Eng Mater Struct 1994;17(3):243–52.

[21] – Wagner L., "*Mechanical surface treatments on titanium, aluminum and magnesium alloy*", Mater Sci Eng 1999; A263:210–6.

[22] – Benedetti M, Bortolamedi T, Fontanari V, Frendo F., "*Bending fatigue behavior of differently shot peened Al 6082 T5 alloy*", Int J Fatigue 2004; 26:889–97.

[23] – Turnbull A, de los Rios ER, Tait RB, Laurant C, Boabaid JS., "*Improving the fatigue resistance of wasp alloy by shot peening*", Fatigue Fract Eng Mater Struct 1998; 21:1513–24.

[24] – Luo W, Noble B, Waterhouse RB., "*The effect of shot peening intensity on the fatigue and fretting behaviour of an aluminium alloy*", In: Niku-Lari A, editor. Advances in surface treatments, vol. 2. Oxford: Pregamon Press; 1988. p. 145–153.

[25] – Benedetti, V. Fontanari, P. Scardi, C.L.A. Ricardo, M. Bandini., "*Reverse bending fatigue of shot peened 7075-T651 aluminium alloy: The role of residual stress relaxation*", International Journal of Fatigue 31 (2009) 1225–1236.

[26] – K. Sanada, T. Kakiuchi, Y. Uematsu, K. Hattori, and Y. Watanabe, "*Effect of ultrasonic shot peening treatment on fatigue behavior of AZ61 magnesium alloy", Conference Proceedings,* Sydney*, 9-12 December,* Woodhead Publishing Limited, 2014.

[27] – Y. M. Xing and J. Lu, "*An experimental study of residual stress induced by ultrasonic shot peening*", J. Mater. Process. Technol., vol. 152, no. 1, pp. 56–61, 2004.

[28] – Janosch JJ, Koneczny H, Debiez S, Statnikov EC, Troufiakov VJ, Mikhee PP., "*Improvement of fatigue strength in welded joints (in HSS [High strength stell] and in aluminum alloys) by ultrasonic hammer peening*", Welding in the World, 1996; 37(2): 72-83.

[29] – Lixing Huo, Dongpo Wang, Yufeng Zhang, "*Investigation of the fatigue behaviour of the welded joints treated by TIG dressing and ultrasonic peening under variable-amplitude load*", International Journal of Fatigue 27 (2005) 95–101.

[30] – Wang Ting, Wang Dongpo, Huo Lixing, Zhang Yufeng, "*Discussion on fatigue design of welded joints enhanced by ultrasonic peening treatment (UPT)*", International Journal of Fatigue 31 (2009) 644–650.

[31] – Roy Sougata, Fisher John W, Yen Ben T, "*Fatigue resistance of welded details enhanced by ultrasonic impact treatment (UIT)*", Int J Fatigue 2003; 25:1239–47.

[32] – A. Berkovits, "*Variation of the cyclic strain- hardening exponent in advanced aluminium alloys*," Int. J. Fatigue, vol. 4, no. 4, pp. 229–232, 1987.

[33] – ASM Handbook Fatigue and Fracture, ASM International - The Materials Information Society, Volume 19.

[34] – O. P. Ostash, V.V. Panasyuk, "*Fatigue process zone at notches*", *Int. J. Fatigue* 23 (2001) 627-636.

CHAPTER 4 – Effect of Shot Peening and Stress Ratio on the fatigue Crack Propagation of Al 7475 T7351 alloy specimens

Published in: Applied Sciences, 2018, 375, doi:10.3390/app8030375

N. Ferreira[1], P.V. Antunes[1], J.A. Ferreira[1], J.D. Costa[1] and C. Capela[2]

[1] CEMUC, Department of Mechanical Enginnering, University of Coimbra, Rua Luís Reis Santos, 3030-788, Coimbra, Portugal.

[2] ESTG, Department of Mechanical Enginnering, Instituto Politécnico de Leiria, Morro do Lena- Alto Vieiro, 2400-901 Leiria, Portugal

Abstract

Shot peening is an attractive technique for fatigue enhanced performance of metallic components, because it increases fatigue crack initiation life prevention and retards early crack growth. Engineering design based on fatigue crack propagation predictions applying the principles of fracture mechanics is commonly used in aluminum structures for aerospace engineering. The main purpose of present work was to analyze the effect of shot peening on the fatigue crack propagation of the 7475 aluminum alloy, under both constant amplitude loading and periodical overload blocks. The tests were performed on 4 and 8 mm thickness specimens with stress ratios of 0.05 and 0.4. The analysis of the shot-peened surface showed a small increase of the micro-hardness values due to the plastic deformations imposed by shot peening. The surface peening beneficial effect on fatigue crack growth is very limited; its main effect is more noticeable near the threshold. The specimen's thickness only has marginal influence on the crack propagation, in opposite to the stress ratio. Periodic overload blocks of 300 cycles promotes a reduction of the fatigue crack growth rate for both intervals of 7500 and 15000 cycles.

Keywords: Aeronautical aluminium alloys; Fatigue crack propagation; Overloads; Shot Peening; Paris law

4.1 Introduction

High-strength aluminum alloys are widely used in aerospace applications due to the high strength-to-weight ratio, good corrosion resistance and high toughness combined with good formability and weldability. High-strength aluminum alloys are broadly employed in aerospace applications owing to the high strength-to-weight ratio, excellent corrosion resistance and great toughness associated with good weldability capabilities and formability. On the other hand, one of the main issues for the contemporary aircraft industry is to ensure simultaneously reliability, high durability, minimum weight and economic efficiency of transport aircraft. To obtain such crafted aircraft characteristics, it is necessary to design structures that ensure high damage tolerance. The approach to engineering design based on the assumption that flaws can exist in any structure and cracks propagate in service, is commonly used in aerospace engineering. Therefore, the prediction of crack growth rates based on the application of fracture mechanics theory is an important aspect of a structural damage tolerant assessment. Many metal components, such as turbines blades, used in aerospace and power industries are subjected to dynamic mechanical loading, leading to the initiation of fatigue cracks. One way to reduce the risk of fatigue crack initiation is to introduce compressive stresses in the region of higher stresses concentration, for example by shot peening. At the industrial level, this is a well-established surface treatment technology, despite generating a meaningful rougher surface and therefore surface defects [1]. Considering that most fatigue cracks initiate at the surface, the conditioning of the surface to resist crack initiation and earlier crack growth is a convenient method to enhance fatigue performance. The indentation of each impact, in shot peening process, produces local plastic deformation given rise to a field of surface compressive stresses. Studies by many researchers have shown a positive shot peening effect [2–4], resulting from the introduction of residual compressive stresses in the subsurface layers of material. Depending on peened material, there is an Almen intensity for which the optimum fatigue strength is achieved, corresponding to a certain balance between residual compressive stress field and surface roughness damage. Paris's law, which relates fatigue crack growth rate (da/dN) and stress intensity range (ΔK) is the prime approach adopted for characterizing fatigue crack propagation in engineering structures. Fatigue crack growth of the aluminum alloys in the Paris's law regime is affected by microstructure [5–7] and by the crack closure induced by plasticity, oxidation and surface roughness, especially

near threshold regime. Paris law characterizes the rate of crack advance per cycle: $da/dN = C\Delta K^m$. The rate of crack advance per cycle is related to the stress intensity factor range ΔK. C and m are constants that depend on the material, environment and stress ratio. Crack closure is considered a very good approach to explain the influence of mean stress on the fatigue crack growth rate [6,8]. Bergner and Zouhar [6] showed that crack growth rates of various aluminum alloys varied by a factor of about 20 for some ΔK values, suggesting that the main factor to explain that discrepancies was the crack closure effect and the environment. Fatigue cracks tends to grow into a material region that has experienced large plastic strains due to its location in the crack tip plastic zone. Typically, this material is deformed beyond its elastic domain in the direction normal to the crack flanks. The trace of the plastic deformation produced is left in the crack's path. It acts in the same way to an additional wedge stick between flanks, thus pre-straining them and partly protecting the crack tip from the action of posterior loads. This phenomenon is called plasticity induced crack closure and tends to decrease the effective stress intensity range, thereby resulting in slower crack propagation rates [8]. In compact tension (CT) specimens, the crack progresses more rapidly in center than at the surface conducting to a crack tunneling effect, due to the prevailing tri-axial state of stress at the center, promoting plain strain in contrast with plain stress at surface. Striation spacing between beach marks on fatigue crack surfaces is also affected by shot and laser peening effect. Zhou et al. [9] have observed a decrease in striation spacing with increase in the number of laser peening impacts for Ti6Al4V specimens. For the same alloy, Pant et al. [10] studied the effect of shot peening and laser peening on the fatigue crack propagation and compared with the untreated one with respect to the striation spacing; this was done using R = 0.1 and R = 0.7. Both peening surfaces presented a reduction on the striation spacing when compared to the untreated specimens. Overloads can lead to significant interaction effects on crack propagation, as has been reported in many studies [11–22]. Crack growth retardation can be explained by many mechanisms, including models based on crack closure, residual stresses, crack tip blunting, strain hardening, reversed yielding and crack branching. The residual plastic deformation effect leads to compressive stresses in the wake of the crack and raises the crack opening load on subsequent crack growth (crack closure), becoming the most important phenomena for what concerns the explanation for the variation of characteristic features of post-overload transients [19–23]. Donald and Paris [23] observed for 6061-T6 and 2024-T3 aluminum alloys that closure measurements produced good data correlation between distinct stress ratio

crack growths obtained in tests with increasingly K conditions. However, in the near-threshold regime with crack growth data obtained by the K-decreasing method, measured opening loads were excessive. This discrepancy was justified by Paris et al. [24], who suggested the "partial closure model". Borrego et al. [25] concluded that crack closure explained the bias of stress ratio on the fatigue crack growth rate for the 6082-T6 aluminum alloy and the influence of several load parameters for overloads interactions if the partial crack closure model is included in the analyses. The present work analyzes the effect of shot peening, specimen thickness and stress ratio on the fatigue crack propagation of 7475 aluminum alloy with T7351 heat treatment. T7351 provides an aged material abler to resist to stress-corrosion, the heat-treatment produces stress-relieved by control stretching and after artificially overaged to achieve the best stress corrosion resistance. A more extensive analysis of the crack growth following periodical tensile overloads blocks is also evaluated.

4.2 Materials and Experimental Procedures

4.2.1 Material and Samples

This research was conducted using the 7475 aluminum alloy with a T7351 heat treatment. These alloys are widely used in aeronautical applications where the combination of high strength, fracture toughness, good fatigue crack propagation and corrosion resistance are required. The chemical composition is shown in Table 4.1. The material bars from which the specimens were produced had following the dimensions in mm: 4000 x 1000 x 250. According to the material manufacturer, the ultimate tensile stress and yield stress are σ_{UTS} = 490 MPa and σ_{YS} = 414 MPa, respectively.

Table 4.1 – Chemical composition of Al 7475-T T7351 aluminium alloy (% weight).

Si	Fe	Cu	Mn	Mg	Cr	Zn	Ti	Other	Al
0.1	0.12	1.2-1.9	0.06	1.9-2.6	0.18-0.25	5.2-6.2	0.06	0.15	Remaining

To study the surface shot peening effect on crack propagation, two CT specimen batches were prepared: one with shot peening (SP) and another without shot peening but with the lateral surfaces mechanically polished (MP). MP specimens were polished to ensure a good visualization

of crack propagation. Manual grinding was performed using a LaboPol-5—Struers A/S, DK-2750 machine, passing progressively 240, 320, 600, 1000 and 2500-grit grinding paper. After specimen grinding, diamond paste of 3 μm and 1 μm were used to give the specimens a mirrored surface aspect. Shot peening was done at OGMA – Indústria Aeronáutica de Portugal S.A. Company (Alverca do Ribatejo, Portugal) with a large experience in producing components and aeronautics repair. Both sides of the specimen were subjected to a manual shot peening process, using a SURFATEC machine, as shown in Figure 4.1a), and an Almen strip type A, according to SAE J443 standard [26]. Coverage assessment was done by the surface visual inspection, using a 10× magnifying lens. One hundred-percent coverage was achieved when this analysis showed a completely attained surface by particles. The beads used in current study were of the type S170 with 0.43 mm diameter and Almen type A with intensity 0.20 A (mm), according SAE AMS2430 standard [27] for aluminum alloys. Figure 4.1b) shows one sample after the shot-peening process.

The studies of fatigue crack propagation were performed using the standard Compact Tension (CT) specimen with the geometry shown in Figure 4.1c), according with ASTM E647 standard [28]. For each batch of specimens, two different thickness (B) were manufactured: 4 mm and 8 mm. The specimens were machined in the longitudinal transverse (LT) direction from laminated plates. The loading specimen's direction coincides with bars lamination direction (Figure 1b, c). For each test condition, three specimens were used.

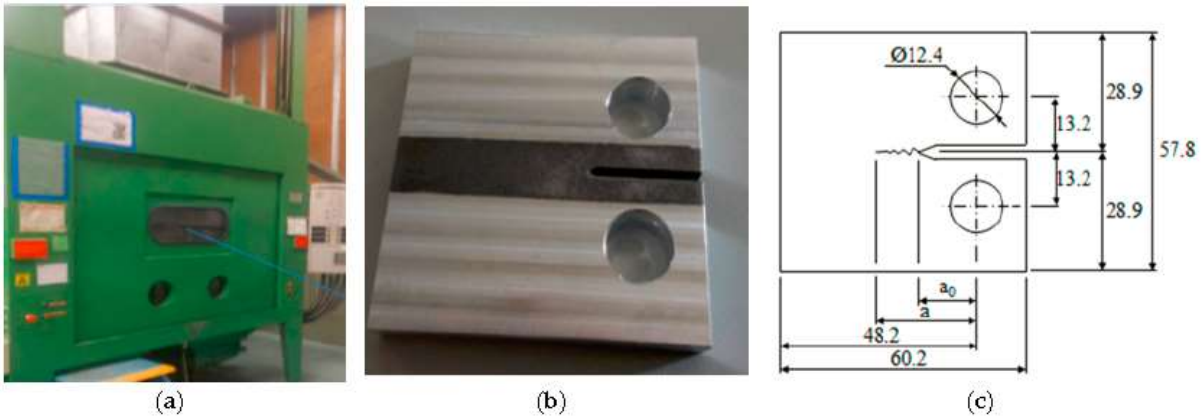

Figure 4.1 – a) Shot peening machine; b) Shot peened specimen; and c) Dimensions of Compact Tension (CT) Specimens in mm.

The surface roughness was evaluated according to DIN EN ISO 4288 standard [29] using a Surftest SJ-500 Mitutoyo surface roughness measuring system. The evaluated parameters for

each superficial treatment were: roughness average R_a, root mean square (RMS) roughness R_q and mean roughness depth R_z. Table 4.2 summarizes the roughness parameters showing an increasing of more than 300% in the three roughness parameters for the peened surfaces.

Table 4.2 – Surface roughness parameters for Mechanically Polished (MP) and Shot Penned (SP) specimens.

Specimen	**Parameter**	**Mean value±standard deviation (µm)**
MP	R_a	1.22±0.02
	R_q	1.50±0.02
	R_z	7.74±0.13
SP	R_a	3.70±0.17
	R_q	4.60±0.21
	R_z	23.50±2.00

To analyze the material microstructure, some samples of the specimens were selected to observe their cross section. The specimen's surface was gradually polished with several silicon carbide papers. The papers' granulometry ranged from high to low. Afterwards, 1µm diameter diamond particles were used until specimen's surface became mirror-like. Surfaces were then etched with Keller reagent (2.5% HNO_3, 1.5% HCl, 1% HF, and 95% H_2O (volume) (Coventry, UK)) and taken micrographs using an optical microscope Leica DM 4000 M LED (Wetzlar, Germany). Figure 4.2 shows typical micrographs indicating that base material microstructure (Figure 4.2 a)) with elongated grains in the rolling direction. The plane selected to take micrograph was normal to the loading direction to demonstrate the shot-peening effect. Around the shot peened surface (Figure 4.2 b)), an increasing of grain deformation and roughness was observed.

Surface Vickers hardness tests were performed according to ASTM C1327-15 [30] using a Struers Duramin micro-hardness tester with 0.5N load for 15s. Micro-hardness measurements were done in the cross-section of the sample at 0.3 mm from the surface, and spaced out 0.5 mm,

for both specimen types, MP and SP. The average values obtained from twenty measurements were: Hv0.05 = 157 for MP surfaces and Hv0.05 = 167 for SP surfaces. Therefore, shot peening surface hardness increased is more than 6%.

Residual stresses were measured, in-depth and on the longitudinal surface. Residual stresses analysis was performed by X-ray diffraction using a Proto iXRD equipment. Lattice deformations of the {222} diffraction planes were measured using Cr-Kα X-ray radiation, with 22° ψ angles, in the range ±42°, an acquisition time of 30s by peak and ±2° oscillations in ψ. For the analyzed material, and considering the radiation used, the average penetration depth of the X-rays was about 11 μm. Measurements were made for all studied treatments at four points along the surface of one specimen: one point for each longitudinal surface and one point for each notch surface in the central position. Analysis of indepth evolution of residual stresses in the longitudinal surface was performed by X-Ray diffraction after successive layer removal by electro polishing.

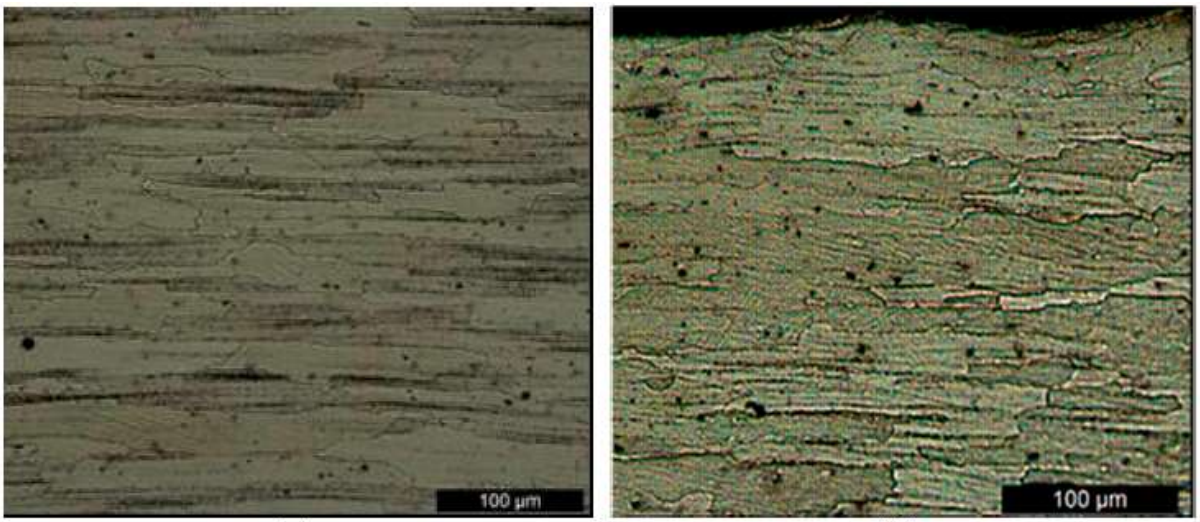

Figure 4.2 – Microstructure micrographs: a) Base material; and b) Shot peening (SP) sample.

4.2.2 Fatigue Tests

Fatigue crack propagation tests were carried out, in agreement with ASTM E647 standard [28], using 4 and 8 mm thick compact specimens (CT). The tests were performed under load

control at room temperature using a 100 kN capacity servo-hydraulic Instron 1341, with a frequency within the range 15–20Hz and stress ratios of R=0.05 and 0.4. The specimen's geometry and dimensions are shown in Figure 4.1 c). For both specimens' batches two types of tests were conducted: constant amplitude loading tests with the stress ratios R=0.05 and 0.4 and variable amplitude loading tests in which periodic overload blocks of 300 cycles are applied with intervals of N_{int} cycles, as shown schematically in Figure 4.3. The main purpose of these tests is to obtain the a-N and da/dN curves as a function of the stress intensity factor range ΔK, to analyze the effects of shot peening, specimen thickness and stress ratio.

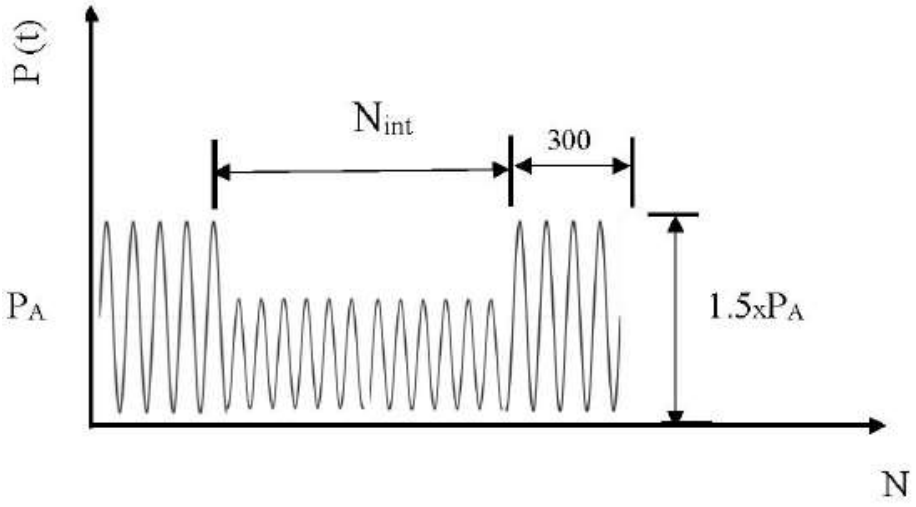

Figure 4.3 – Scheme of variable amplitude loadings with periodic overloading blocks.

For the surface polished specimens, the surface crack length was measured using a travelling microscope (45x) with 10μm accuracy. Crack growth rates under constant amplitude loading were determined by the incremental polynomial method using five consecutive points [28]. For the surface peened specimens, the crack length was obtained by using experimental calibration curves based on the compliance variation, previously obtained with the polished specimen's tests, considering the compliance (C) definition and ratio of displacement to load increment (Equation (4.1)).

$$C=\frac{(u_{max}-u_{min})}{(P_{max}-P_{min})} \quad (4.1)$$

where u and P are the axial grip displacement and the load, respectively, which were monitored during the test. From the non-peened specimen tests with constant amplitude loading, it was monitored a set of data for C calculation and the correspondent values of the crack length. The collected data are plotted in Figure 4.4, in terms of the crack length (a in mm) versus the compliance, and fitted by Equations (4.2) and (4.3) for specimens with 8 mm and 4 mm thickness, respectively, both with a 0.99 correlation factor. Equations (4.2) and (4.3) were afterwards used for the evaluation of the crack length in the tests with peened specimens and in the periodical overloading block tests.

$$a=39{,}515\times C^5 - 53{,}199\times C^4 + 27{,}962\times C^3 - 7278{,}2\times C^2 + 980{,}36\times C - 23{,}559 \quad (4.2)$$

$$a=2905{,}2\times C^5 - 6399\times C^4 + 5393{,}9\times C^2 + 2275{,}3\times C^2 + 502{,}82\times C - 16{,}62 \quad (4.3)$$

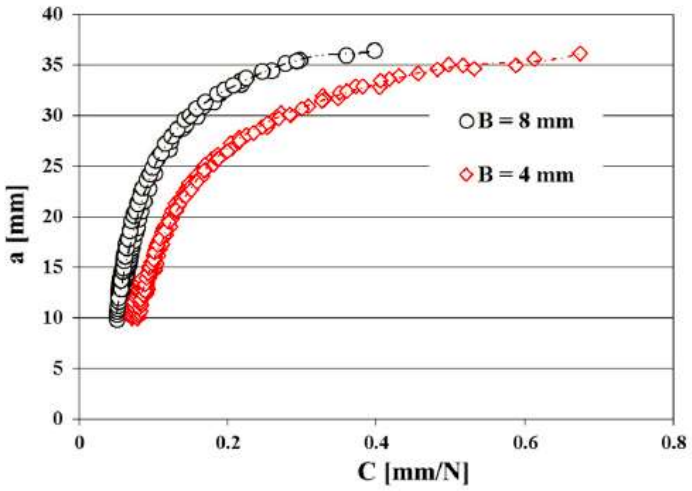

Figure 4.4 – Calibration curves based on the compliance, C, for 4 or 8 mm thick specimens.

4.3 Results and Discussion

Figures 4.5 and 4.6 highlight the effects of the specimen's thickness and surface peening on the crack propagation curves, respectively. Figure 4.5a–d) shows the influence of the thickness on the da/dN-ΔK curves. It is well known [31] that the thickness influence on the fatigue crack

propagation is related both to the microstructure and stress state. In the present study, specimens were machined from the same thickness bars, so there is no microstructure change between 4 and 8 mm thickness specimens. Therefore, the effect of thickness is only caused by changes in stress distribution along cross section and consequent variation on crack closure level [31]. The analysis of Figure 4.5 shows a reduced thickness effect on da/dN for both surface treatments (MP and SP specimens), including in the near-threshold region. The higher thickness specimens have higher da/dN for the same ΔK values in all conditions analyzed in Figure 4.5. It is also possible to notice that, for R = 0.05, the increase in da/dN is higher with increasing ΔK. Specimen's thickness effect is more noticeable for lower R-values and MP samples. As expected, independently of the surface treatment, the thicker specimens have higher crack growth rates over all the ΔK range analyzed.

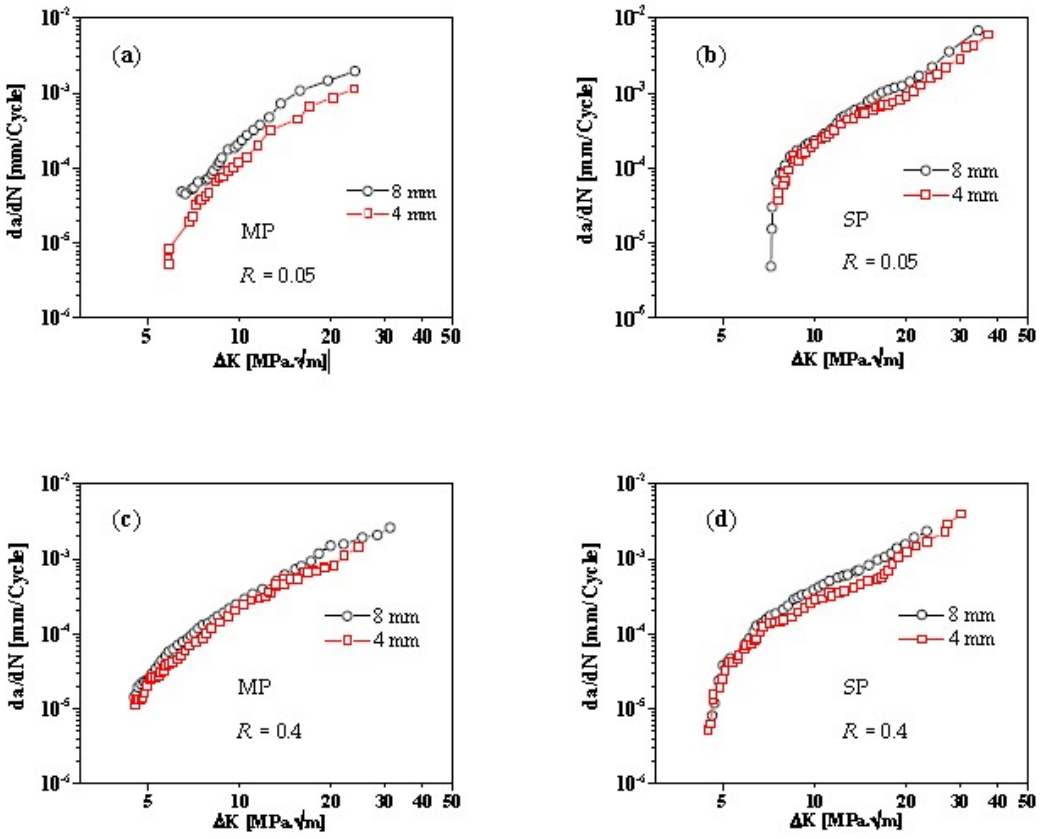

Figure 4.5 – Thickness effect on the da/dN-ΔK curves for specimens: a) MP, R = 0.05; b) SP, R = 0.05; c) MP, R = 0.4; and d) SP, R = 0.4.

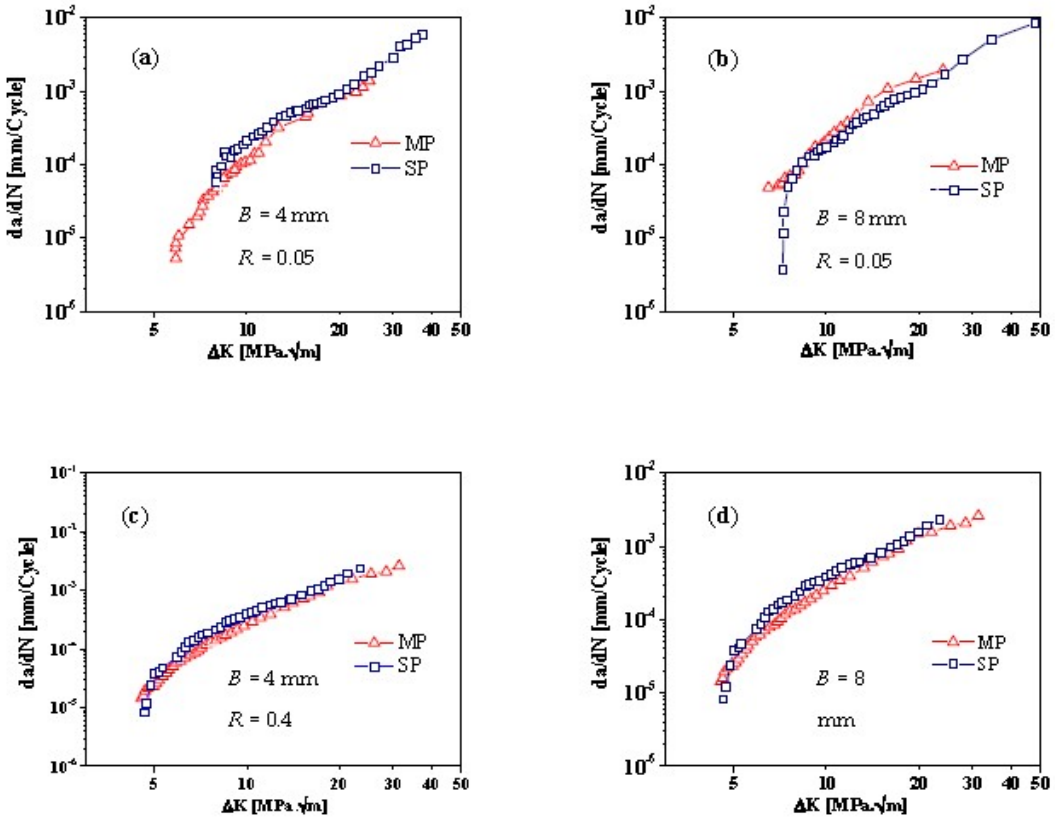

Figure 4.6 – Shot peening effect on da/dN-ΔK curves for specimens: a) B = 4 mm, R = 0.05; b) B = 8 mm, R = 0.05; c) B = 4 mm, R = 0.4; and d) B = 8 mm, R = 0.4.

The main purpose of current work was the analysis of the surface peening effect on the crack propagation. Figure 4.6 a)–d) shows the influence of the shot peening on the da/dN-ΔK curves for both thicknesses and stress ratios. Taking into account that shot peening has a much localized effect near the surface, which results in the introduction of compressive residual stresses, the propagation of cracks will be affected only in these areas. To analyze the retardation of crack propagation around the surface, the fractured specimens were observed by optical microscopy.

Figure 4.7 a), b) presents exemplary photos showing the marks of crack growth shape for machined and shot peening specimens, with 8 mm thickness, respectively. These marks were produced during variable amplitude loading with periodic overload blocks tests. Although the specimen's thickness is small to ensure tri-axial plain strain conditions in the center of the sample, the crack path presents a significant tunnel effect, as shown in Figure 4.7 a), b), and also according

to Zhou et al. [9]. The visual observation of the images does not show a clear evidence of the shot peening effect on the crack path.

For a detailed analysis, a tunnel effect parameter was defined by the Equation (4.4):

$$tunnel\ effect = \frac{a_2 - \left(\frac{a_1 - a_3}{2}\right)}{a_0} \quad (4.4)$$

where a_1 and a_3 are the crack lengths at the specimen's surfaces, a_2 is the current crack length at the center and a_0 is the initial crack length. The tunnel effect is a well-studied manifestation in fatigue crack propagation. Specimens stress state affect fatigue crack propagation, thus propagation rate is distinct at the crack flanks front relatively to specimens' central points. The effect of stress state is usually explained by crack closure mechanisms. Typically, a plane stress state occurs at the surface that promotes crack tip plastic deformation and accordingly plasticity induces crack closure [32]. In turn, inside the specimen, there is a tri-axial stress state that prevents plastic deformation. As fracture surface roughness may be different, promoting roughness induces crack closure, especially for low values of ΔK [33]. This stress state effect on fatigue crack propagation slows down crack growth at the surface and hence promotes the tunnel effect. Several different parameters are used to understand to what extend tunnel affects the specimens' behavior. The simplest and most common parameter is d/B (Figure 4.7 c)). Other used parameters are presented in the literature [34, 35]. Note that the stable shape of crack front has a uniform distribution of effective stress intensity factor range.

The tunnel effect parameter is plotted in Figure 4.7 d) against the fatigue crack length (a_2-a_0).

As expected, shot peening increases the retardation of the surface crack propagation observed by a higher tunnel effect parameter for crack length lesser than 10 mm. As mentioned above, tunnel effect can be caused by residual stresses profiles.

For MP specimens, average residual stress in load direction obtained from four measurements at the surface was about +290 MPa, while for SP samples compressive residual stresses occur around the surface. Figure 4.8 shows the profile of residual stresses and X-ray diffraction peak breadth against the depth from surface. According to the diffraction peak breadth profiles, the thickness layer affected by all surface treatments is circa 200 μm. The average value of the compressive residual stresses occurring trough a layer below the free surface with a 150

μm depth is about 200 MPa. Regarding the MP specimens, the residual stress measurements, for the same depth of the SP specimens presented an average value of 180 MPa. The reduced thickness of this layer, justifies the reduced influence on the overall propagation of fatigue cracks observed, in accordance to He et al. [36].

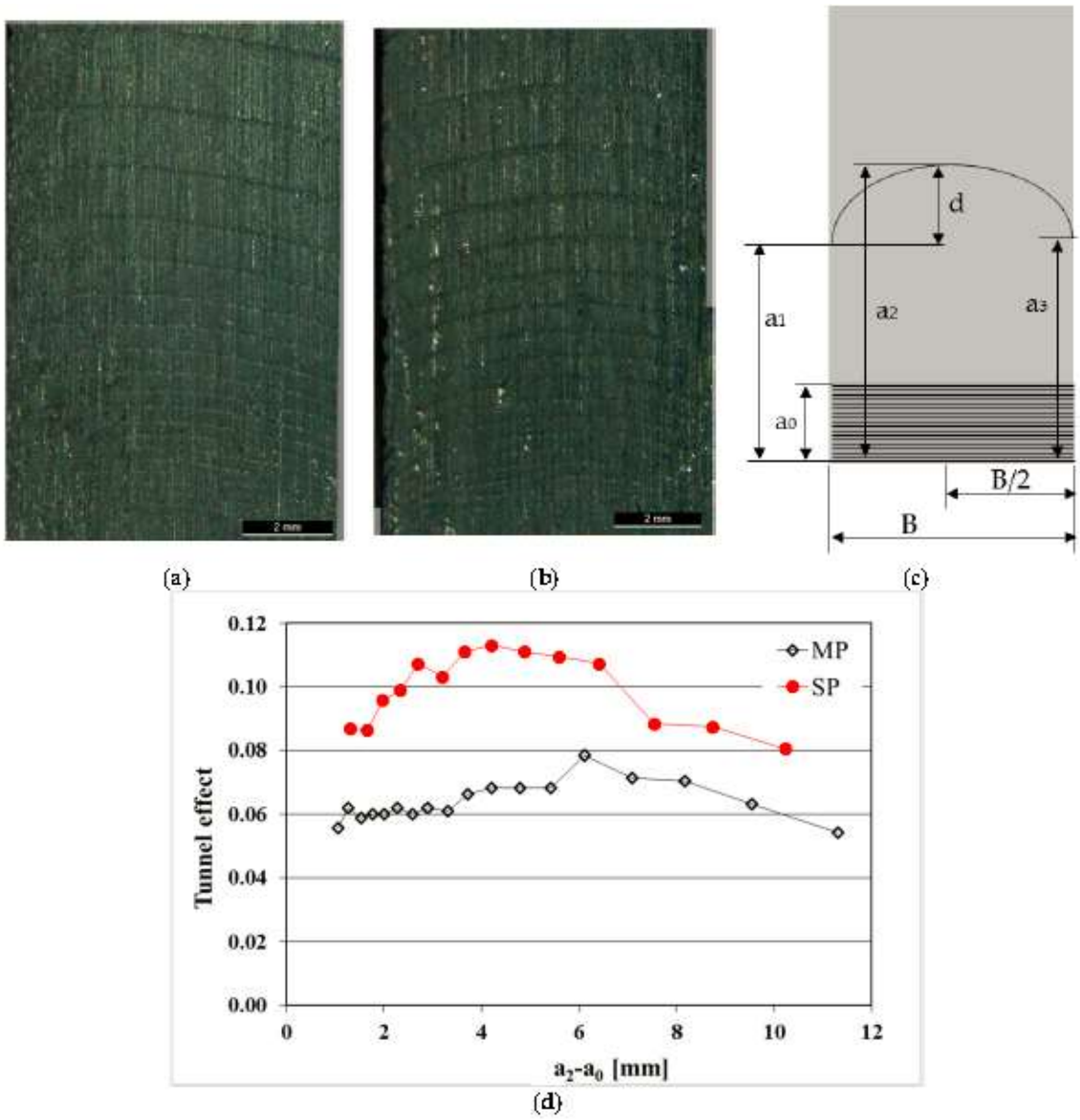

Figure 4.7 – Impression marks of the crack path and tunnel effect: a) MP specimens; b) SP specimens; c) Schematic indication for tunnel effect parameters; and d) Tunnel effect value distribution for MP and SP specimens.

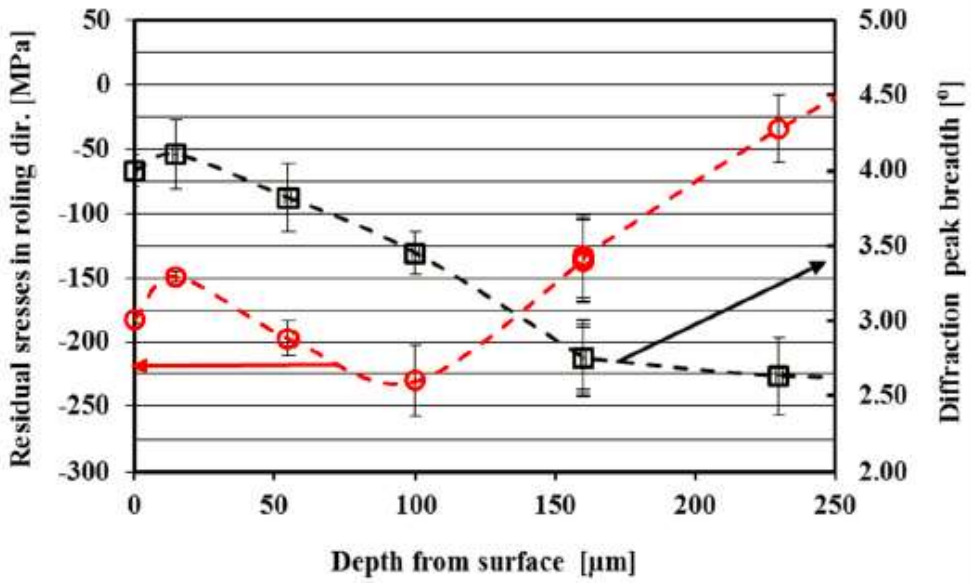

Figure 4.8 – Residual stresses profile and X-ray diffraction peak breadth against the depth from surface for SP specimens. "O" corresponds to the residual stress in rolling direction (MPa) and "□" to the diffraction peak breadth (°).

Results obtained for both stress ratios R = 0.05 and R = 0.4 are compared in Figure 4.9, for both surface treatments and thicknesses. As expected, a meaningful influence of the stress ratio was noticed in both Paris law regime and near-threshold condition. As reported in the literature, this effect is mainly consequence of the significant reduction on crack closure level for higher stress ratio R = 0.4 [31].

This is why above 15 $MPa.\sqrt{m}$ the R does not present any significate effect.

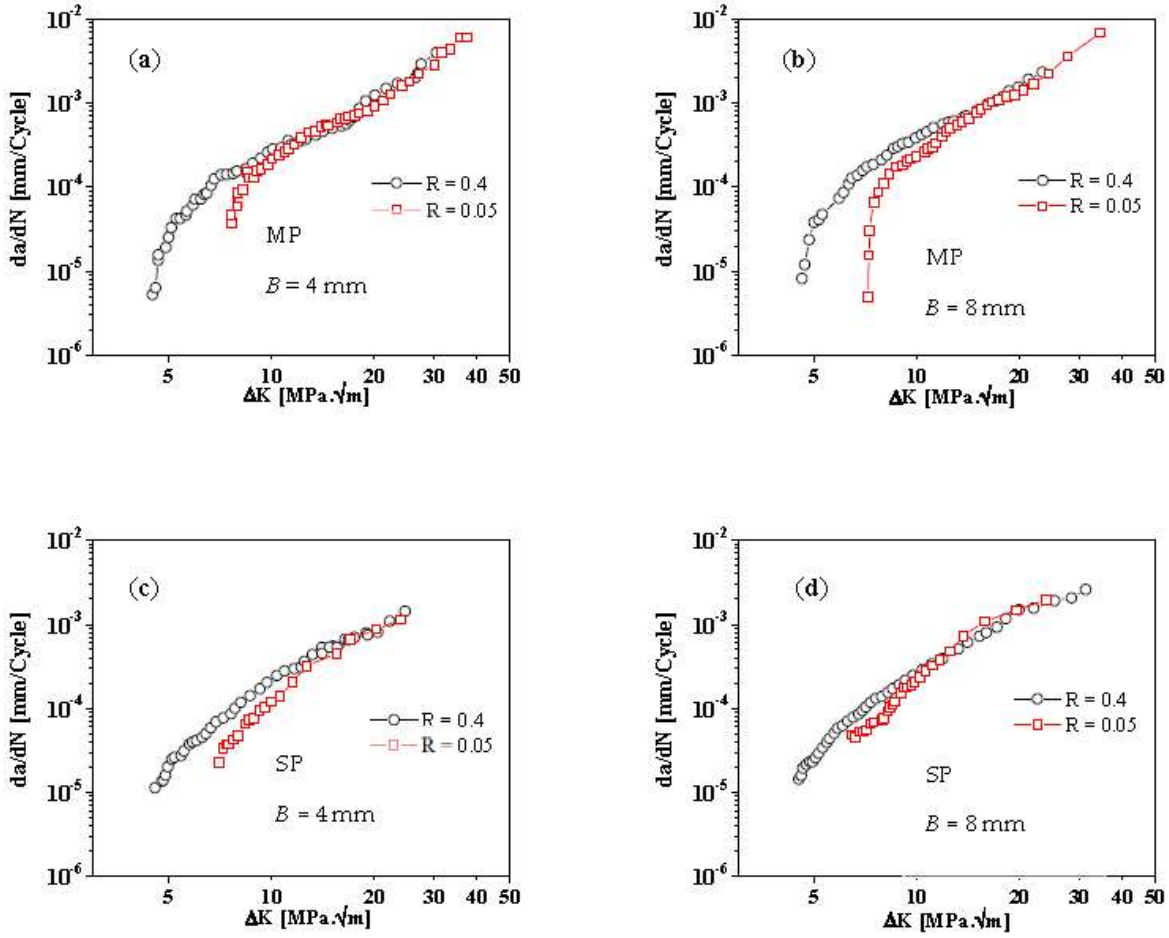

Figure 4.9 – R effect on da/dN-ΔK curves for specimens: a) B=4mm, MP; b) B=8mm, MP; c) B=4mm, SP; and d) B=8mm, SP.

Fatigue crack propagation resulting in the stable regime were modeled by Paris' law equation. Table 4.3 summarizes the values of the coefficients and intervals of validity of Paris' law and the correlation coefficients for all test conditions.

Table 4.3 – Paris' law parameters, $\boldsymbol{C}$ and $\boldsymbol{m}$ determined from $\boldsymbol{da/dN}$ vs. $\Delta\boldsymbol{K}$curves (mm/cycle; MPa $m^{1/2}$).

B [mm]	Specimen	R	C	m	Validity [MPa $m^{1/2}$]	Correlation factor
4	MP	0.05	1.41×10^{-8}	3.94	7-13	0.995
4	MP	0.4	2.42×10^{-6}	2.04	12-24	0.996
4	SP	0.05	2.95×10^{-7}	2.94	8-14	0.970
4	SP	0.4	2.70×10^{-7}	3.05	5-10	0.982
8	MP	0.05	2.72×10^{-8}	3.89	7-12	0.996
8	MP	0.4	1.96×10^{-6}	2.16	13-22	0.998
8	SP	0.05	2.53×10^{-7}	2.97	9-16	0.991
8	SP	0.4	2.63×10^{-7}	3.25	5-17	0.973

To analyze the transient effects after overloads, variable amplitude loading with R = 0.04 were carried out, in which periodic overload blocks of 300 cycles were applied with intervals of N_{int} of 7500 and 15000 cycles, as shown in Figure 4.3. The results obtained were compared with the reference constant amplitude loading tests. Figure 4.10 a)–d) shows the collected results from the tests performed in specimens with 8 mm thick. The typical transient behavior after overloads is not detected in all blocks because of the reduced transient zone and the crack measuring method. The analysis of the figure shows that for MP specimens the fatigue crack growth rate reduction reaches the maximum value for N_{int} = 7500 cycles, while for the SP specimens the crack growth rate continues to decrease, although slightly, when N_{int} increases from 7500 to 15000 cycles. For MP specimens, fatigue crack growth decreases more for 7500 cycles because induced plasticity of crack closure retardation is more critical (Figure 4.10 d). This behavior cannot be confirmed when crack closure is not measured. For the SP specimens with R = 0, the behavior is similar. This effect is more noticeable for N_{int} = 7500 cycles then for 15000 cycles.

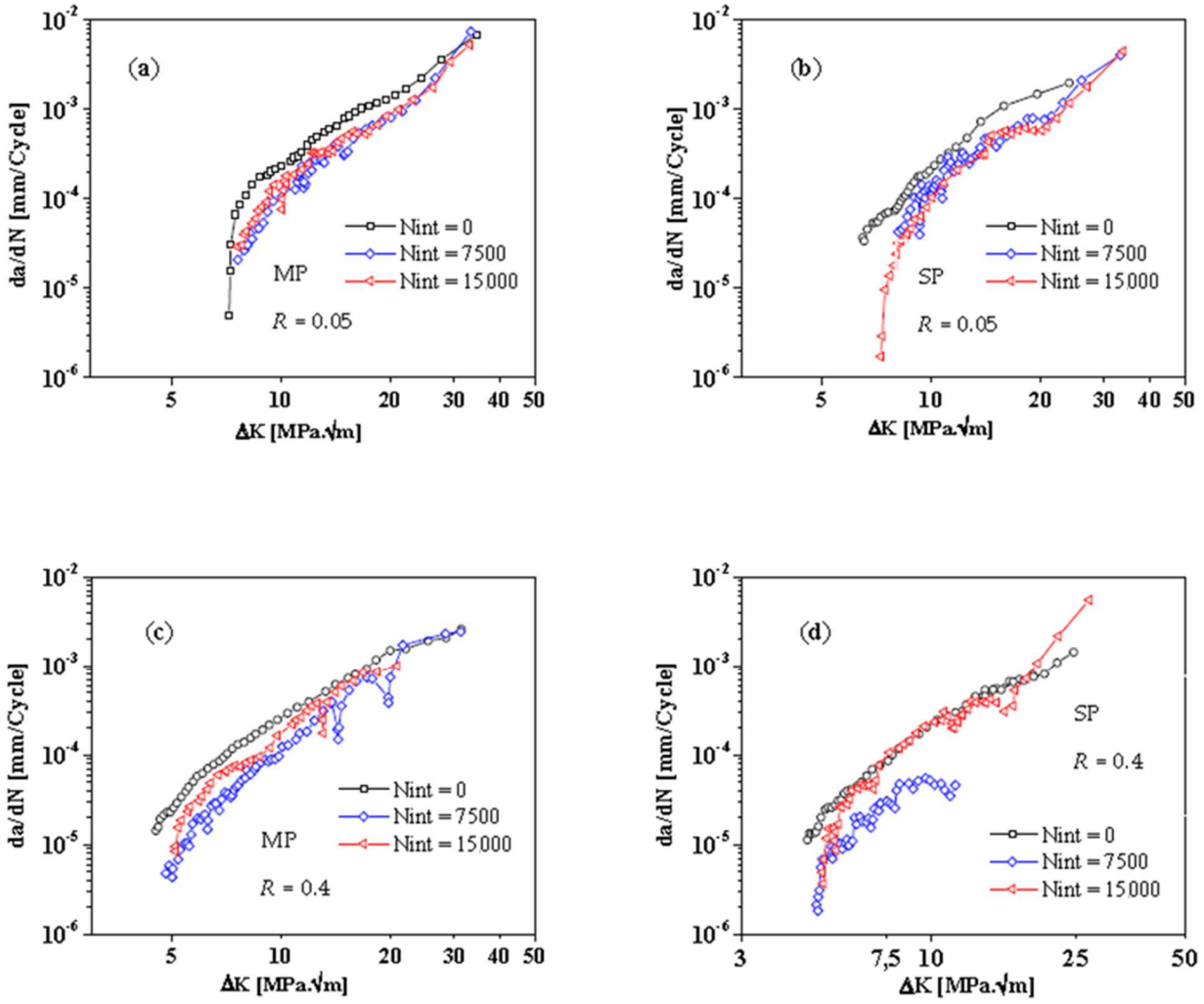

Figure 4.10 – Block overload effect on effect on da/dN-ΔK curves for curves for 8mm tick specimens: a) R=0.05, MP; b) R=0.05, SP; c) B=0.4, MP; and d) B=0.4, SP.

To understand better the fatigue mechanisms processes, fracture surfaces of the samples were observed in a Philips XL30 scanning electron microscope. Figure 4.11 shows two exemplary photos with different magnification of the crack propagated region in Paris' law regime, representative of various observations done during the study. Both images in Figure 4.11 show that fatigue crack propagation occurs mainly by striation.

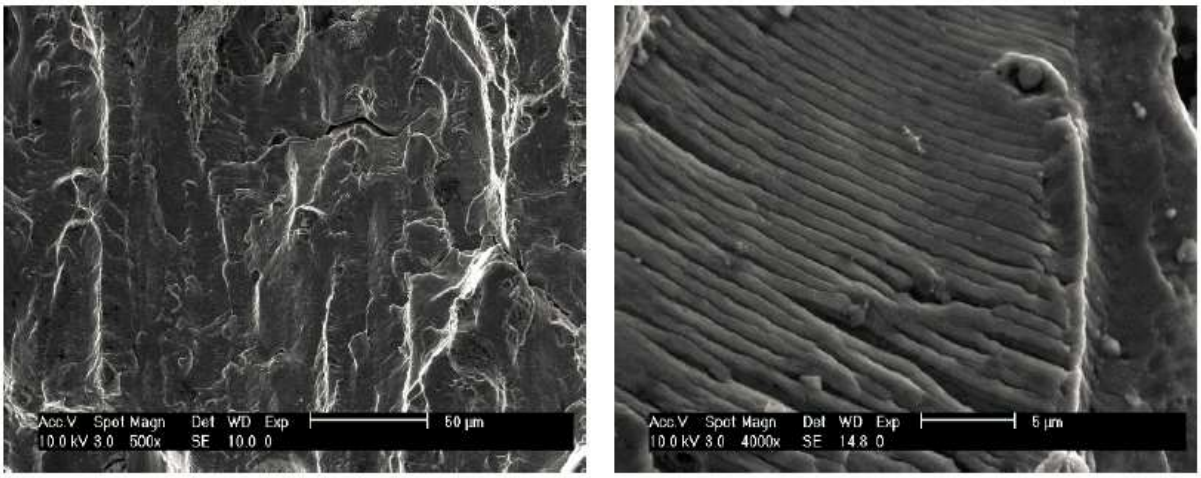

(a) (b)

Figure 4.11 – Exemplary fracture surface morphology from SEM observations.

4.4 Conclusions

The present work studied the effects of the shot peening and the stress ratio on the fatigue crack propagation of the 7475 aluminum alloy with a T7351 heat treatment, using two specimens' thickness: 4 and 8 mm. The analysis of the results draws the following conclusions:

- As a result of its small influence depth, the beneficial effect of shot peening on $da/dN - \Delta K$ curves is negligible, particularly for R = 0.4. However, this effect seems to increase near the threshold condition;
- For both mechanically polished and shot-peened samples, a specimen's thickness has only marginal influence on the stable crack propagation regime;
- A significant effect of the mean stress was observed, particularly in near- threshold region;
- Periodic overload blocks promote a reduction of the fatigue crack growth rate. For MP specimens, the reduction reaches the maximum value for the interval between blocks of 7500 cycles, while, for SP specimens, the crack growth rate continues to decrease for intervals of 15000 cycles.

4.5 Acknowledgments

This research is sponsored by FEDER funds through the program COMPETE—Programa Operacional Factores de Competitividade—and by national funds through FCT—Fundação para a Ciência e a Tecnologia—under the project PEst-C/EME/UI0285/2013. The authors would also like to acknowledge OGMA – Indústria Aeronáutica de Portugal, Alverca, Portugal, and Dr. Ana Guimarães and Eng. João Miranda for the collaboration in the shot-peening processing.

4.6 References

[1] – Fathallah, R.; Laamouri, A.; Sidhom, H.; Braham, C.; "*High cycle fatigue behavior prediction of shot-peened parts*"; Int. J. Fatigue; 26, p.1053–1067; 2004.

[2] – Miková, K.; Bagherifard, S.; Boku°vka, O.; Guagliano, M.; Trško, L.; "*Fatigue behavior of X70 microalloyed steel after severe shot peening*"; Int. J. Fatigue, 55, p.33–42; 2013.

[3] – Bagherifard, S.; Guagliano, M.; "*Fatigue behavior of a low alloy steel with nanostructured surface obtained by severe shot peening*"; Eng. Fract. Mech., 81, p.56–68, 2012.

[4] – Zhang, P.; Lindemann, J.; Leyens, L.; "*Shot peening on the high-strength magnesium alloy AZ80—effect of peening media*"; J. Mater. Process. Technol., 210, p. 445–450; 2010.

[5] – Petit, J.; Mendez, J.; "*Some aspects of the influence of microstructure on fatigue resistance*"; In Fatigue 96, Proceedings of the Sixth International Fatigue Congress, Berlin, Germany, 6–10 May 1996; Lutjering, G. Nowack, H., Eds.; Pergamon: Oxford, UK, 1996; Volume I, pp. 15–26.

[6] – Bergner, F.; Zouhar, G.; "*A new approach to the correlation between the coefficient and the exponent in the power law equation of fatigue crack growth*"; Int. J. Fatigue, 22, p.229–239; 2000.

[7] – Bergner, F.; Zouhar, G.; Tempus, G.; "*The material-dependent variability of fatigue crack growth rates of aluminium alloys in the Paris regime*"; Int. J. Fatigue, 23, p.383–394, 2001.

[8] – Sunder, R.; Dash, P.K.; "*Measurement of fatigue crack closure through electron microscopy*"; Int. J. Fatigue, 4, p.97–105; 1982.

[9] – Zhou, J.Z.; Huang, S.; Sheng, J.; Lu, J.Z.; Wang, C.D.; Chen, K.M.; Ruan, H.Y.; Chen, H.S.; "*Effect of repeated impacts on mechanical properties and fatigue fracture morphologies of 6061-T6 aluminium subject to laser peening*"; Mater. Sci. Eng. A, 539, p.360–36; 2012.

[10] – Pant, B.K.; Pavan, A.H.V.; Prakash, R.V.; Kamaraj, M.; "*Effect of laser peening and shot peening on fatigue striations during FCGR study of Ti6Al4V*"; Int. J. Fatigue, 93, p.38–50; 2016.

[11] – Vecchio, R.S.; Hertzberg, R.W.; Jaccard, R.; "*On the overload induced fatigue crack propagation behavior in aluminium and steel alloys*"; Fatigue Fract. Eng. Mater. Struct., 7, p.181–194; 1987.

[12] – Ward-Close, C.M.; Blom, A.F.; Richie, R.O.; "*Mechanisms associated with transient fatigue crack growth under variable amplitude loading: An experimental and numerical study*"; Eng. Fract. Mech., 32, p. 613–638; 1989.

[13] – Krumar, R.; Garg, S.B.L.; "*Effect of yield strength and single overload cycles on effective stress intensity range ratio in 6061-T6 Al alloy*"; Eng. Fract. Mech., 34, p. 403–412; 1989.

[14] – Ling, M.R.; Schijve, J.; "*The effect of intermediate heat treatments on overload induced retardations during fatigue crack growth in an Al-alloy*"; Fatigue Fract. Eng. Mater. Struct., 15, p.421–430; 1992.

[15] – DDamri, D.; Knott, J.F.; "*Fracture modes encountered following the application of a major tensile overload cycle*"; Int. J. Fatigue, 15, p.53–60; 1993.

[16] – Shuter, D.M.; Geary, W.; "*Some aspects of fatigue crack growth retardation behaviour following tensile overloads in a structural steel*"; Fatigue Fract. Eng. Mater. Struct., 19, p. 185–199; 1996.

[17] – Robin, C.; Louah, M.; Pluvinage, G.;"*Influence of the overload on the fatigue crack growth in steels*"; Fatigue Fract. Eng. Mater. Struct., 6, p.1–13; 1983.

[18] – Shercliff, H.R.; Fleck, N.A.; "*Effect of specimen geometry on fatigue crack growth in plane strain—II. Overload response*"; Fatigue Fract. Eng. Mater. Struct., 13, p. 297–310; 1990.

[19] – Shin, C.S.; Hsu, S.H.; "*On the mechanisms and behaviour of overload retardation in AISI 304 stainless steel*"; Int. J. Fatigue, 15, p. 181–192; 1993.

[20] – Dexter, R.J.; Hudak, S.J.; Davidson, D.L.; "*Modelling and measurement of crack closure and crack growth following overloads and underloads*"; Eng. Fract. Mech., 33, p. 855–870; 1989.

[21] – Tsukuda, H.; Ogiyama, H.; Shiraishi, T.; "*Transient fatigue crack growth behaviour following single overloads at high stress ratios*"; Fatigue Fract. Eng. Mater. Struct., 19, 879–891, 1996.

[22] – Borrego, L.P.; Ferreira, J.M.; Pinho da Cruz, J.M.; Costa, J.M.; "*Evaluation of overload effects on fatigue crack growth and closure*"; Eng. Fract. Mech., 70, p. 1379–1397; 2003.

[23] – Donald, K.; Paris, P.C.; "*An evaluation of DKeff estimation procedures on 6061-T6 and 2024-T3 aluminium alloys*"; Int. J. Fatigue, 21, S47–S57; 1996.

[24] – Paris, P.C.; Tada, H.; Donald, J.K.; "*Service load fatigue damage - A historical perspective*", Int. J. Fatigue, 21, S35–S46; 1999.

[25] – Borrego, L.P.; Ferreira, J.M.; Costa, J.M.; "*Fatigue crack growth and crack closure in an AlMgSi alloy*"; Fatigue Fract. Eng. Mater. Struct., 24, p. 255–265; 2001.

[26] – The American Standard SAE J443, "*Procedures for Using Standard Shot Peening Test Strip*"; American Standard: Piscataway Township, NJ, USA, 1968.

[27] – The American Standard. Aerospace Materials Division; SAE, Shot Peening, SAE AMS 2430; American Standard: Piscataway Township, NJ, USA, 2009.

[28] – American Society for Testing and Materials, "*Standard Test Method for Microhardness of Materials*", In Annual Book of ASTM Standards; ASTM: West Conshohocken, PA, USA, 2000; Volume 03.01, p. E647.

[29] – International Organization for Standardization, "*DIN EN ISO 4288: Geometrical Product Specifications (GPS). Surface Texture: Profile Method: rules and procedures for the Assessment of Surface Texture*"; ISO: Geneva, Switzerland, 1996.

[30] – American Society for Testing and Materials., "*Standard Test Method for Vickers Indentation Hardness of Advanced Ceramics*"; ASTM: West Conshohocken, PA, USA, 2015; p. C1327.

[31] – Borrego, L.P.; Costa, J.D.M.; Silva, S.; Ferreira, J.M.; "*Microstructure dependent fatigue crack growth in aged hardened aluminium alloys*"; Int. J. Fatigue, 26, p. 1321–1331; 2004.

[32] – Antunes, F.V.; Chegini, A.G.; Branco, R.; Camas, D.; "*A numerical study of plasticity induced crack closure under plane strain conditions*"; Int. J. Fatigue, 71, p. 75–86; 2005.

[33] – Antunes, F.V.; Ramalho, A.L.; Ferreira, J.A.M.; "*Identification of Fatigue Crack Propagation Modes with Roughness Measurements*"; Int. J. Fatigue, 22, p. 781–788; 2000.

[34] – Lin, X.B.; Smith, R.A.; "*Fatigue shape analysis for corner cracks at fastener holes*"; Eng. Fract. Mech., 59, p. 73–87; 1998.

[35] – Branco, R.; "*Numerical Study of Fatigue Crack Growth in MT Specimens*"; Master's Thesis, Department of Mechanical Engineering, University of Coimbra, Coimbra, Portugal, 2006.

[36] – He, B.Y.; Soady, K.A.; Mellor, B.G.; Harrison, G.; Reed, P.A.S; "*Fatigue crack growth behaviour in the LCF regime in a shot peened steam turbine blade material*"; Int. J. Fatigue, 82, p. 280–291; 2016.

CHAPTER 5 – Effect of Bead Characteristics on the fatigue life of shot peened Al 7475 T7351 specimens

Published in: International Journal of Fatigue 134, 2020, 105521

N. Ferreira[1], J. S. Jesus[1], J.A.M. Ferreira[1], C. Capela[1,2], J.M. Costa[1] and A. C Batista[3]

[1] CEMMPRE, Department of Mechanical Engineering, University of Coimbra, Rua Luís Reis Santos, 3030-788, Coimbra, Portugal

[2] ESTG, Department of Mechanical Engineering, Instituto Politécnico de Leiria, Morro do Lena - Alto Vieiro, 2400-901 Leiria, Portugal

3 CFisUC, Department of Physis, University of Coimbra, 3004-516 Coimbra, Portugal

Abstract

The present work aims to analyze the effect of shot peening processing parameters, material and size of beads on the fatigue behavior of aluminum alloy Al 7475-T7351. A systematic study was carried out under both three points bending (3PB) and tensile loadings. For 3PB tests it was concluded that shot peening does not introduce significant improvement on fatigue life and that the use of low size glass beads is potentially beneficial, with roughness being as or more important than residual stresses. All tensile treated specimens presented an improvement of fatigue life in comparison to the untreated specimens, particularly when the crack initiated internally. Internal crack propagation generates a conical fracture surface until transition to mode I propagation.

Keywords: Aluminum alloys; Shot Peening; Fatigue Life Enhancement; Internal Crack Initiation

5.1 Introduction

Aluminum alloys are widely used in the aerospace and aeronautical industries due to their high strength-to-weight ratio. Al 7475-T7351 alloy is a new aerospace material with improved mechanical properties compared to others, such as 7050 and 7075 alloys [1-3]. Fatigue cracks initiate mainly on the surface, which explains why the preparation of the surface to resist crack initiation and earlier crack growth is an attractive method of improving fatigue performance. Shot peening is a widely used mechanical surface treatment to improve the fatigue life of metallic components. During the shot peening process, the beads are bombarded into the material's surface by a nozzle. The main process parameters are: the beads size and material, Almen intensity (Almen intensity is a measure of the shot peening intensity obtained by the "Almen" test [4]) exposure time, coverage, air pressure, impact angle and nozzle characteristics [5, 6]. Each impact produces local plastic deformation which expansion is constrained by the adjacent material, resulting in a field of surface compressive stresses. A positive effect of shot peening was observed in many researches [7-9], due to the introduction of compression residual stresses in the subsurface layers of the material.

As with steels, most of the improvement in the fatigue life of an aluminum alloy may be attributed to the compressive residual stresses in the surface region, which often overcompensates the worsening of the surface's morphology [10-14]. However, the increase of aluminum alloys' fatigue resistance by shot peening is more difficult to achieve. The roughness of the peened surface is generally worse, which may cancel or reduce the beneficial effect of the compressive residual stress field. Therefore, shot peening in aluminum alloys produces both balancing beneficial and detrimental effects (residual stresses and surface roughness), with the determination of optimized process parameters becoming a difficult and time-consuming task to accomplish. In order to reduce the surface roughness and enlarge compressive residual stress field, new technologies have been developed, such as laser peening [15-17] and ultrasonic peening [18, 19].

In addition to the effect of surface roughness, shot peening in aluminum alloys causes the work hardening, which enhances resistance to crack initiation. On the other hand, it reduces fatigue crack propagation resistance during early crack growth due to the material's embrittlement. In addition, the material of the shot bead plays an important role on the shot

peening of aluminum alloys. Using steel beads, which caused rough peened surface, Luo et al. [20], obtained only an increase of 7% in fatigue life while Sharp et al. [11], by peening with lighter materials (glass and ceramic beads), decreased surface roughness and improved the fatigue strength significantly.

Recently, Benedetti et al. [21] studied the effect of shot peening treatments on the plain bending fatigue strength of aluminum alloy Al 7075-T651, concluding that shot peening conducted with small beads promotes a more effective improvement of the fatigue resistance, as it causes a lower surface roughness and induces the maximum compressive residual stress in the region closer to the surface. These authors also obtained additional improvement of fatigue strength by eliminating surface roughness by the tribo-finishing process.

The improvement in fatigue strength due to surface peening on aluminum alloys needs to be more studied in order to enable the development of the curves' designs based on more accurate fatigue life and prediction models. The main purpose of this paper is to evaluate the effect of shot peening parameters, bead diameter and material on fatigue design curves under both 3PB and tensile cyclic loadings in the aluminum alloy Al 7475-T7351.

5.2 Materials and Experimental Procedures

5.2.1 Material and Samples

Test specimens were performed from Al 7475-T7351 aluminum alloy. This material was heat treated at 470°C, then subjected to water quenching and controlled stretching from 1.5% to 3%, followed by artificial aging in two phases: first at 121°C for 25 hours and then at 163°C in the range of 24 to 30 hours. The chemical composition is indicated in Table 5.1, according with the specifications provided by supplier ALCOA Company. The main mechanical properties are yield stress of 414 MPa, tensile strength of 490 MPa and a maximum elongation of 9% (according to ALCOA Company).

Table 5.1 – Chemical composition of Al 7475 - T7351 aluminum alloy (% weight).

Si	Fe	Cu	Mn	Mg	Cr	Zn	Ti	Other	Al
0.1	0.12	1.2-1.9	0.06	1.9-2.6	0.18-0.25	5.2-6.2	0.06	0.15	Remaining

Five batches of samples were prepared for each loading mode: an untreated reference batch was grounded with 1000 grit SiC paper and additionally polished with diamond pastes up to 1μm; in the other four batches, the specimens' surface was submitted to shot peening treatments. Table 5.2 indicates the diameters and materials of the beads used in the different batches. It was assumed that the particles have spherical shape. Bead sizes are in accordance with the standard specifications and recommendations on ASM 2430 [4] for the shot peening of aluminum alloys.

Table 5.2 – Parameters for the different shot peening batches.

Code	Bead material	Mean bead size (μm)	Standard deviation size (μm)
Polished	-	-	-
GB 8	Glass	166	28
GB 35	Glass	377	32
SB 110	Steel	348	21
SB 170	Steel	670	75

Shot peening was done in OGMA - Indústria Aeronáutica de Portugal S.A., a company with great experience in surface treatment of components for the aeronautical industry, using a SURFATEC machine and with a type A Almen strip. The samples were rotated in order to promote an approximate impact angle of the beads on surfaces of 90º in all zones. The coverage of the shot peening was 100% for an Almen intensity of 0.20 A (mm), according to the ASM 2430 standard [4].

Fatigue tests were carried out using round dog bone specimens with 6 mm diameter in the center region and tested in three points bending (3PB) under tensile loadings with the stress axis parallel to the microstructure's longitudinal direction. All tests were conducted in load control mode, at air and room temperature and at a frequency ranging from 10 - 20 Hz. Bending tests were carried out using an Instron EletroPuls E10000 machine, while for the tensile tests a 100kN capacity Instron servo hydraulic machine was used. Tensile fatigue tests were performed at the load ratio R=0 and the 3PB tests at R=0.1.

Figures 5.1 a) to c) show the geometry of the tensile tests, a schematic view of the apparatus for 3PB tests and the geometry of the 3PB test specimens, respectively. For the tensile tests, the load amplitude and mean load required as input data were calculated as $P_a = P_m = \sigma_a A$, while for 3PB tests the amplitude load was calculated taking into account the values of the nominal bending stresses, according to Equation (5.1):

$$P_a = \frac{\pi D^3 \sigma_a}{16L} \tag{5.1}$$

where σ_a is the stress amplitude, P_a is the bending or axial load amplitude, L is the specimen span, D is the diameter of the specimen and A the cross section area.

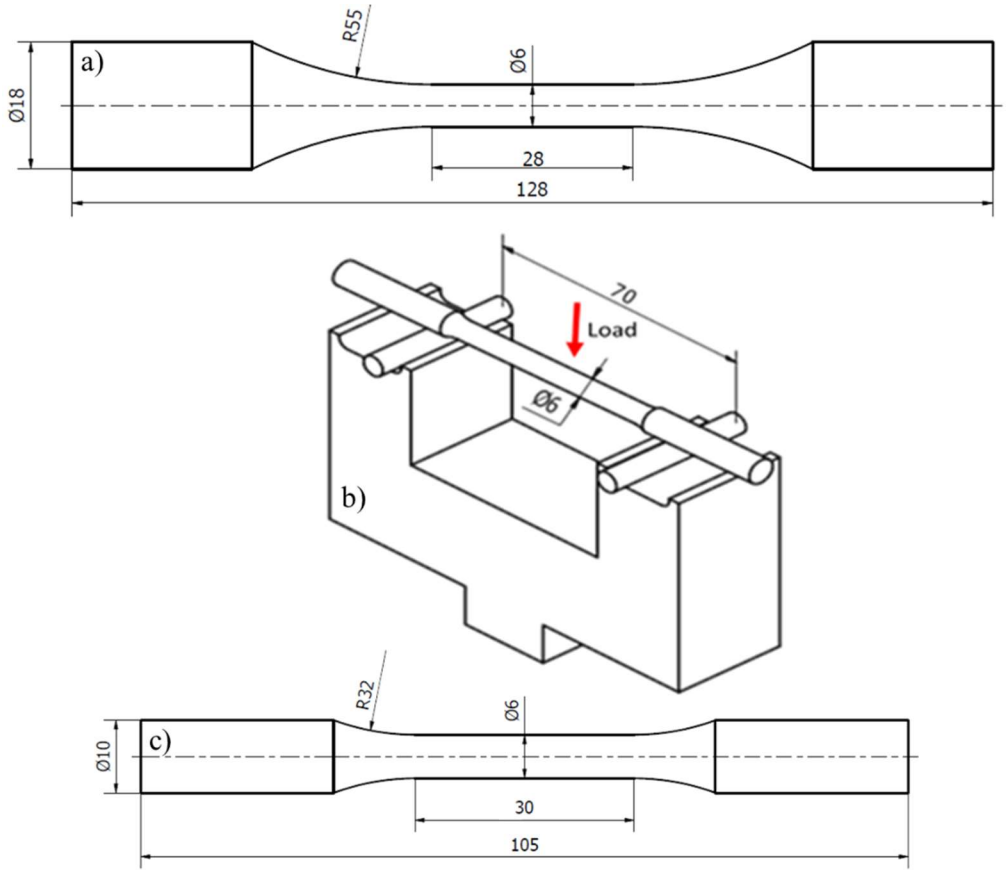

Figure 5.1 – a) Geometry of the tensile test specimens; b) 3PB testing apparatus; c) Geometry of 3PB tests specimens. (Dimensions in mm).

One specimen of each batch was cut through a plane containing longitudinal axle and afterwards the surface was gradually polished with smaller granulometry silicon carbide papers,

while at the end diamond particles with a 1μm diameter were used until the surface became mirror-like. Afterwards, said surfaces were etched with Keller reagent (2.5% HNO_3; 1.5% HCl; 1% HF; 95% H_2O) and observed with an optical microscope Leica DM 4000 M LED.

Roughness evaluation was carried out in accordance with the DIN EN ISO 4288 [22] standard, using the Mitutoyo, Surftest SJ-500, surface roughness measuring system. Vickers nanohardness measurements were performed in cross section specimens using a Berkovich three-sided diamond pyramid indenter with a half angle of 65.35º. The maximum load applied was 30 mN. The equipment has a load and displacement resolution of 0.5 mN and 80 nm, respectively. The wait time was 5 seconds while the loading and unloading time was 10 seconds. Measurements started at a distance from surface of 5μm with increments of 20μm up to 185μm depth. An additional test was also performed at the center of the specimen to estimate the base material's nanohardness value.

The residual stress analysis was performed by X-ray diffraction using a Proto iXRD equipment in the longitudinal direction of the samples. Lattice deformations of the {222} diffraction planes ($2\theta \approx 157°$) were measured using Cr-K_α X-ray radiation, with 21 β angles in the range ±30° (42 ψ angles in the range ±42°), an acquisition time of 60 seconds by peak and ±2° oscillations in ψ. The stress was evaluated with an elliptical regression of $\sin^2\psi$ data and the X-Ray elastic constants values of 18.56×10^{-6} MPa^{-1} for $(1/2)\cdot S_2$ and -4.79×10^{-6} MPa^{-1} for S_1. For the analyzed material, and considering the radiation used, the average penetration depth of the X-Rays was about 11 μm. The analysis of the in-depth evolution of the residual stresses was performed step-by-step, by removing successive thin layers of material by electrolytic polishing. For some of the deeper layers both ψ and φ oscillations were used, to get better diffraction peak profiles.

Finally, the fatigue fractured surfaces of the broken specimens were analyzed with a scanning electron microscope (SEM), Philips® XL30 TMP.

5.3 Results and Discussion

5.3.1 Metallographic analysis

The region near the surface was observed by optical microscopy, in order to study shot peening effect on microstructure. Figure 5.2 a) to e) shows exemplary photos. Figure 5.2 a) shows the microstructure of the aluminum alloy, presenting the grains elongated in the rolling direction, typical of extruded rods. Figures 5.2 b) and c) highlight the surface area where the shot peening occurred in the cases of steel beads, SB170 and SB110, respectively. It was noticed that SB170 and SB110 steel beads, which have a much higher mass than glass beads, promote a larger damaged area (presenting a surface damaged layer with about 100μm depth). A visual analysis of Figures 5.2 c) and d) seems to indicate that SB110 and GB35 beads have similar roughness, lower than SB170 series, and a few surface defects, with a significantly lower depth than the plastically deformed layer created by the shot peening treatment, which may promote the onset of fatigue cracking. Figure 5.2 e) shows that GB8 beads reduced significantly the plastic deformed layer and the roughness in comparison with the other shot peening series. On the other hand, a visual analysis of Figure 5.2 d) did not reveal the presence of surface defects in the GB8 specimens.

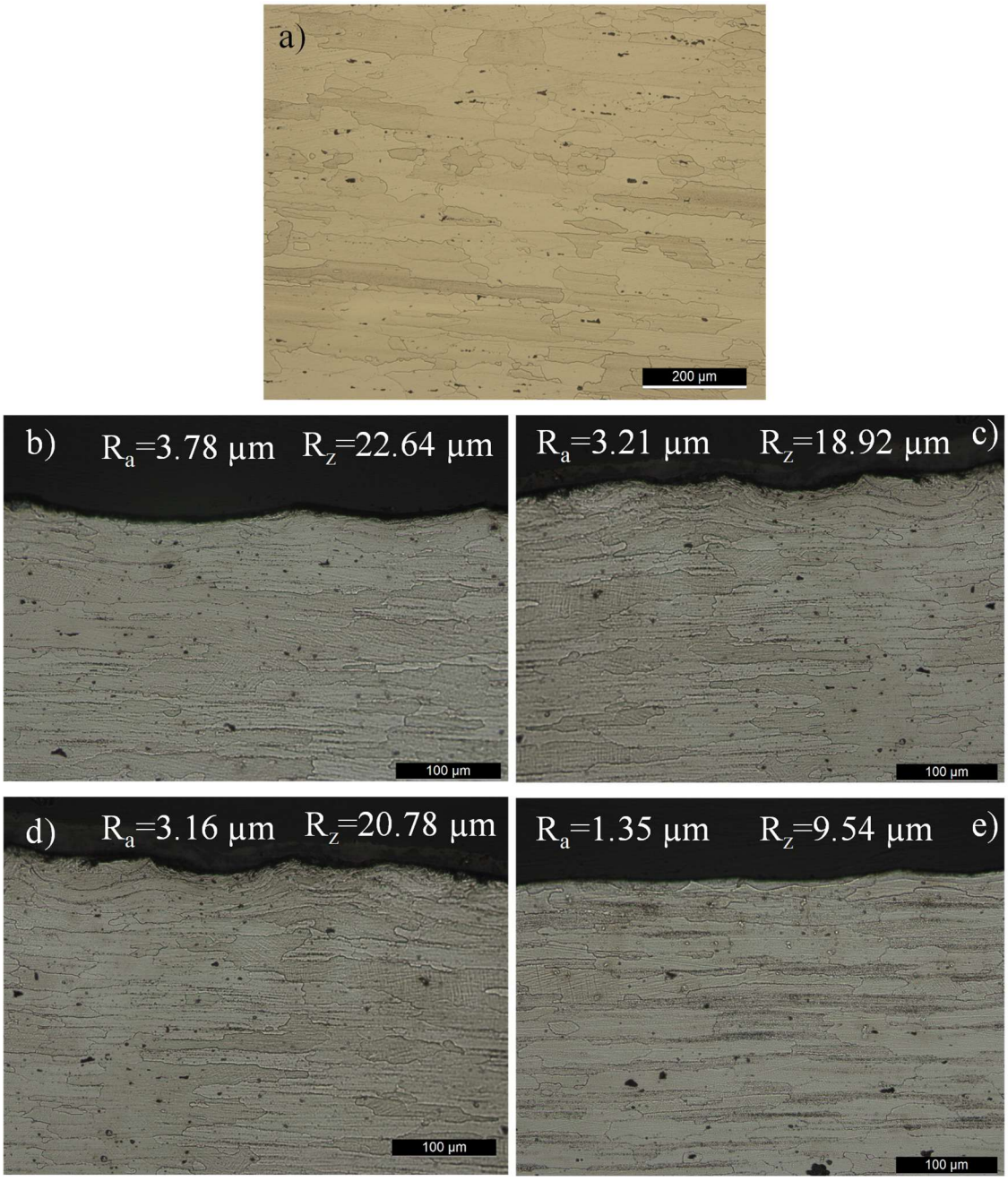

Figure 5.2 – Microstructures: a) Aluminum alloy; b) Peened with SB170; c) Peened with SB110, d) Peened with GB35; e) Peened with GB8.

5.3.2 Roughness Evaluation

The roughness parameters evaluated for each superficial treatment are summarized in Table 5.3: roughness average R_a, maximum peak-to-valley height R_y, the average maximum peak to valley of five consecutive sampling lengths within the measuring length R_z, the average spacing

of adjacent peaks in the surface profile D_p, the elastic stress concentration factor K_t and the notch factor K_f. The elastic stress concentration factor K_t, introduced by multiple micro-notches after shot peening, according to Li et al. [23] is given by Equation (5.2):

$$K_t = 1 + 2.1\left(\frac{R_z}{D_p}\right) \tag{5.2}$$

and the notch factor K_f can be calculated by the Peterson formulation, Equation (5.3):

$$K_f = 1 + \frac{K_t - 1}{1 + \frac{a}{r}} \tag{5.3}$$

where *a* and *r* are a material characteristic length of the crack initiation processing zone and the mean radius of beads indicated in Table 5.2, respectively. For aluminum alloys *a* is estimated as 0.51mm.

Table 5.3 – Roughness parameters for the treated and untreated series.

Series	Roughness	Average	Standard Deviation	K_t	K_f
GB8	R_a [µm]	1.35	0.096		
	R_y [µm]	11.78	0.994		
	R_z [µm]	9.54	0.524		
	D_p [µm]	98.10	2.686	1.204	1.028
GB35	R_a [µm]	3.16	0.155		
	R_y [µm]	26.21	1.976		
	R_z [µm]	20.78	1.816		
	D_p [µm]	221.95	9.218	1.197	1.053
SB110	R_a [µm]	3.21	0.350		
	R_y [µm]	25.69	3.642		
	R_z [µm]	18.92	2.390		
	D_p [µm]	162.67	5.104	1.244	1.062
SB170	R_a [µm]	3.78	0.277		
	R_y [µm]	30.78	3.512		
	R_z [µm]	22.64	2.342		
	D_p [µm]	367.62	7.761	1.129	1.051
Non treated	R_a [µm]	0.06	0.011		
	R_y [µm]	0.49	0.131		
	R_z [µm]	0.41	0.080		

Figure 5.3 shows the average of roughness parameters for the different batches used in 3PB and tensile tests. The roughness values indicated in Figure 5.3, along with the images shown in Figure 5.2, indicate that even the higher roughness caused by SB170 beads presents a smoother surface profile with fewer localized notches when compared to GB35 and SB110 beads.

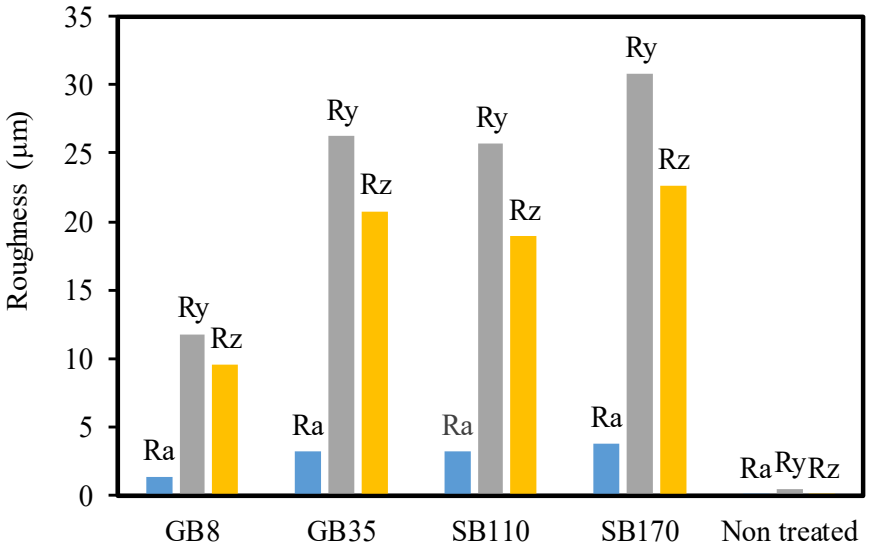

Figure 5.3 – Average roughness parameters for the different batches.

Table 5.3 and Figure 5.3 show that the shot peening treatments increase the surface roughness relatively to the untreated specimens and that the steel SB110 and SB170 beads and glass GB35 beads produce similar and significantly higher levels of roughness than GB8 beads. In all cases, it can be said that the layer treated by shot peening is very shallow, affecting only a few surface grains with a depth of generally less than 100µm.

5.3.3 Hardness analysis

Shot peening promotes surface densification, the increase of hardness and the accumulation of compressive residual stresses. Figure 5.4 presents the averages of hardness of all indentions performed around the surface for the different samples batches. All series show a similar trend, with a slight increase (lesser than 10%) in surface hardness and a progressive attenuation of the

effect of the impact of the beads until they converge to the hardness of the base material of about 246 Hv to about 200 µm depth. The GB8 series presents the lower values of hardness for depths until 60µm. These results partially coincide with those obtained by Ramos et al. [19] for the same material, which also found only a slight increase of hardness in the shot peened surface in comparison with the base material, due to the cold work and the consequent plastic deformation induced by the beads' impact.

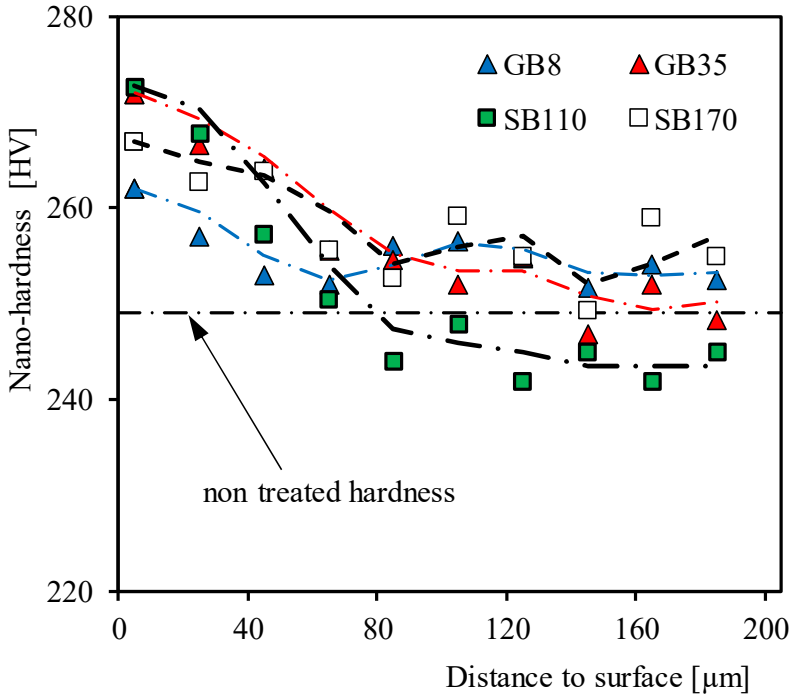

Figure 5.4 – In depth hardness distribution for the different beads.

5.3.4 Residual Stress Evaluation

The surface and in-depth measurements of residual stresses in the longitudinal direction are shown in Figure 5.5. Fitted residual stress profiles of the shot peened series using the Robertson formula [24] are also superimposed, as seen in Equation (5.4):

$$\sigma_{res} = A \cdot exp\left(\frac{-2(x-x_d)^2}{W^2}\right) + B \tag{5.4}$$

where σ_{res} is the residual stress, x, the depth below the surface, $A+B$, the maximum residual stress, W, a measure of the width of the curve and x_d, is the depth to the maximum residual stress.

All surface treatments induce compressive residual stresses on the surface layer, which is the first measurable layer by X-Ray diffraction at a depth of 11 μm. The values obtained for the surface residual stresses are indicated in Table 5.4.

Table 5.4 – Residual stress values on the surface.

Treatment	Residual Stress [MPa]
Polished	-66±14
GB8	-210±9
GB35	-206±6
SB110	-271±6
SB170	-181±3

Shot peening treatments increased the surface residual compressive stresses to values in the range 180-270 MPa. However, it was not possible to establish a direct connection between the residual stress values and the diameter of the beads or the impact energy.

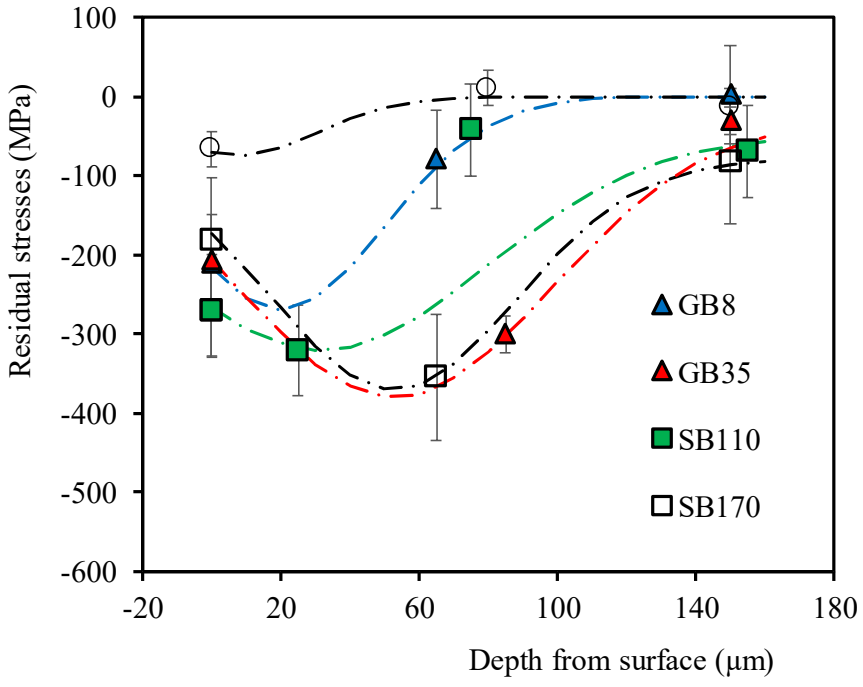

Figure 5.5 – In depth residual stresses for the different beads.

A more detailed observation of the results plotted in Figure 5.5 indicated that they agree with those obtained by Gao [17], showing that the maximum compressive residual stresses did not occur at the surface but at inner layers with about 25-60 μm depth, depending of the beads' type. Regardless of the bead type used in shot peening, the residual stresses caused by the impacts tends to zero for about 150μm depth.

5.3.5 Fatigue Tests Results

The results of the fatigue tests are shown in Figures 5.6 a) to b) in terms of the stress amplitude against the number of cycles to failure, comparing the S-N curves for shot peened series with polished specimens for 3PB tests and tensile tests, respectively. As is well known, fatigue crack initiation is a localized process, causing a significant dispersion of results by the combined effect of the residual stresses, hardness and roughness.

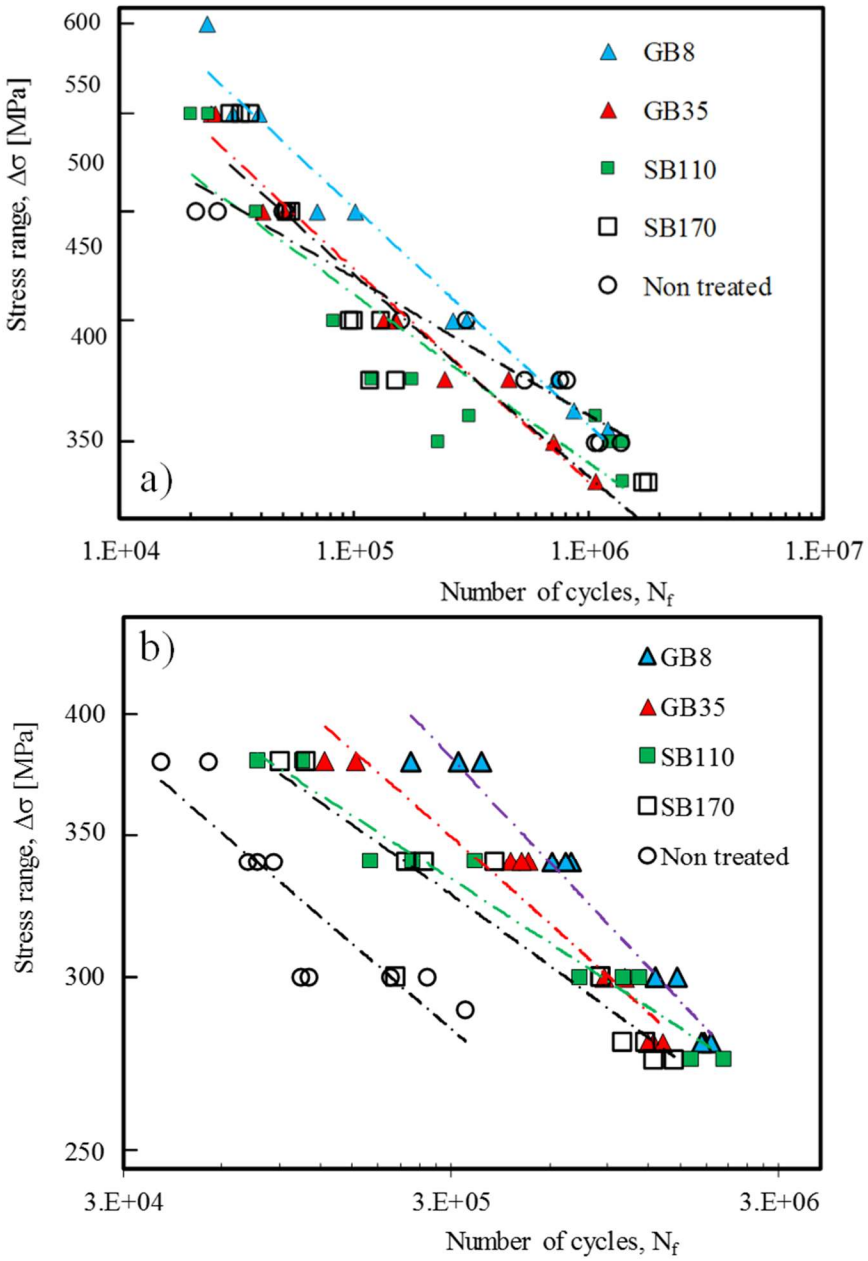

Figure 5.6 – S-N curves for the batches with different shot peening beads and the reference polished samples: a) 3PB tests; b) Tensile tests.

The S-N curves were fitted using Basquin's law, Equation (5.5):

$$\sigma_a = \sigma'_f \times (N_f)^b \tag{5.5}$$

where: σ'_f is the cyclic resistance coefficient, b is the cyclic resistance exponent and N_f the number of cycles to failure. The values of σ'_f and b are summarized in Table 5.5 for all the series tested. Table 5.5 also presents the fatigue resistance improvement of the different treatments, for a fatigue life of $5x10^5$ cycles, in comparison with simply polished specimens.

Table 5.5 – Analysis of the S-N Curves for all treatments.

Treatment	σ'_f [MPa]	b	Loading mode	Improvement [%]*
Non treated	457	-0.058	3PB	-
GB8	718	-0.091	3PB	2
GB35	668	-0.09	3PB	-4
SB110	528	-0.072	3PB	-4
SB170	632	-0.086	3PB	-4
Non treated	1169	-0170	Tensile	-
GB8	1987	-0.184	Tensile	42
GB35	2459	-0.204	Tensile	35
SB110	896	-0.130	Tensile	30
SB170	1968	-0.189	Tensile	31

* (in relation to polish specimens for $5x10^5$ cycles)

For a fatigue life of $5x10^5$ cycles, the 3PB fatigue resistance of GB8 series is similar of the untreated series, while the other treated series present slightly lower resistances to fatigue. As expected, in all specimens tested in 3PB loading the crack initiation occurs from the surface, due to the high stress gradient created by the bending loading. For lower lives the GB8 series show better fatigue performance than untreated series. The only parameter where GB8 series present better results than the other series is the roughness (see Figure 5.3 and Table 5.3). In what concerns the residual stresses and hardness profile, all series present similar values. The S-N curves obtained for the other treated series present lower resistance than the untreated series for fatigue lives above 10^5 cycles. Despite the increase of surface hardness and the introduction of compressive residual stresses in a surface layer with 150μm depth, the shot peening treatment did not produce a beneficial effect with GB35, SB110 and SB170 beads. It seems that with 3PB tests the roughness has a detrimental effect, equivalent to the potential beneficial effect of the compressive residual stresses resulting from the shot peening. Therefore, it can be concluded that

the shot peening treatment does not introduce significant improvement on fatigue life and that the use of small glass beads is potentially beneficial for specimens tested in 3PB.

Table 5.6 summarizes the fatigue results obtained in the tensile tests. The number of cycles N_{est} was calculated from Equation 5.5 for each value of the stress range. For the majority of the specimens, crack initiation occurs internally at the depth *f* indicated in this table. For the GB8 series internal crack initiation occurs 92% of times, for the GB35 series 80%, and for SB110 and SB170 series 55%.

Table 5.6 – S-N curves parameters.

Ref.	Δσ [MPa]	f [mm]	N_f [cycles]	N_{est} [cycles]	N_f/N_{est}	Ref.	Δσ [MPa]	f [mm]	N_f [cycles]	N_{est} [cycles]	N_f/N_{est}
GB8_1	300	1.18	1261038	1275635	0.989	**SB110_1***	300	0.00	293943	939865	0.313
GB8_2	340	0.93	695965	645628	1.078	**SB110_2***	340	0.00	171484	358716	0.478
GB8_3	380	0.23	371161	352510	1.053	**SB110_3***	380	0.00	77102	152411	0.506
GB8_4	280	2.25	1783084	1856724	0.960	**SB110_4**	275	0.45	2050486	1835994	1.117
GB8_5	380	0.22	315074	352510	0.894	**SB110_5**	300	1.30	741971	939865	0.789
GB8_6	340	0.79	609907	645628	0.945	**SB110_6**	275	0.90	1627259	1835994	0.886
GB8_7	300	1.33	1466090	1275635	1.149	**SB110_7***	340	0.00	230404	358716	0.642
GB8_8*	380	0.00	227562	352510	0.646	**SB110_8***	380	0.00	106510	152411	0.699
GB8_9	340	0.90	673857	645628	1.044	**SB110_9**	300	1.68	1003861	939865	1.068
GB8_10	300	1.29	1256335	1275635	0.985	**SB110_10**	340	0.25	356328	358716	0.993
GB8_11	280	2.31	1862700	1856724	1.003	**SB110_11**	300	1.12	1126466	939865	1.199
GB8_12	280	2.12	1736114	1856724	0.935	**SB170_1**	300	0.99	858755	815102	1.054
GB35_2	340	1.06	455600	492120	0.926	**SB170_2**	340	0.93	407785	420550	0.970
GB35_3	340	1.13	516811	492120	1.050	**SB170_3**	280	2.22	999830	1173899	0.852
GB35_4*	380	0.00	123869	285166	0.434	**SB170_4***	380	0.00	90803	233575	0.389
GB35_5*	380	0.00	154602	285166	0.542	**SB170_5***	340	0.00	113763	420550	0.271
GB35_6	300	0.91	878902	909366	0.967	**SB170_6***	340	0.00	97062	420550	0.231
GB35_7	300	1.00	1019929	909366	1.122	**SB170_7**	280	2.90	1178237	1173899	1.004
GB35_8	280	1.73	1248000	1275652	0.978	**SB170_8***	380	0.00	108165	233575	0.463
GB35_9	280	1.59	1191270	1275652	0.934	**SB170_9**	300	1.04	857158	815102	1.052
GB35_10	280	1.94	1328353	1275652	1.041	**SB170_10**	275	0.58	1437863	1291232	1.114
GB35_11	340	1.10	492775	492120	1.001	**SB170_11**	275	0.39	1253275	1291232	0.971
						SB170_12*	300	0.00	204174	815102	0.250

* *Surface crack initiation*

In the case of fatigue tensile tests, the S-N curves, presented in Table 5.5 and plotted in Figure 5.7, were fitted using only the fatigue results obtained with the specimens with internal crack initiation.

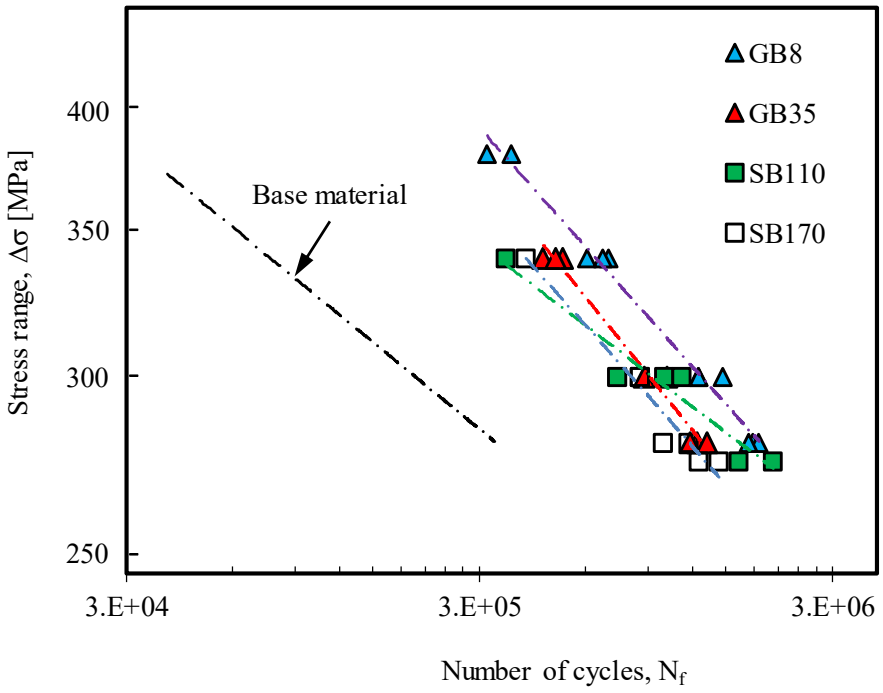

Figure 5.7 – S-N curves for the batches with different shot peening beads. Tensile tested specimens with internal crack initiation.

A very good coefficient of correlation of R above 0.98 was obtained, except for the SB110 series. The GB8 series present the higher fatigue lives (about 7.3x higher than untreated material for a stress range of 300 MPa), while the other treated series present similar fatigue resistances with fatigue lives about 5x also higher than untreated material. For a fatigue life of $5x10^5$ cycles, the GB8 series has an increase of fatigue resistance of 42% relatively to the untreated series. The others treated series present a lower increase of fatigue resistance between 30 and 35%. Therefore, in the case of tensile fatigue tests, all shot peening treatments lead to an important increase of fatigue life in the range of stresses used in the tests, 275-380 MPa, when the crack initiation occurs internally. The GB8 series present the lowest value of roughness and Table 5.3 shows that this series also presents the lower value of K_f, although the same is not very different from the values obtained for the other treated series. This agrees with the higher fatigue performance presented by the GB8 series. In addition, the very low values obtained for the notch

factor K_f, the presence of compressive residual stresses on the surface layer and the uniform stress distribution in tensile loadings justify the higher percentage of specimens that fail from internally initiated cracks under tensile loading. The stress intensity factor ΔK_I, considering an internal defect as a crack, may be calculated by an approximate equation from Murakami [25], Equation (5.6):

$$\Delta K_I = \beta \Delta\sigma \sqrt{\pi\sqrt{A}} \tag{5.6}$$

where A is the area of the defect projected in the plane normal to the tensile stress, β=0.5 for an internal defect and β=0.65 for a surface defect. Therefore, for a given applied stress range, ΔK_I is about 1.3 higher for a surface defect than for an internal defect with the same size. The difference between β values for internal and surface defects and the usually accepted idea that vacuum makes crack growth slower and the threshold higher agree with the results obtained in tensile fatigue tests in Table 5.4, which shows an increase of fatigue resistance between 1.3 and 1.42 for treated specimens that failed from internal crack initiation relatively to untreated specimens which failed from surface crack initiation.

The ratio between the experimental number of cycles N_f and N_{est} (Table 5.6) is used to quantify the deviation between the total fatigue lives of specimens with surface crack initiation and the total fatigue lives of specimens with internal crack initiation, for the same stress range. Figure 5.8 shows the ratio N_f/N_{est} against the ratio f/d, where d is the specimen diameter. For internal crack initiation, N_f/N_{est} has an average value near unity and a standard deviation of 0.088, while for surface initiation these parameters change to 0.45 and 0.166, respectively. It can be concluded that fatigue life increases in average 2.2x when crack initiation occurs internally in comparison to surface crack initiation. However, even in the case of specimens with surface crack initiation there is an increase of fatigue resistance relatively to the untreated series, as can be observed in Figure 5.6 b).

The improvement difference introduced by the shot peening process on bending and tensile test results is caused by the different stress distributions created by bending and tension loadings, leading to different fatigue resistances.

The fatigue strength obtained in the 3PB tests was higher than that obtained in tensile tests, particularly for long lives where the initiation phase is predominant. The strong stress gradient and the restricted volume subjected to higher stresses in specimens tested under 3PB loading are the main causes for its higher fatigue resistance and also explain that crack initiation always occurred on the specimen surface. As indicated in Table 5.5, the slope of S-N curves for 3PB tests is very low (-0.058 to -0.09), indicating that the crack initiation phase is predominant in the total fatigue life. Moreover, the maximum stress applied in 3PB tests ranged from 385 to 600MPa, which is typically greater than the microscopic yield strength (the microscopic yield strength of the material surface is lower than the global yield strength of 414 MPa) and reduces or eliminates the residual stress field with a maximum depth of 140μm. Consequently, in 3PB tests the favorable effect of the compressive residual stresses on fatigue strength was canceled or reduced, leading to surface roughness and the slight increase of hardness became the main parameter that may influence the fatigue strength. For longer lives, the increase of surface roughness effect leads to a reduction in fatigue strength of some treated series compared to the untreated series.

In the case of tensile tests, a uniform stress distribution over the entire specimen volume reduced both crack initiation and propagation phases compared to 3PB tests, leading to a reduction of the fatigue strength. Moreover, the slope of S-N curves obtained in tensile tests, being higher than in 3PB tests (-0.13 to -0.204), indicates that the crack initiation period is lower.

The uniform distribution of stresses over the entire specimen volume makes it possible to initiate the crack superficially or internally, depending on the superficial parameters: residual stresses and roughness. As the fatigue strength was lower in tensile tests, the applied stress ranges were also smaller; the maximum stress ranged from 275 to 380 MPa, always lower than the yield stress of 414 MPa. Therefore, in the case of fatigue tensile tests the compressive residual stresses and eventually the increase of hardness near surface have a higher beneficial effect in the fatigue lives of treated series than the detrimental effect of the roughness. In spite of this, the fatigue strength in tensile tests was significantly lower than in 3PB tests, for both treated and untreated specimens.

Dong et al [26] also achieved an extension in fatigue lifetime due to the failure mode transition from surface crack initiation to internal crack initiation on the FSW joint of the 7075-T651 aluminum alloy, by performing uniaxial fatigue tests in specimens with near-polished, gradient nanostructured surface and high compressive residual stresses provided by a surface

mechanical rolling treatment. He et al [27] studied the effect of ultrasonic peening treatment on the high and very high cycle fatigue resistance of an Al 7075 friction stir welded joint. They also observed a fatigue strength improvement through application of ultrasonic peening treatment and that fatigue cracks can initiate from the interior of the specimen due to the compressive residual stress profile in the surface layers.

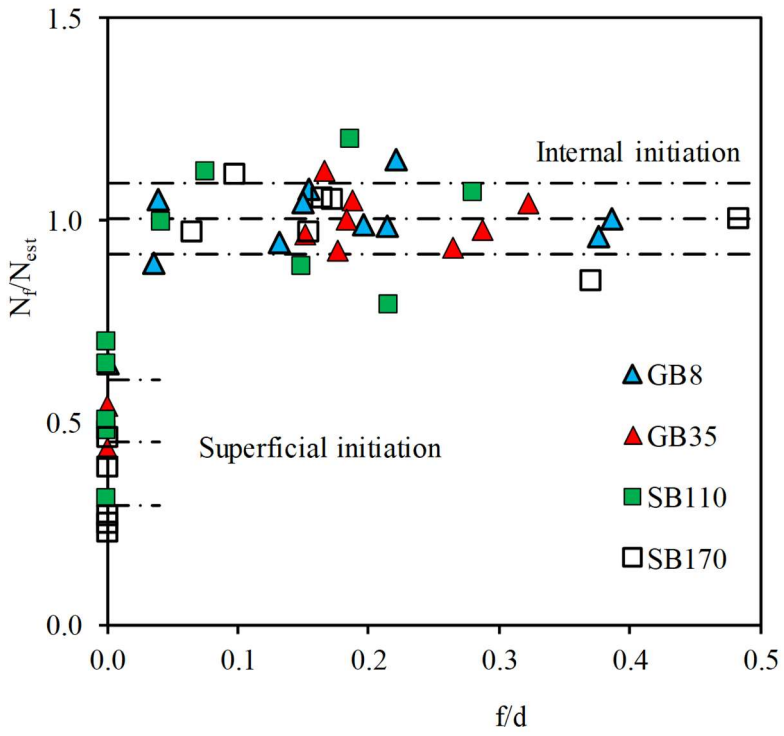

Figure 5.8 – N_f/N_{est} against normalized crack initiation depth f/d for the batches with different shot peening beads. Tensile tests.

Figure 5.9 presents the crack initiation dimensionless depth f/d, where d is also the specimen diameter, against the stress range for all treated series. With exception of the results for the stress range of 275 MPa, a clear trend of an increase of the crack initiation depth with the decrease of the applied stress range may be observed. The cause for the different behavior of specimens tested with the lowest stress range (275 MPa) was not understood.

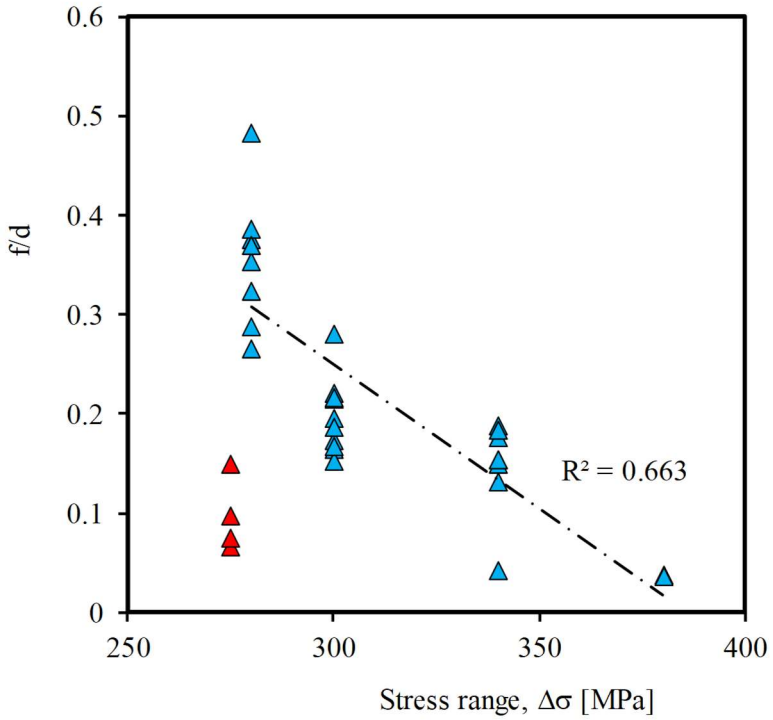

Figure 5.9 – Normalized crack initiation depth f/d against stress range for the batches with different shot peening beads. Tensile tests.

5.3.6 Fracture Surface Analysis

Figure 5.10 shows two macro images of both surface crack initiation (Figure 5.10 a)) and internal crack initiation (Figure 5.10 b)) in treated series. Internal crack initiation occurs due to the increase of surface crack initiation resistance promoted by the compressive residual stresses, for fatigue lives above $3.5x10^5$ cycles.

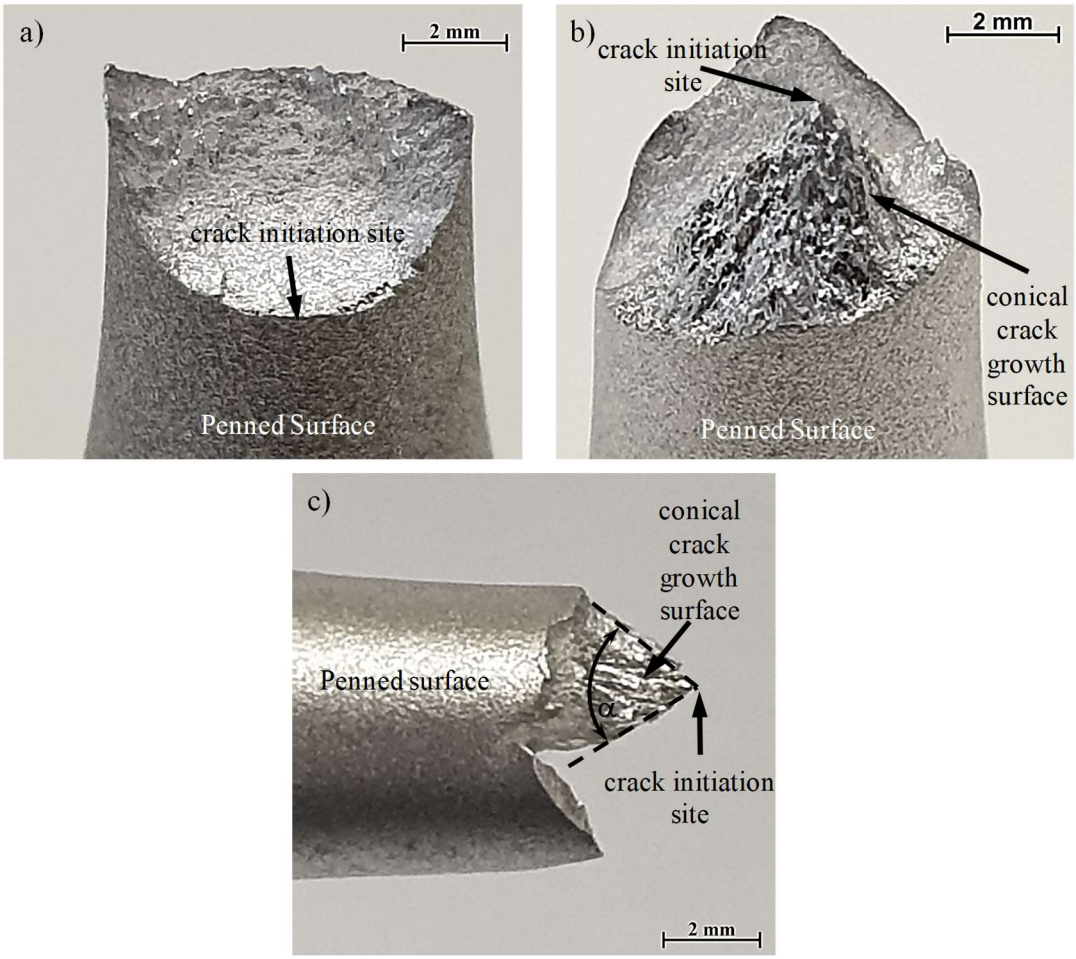

Figure 5.10 – Macro images of fracture surfaces in treated series: a) Crack initiation in S110_11 specimen, b) Internal crack initiation in GB8_11 specimen and c) A lateral image of the conical crack growth surface of GB8_11 specimen.

For fatigue lives below $3.5x10^5$ cycles crack initiation always occurs at surface. Internal crack initiation occurs at the vertices of the conical surface located internally, marked by an arrow in Figure 5.10 b). Figure 5.10 c) shows a lateral image of this conical shape evolution of the crack with internal initiation for the tensile tested specimens. The angle of the cones ranged between 61º and 76º. After the internal crack initiation period, the crack propagates forming the conical shape surface, which size depends on the location of the start point of the crack: the farther the starting point of the crack was from the specimen surface, the larger the conical surface. Therefore, the height of the cones tends to increase with the initial crack distance to surface. The transition from the conical surface to a flat surface, corresponding to mode I crack propagation,

occurs when the point of the base of the cone closest to the specimen surface reaches it. The crack shape evolution shown in Figure 5.10c) is completely different from the usually reported in literature for internal cracks that propagate in mode I with the typical eye of fish aspect. A description of this phenomenon was not found in literature, neither in aluminum alloys nor in other metallic materials.

The surface fracture analysis by SEM was performed only for the fatigue tensile specimens, where both surface and internal crack initiation occurred. In all 3PB treated specimens the crack always initiated on the surface and propagated through the cross section. Figures 5.11 and 5.12 show SEM images of fatigue fractured specimens with surface crack initiation and internal crack initiation, respectively. Figure 5.11a) shows a macrograph of the fracture surface for the SB110_2 tensile specimen with a total fatigue life of 171484 cycles for a stress range of 340 MPa. The white square identifies the crack initiation site from where radial marks following the direction of crack propagation are clearly visible. Figure 5.11b) shows a detail of the crack initiation site. The red arrow indicates the crack initiation origin identified by the convergence of the radial marks. Figure 5.11c) shows a macrograph of the fracture surface for the tensile specimen Al-3 of the untreated series. Crack initiation in untreated series occurs always at the specimen surface. The fracture surface aspect is similar to the one obtained with the treated series S110, but the fatigue life was lower (86833 cycles). Although the field of compressive residual stresses introduced by shot peening in the S110 series is insufficient to prevent surface cracking initiation, it has a favorable effect on fatigue life of this treated series, increasing the initiation period.

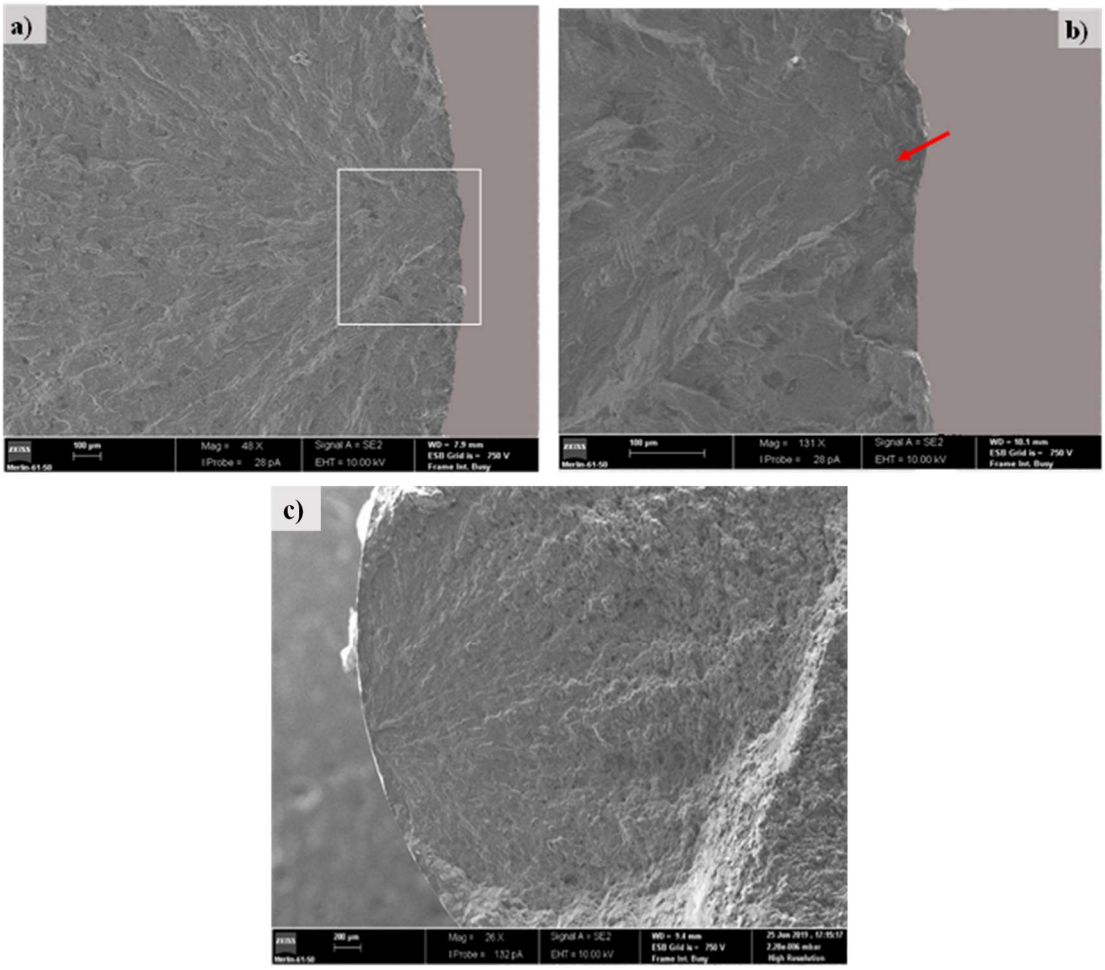

Figure 5.11 – SEM images of a surface crack initiation in SB110_2 tensile specimen. Δσ = 340 MPa: a) Macrograph of fracture surface, b) Detail of the crack initiation zone and c) SEM images of a surface crack initiation in Al_3 non treated tensile specimen. Δσ =340 MPa.

Figure 5.12 a) to b) show macrographs of the fracture surface of two different treated series (S110 and GB8), showing internal crack initiation on a conical shape surface. The overall appearance of both fracture surfaces is similar as well the micromechanisms, which will be analyzed further below. In figure 5.12 a) the black arrow indicates the contour of the specimen cross section. The white square identifies the crack initiation site from where the crack propagates, generating a conical fracture surface which boundary is marked by the dashed red line. This line also defines the transition between the crack propagation along the conical surface and the propagation in mode I in a plane approximately normal regarding the tensile stress. Figure 5.12 c) shows a detail of the crack initiation site corresponding to the cone vertices. It was not

possible to identify precisely the crack initiation site. It seems that early crack growth occurs on a small plateau before changing to the conical surface shape. Figure 5.12 d) shows a detail, near the surface of the specimen, of the transition zone between conical crack growth shape and propagation in mode I. As previously mentioned, this transition occurs when the nearest zone of the base of the cone approximates to the surface of the specimen allowing the contact with external environment. The multiplane aspect of crack propagation in mode I is a consequence of the irregularity of the cone base at the moment of the transition.

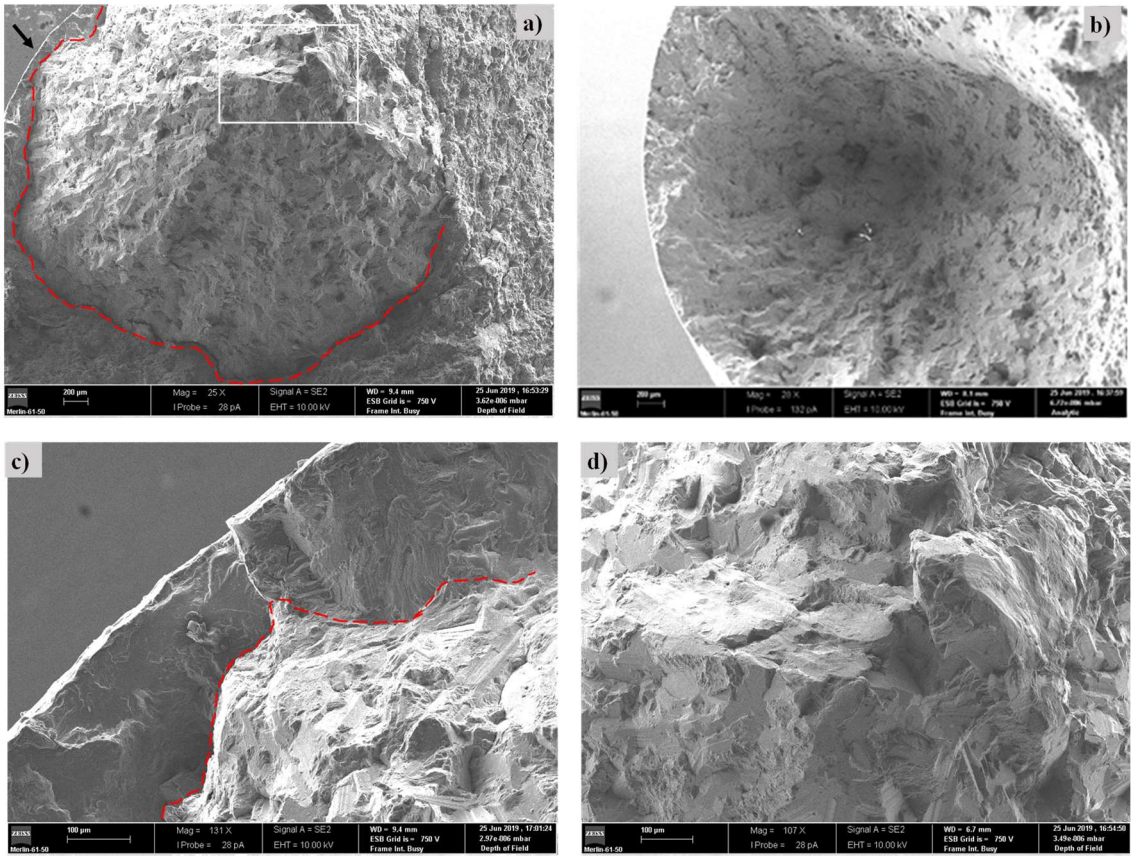

Figure 5.12 – SEM images of an internal crack initiation in treated series showing internal crack initiation on a conical shape surface: a) Macrography of the fracture surface of SB110_9 tensile specimen. Δσ=300 MPa; b) Macrography of the fracture surface of GB8_11 tensile specimen. Δσ=280MPa; c) Detail of the internal crack initiation zone of b) and d) Detail of transition zone between conical crack growth shape and propagation in mode I of image b).

Figure 5.13 shows SEM images of the fractured surface of the GB8-11 specimen with internal crack initiation, showing the crack propagation micromechanisms. Figure 5.13 a) shows that crack propagation on the conical surface occurs by micro cleavage, while Figure 5.13 b)

shows a macrography and a detail of the subsequent mode I fracture zone of crack propagation, showing ductile striations and secondary cracks.

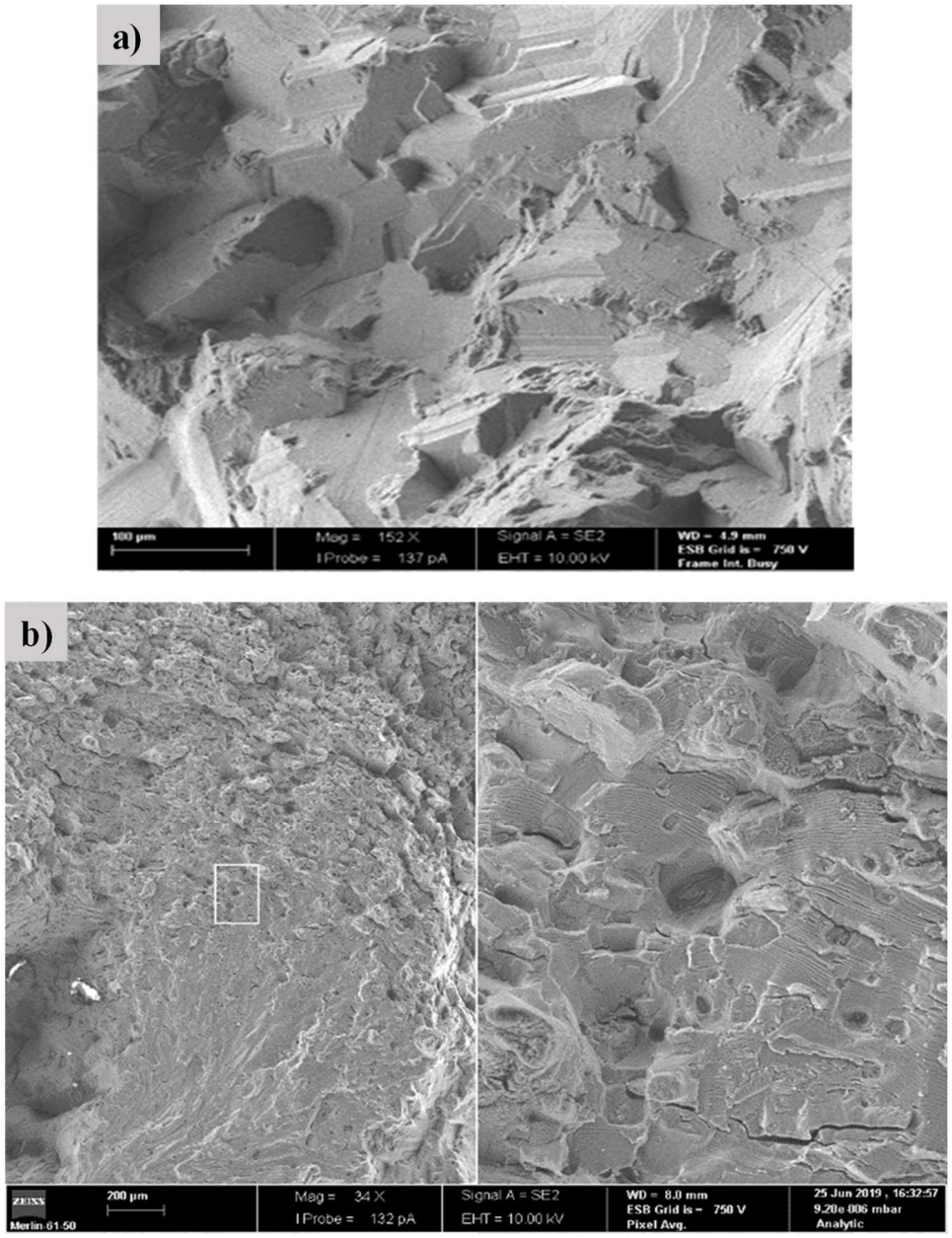

Figure 5.13 – SEM images showing the fatigue crack propagation micromechanisms of specimen GB8-11 with internal crack initiation: a) Micrograph of the conical surface fracture and b) Macrograph and a detail of fracture on mode I crack propagation.

5.4 Conclusions

A systematic study was carried out regarding the roughness, surface hardening and residual stress effects on fatigue life of round specimens of Al 7475-T7351 aluminum alloy tested under 3PB and tensile-tensile. The main conclusions drawn were the following:

- No significant hardening near surface caused by shot peening was observed;
- For 3PB specimens, the surface roughness plays a role as or more important than the residual stresses resulting from shot peening resulting in a surface crack initiation, while for tensile specimens the combination of these factors and the uniform stress distribution in tensile loading leads to a predominant internal crack initiation;
- Shot peening does not introduce significant improvement on fatigue life in 3PB specimens, but the use of small glass beads is potentially beneficial. All tensile treated specimens present an improvement of fatigue life in comparison with the untreated specimens, particularly when the crack initiates internally;
- The internal cracks propagate generating a conical fracture surface until transition to mode I propagation.

5.5 Aknowledgments

The authors would like to acknowledge OGMA-Indústria Aeronáutica de Portugal, in Alverca, for the collaboration in the supplying of samples used in this project, as well as FEDER for the sponsoring by way of funds through the program COMPETE – Programa Operacional Factores de Competitividade – and by national funds through FCT – Fundação para a Ciência e a Tecnologia under the project identified with the number UID/EMS/00285/2013.

5.6 References

[1] – A. Heinz. A. Haszler. C. Keidel. S. Moldenhauer. R. Benedictus. and W. Miller. "*Recent development in aluminum alloys for aerospace applications*". Mater. Sci. Eng. A. vol. 280. no. 1. pp. 102–107, 2000.

[2] – C. Y. Kim. J. M. Choi. and J. H. Song. "*Fatigue crack growth and closure behavior under random loadings in 7475-T7351 aluminum alloy*". Int. J. Fatigue. vol. 47. pp. 196–204, 2013.

[3] – K. Alrubaie. E. Barroso. and L. Godefroid. "*Fatigue crack growth analysis of pre-strained 7475–T7351 aluminum alloy*". Int. J. Fatigue. vol. 28. no. 8. pp. 934–942, 2006.

[4] – SAE AMS 2430, Shot Peening, Automatic AMS2430, SAE International, 4, 1984.

[5] – K. Miková. S. Bagherifard. O. Bokůvka. M. Guagliano. L. Trško., "*Fatigue behavior of X70 microalloyed steel after severe shot peening*", Int. J. Fatigue. 55, 33-42, 2013.

[6] –H. Kumar. S. Singh. and P. Kumar. "*Modified Shot Peening Processes - A Review*". Int. J. Eng. Sci. Emerg. Technol.. vol. 5. no. 1. pp. 12–19, 2013.

[7] – M. Lundberg. R. L. Peng. M. Ahmad. T. Vuoristo. D. Bäckström. and S. Johansson. "*Influence of Shot Peening Parameters on Residual Stresses in Flake and Vermicular Cast Irons*" Mater. Sci. Forum. vol. 768–769. pp. 534–541, 2013.

[8] – S. Bagherifard. M. Guagliano, "*Fatigue behavior of a low alloy steel with nanostructured surface obtained by severe shot peening*", Eng. Fract. Mech. 81, 56-68, 2012.

[9] – P. Zhang. J. Lindemann. L. Leyens., "*Shot peening on the high-strength magnesium alloy AZ80 - effect of peening media*", J. Mater. Process. Technol. 210, 445-450, 2010.

[10] – Mutoh Y. Fair GH. Noble B. Waterhouse RB., "*The effect of residual stresses induced by shot peening on fatigue crack propagation in two high strength aluminum alloys*", Fatigue Fract Eng Mater Struct; 10(4):261–72, 1987.

[11] – Sharp PK. Clayton JQ. Clark G.,"*The fatigue resistance of peened 7050-T7451 aluminum alloy-repair and retreatment of a component surface*", Fatigue Fract Eng Mater Struct; 17(3):243–52, 1994.

[12] – Wagner L., "*Mechanical surface treatments on titanium, aluminum and magnesium alloy*", Mater Sci Eng;A263:210–6, 1999

[13] – Benedetti M. Bortolamedi T. Fontanari V. Frendo F., "*Bending fatigue behavior of differently shot peened Al 6082 T5 alloy*", Int J Fatigue; 26:889–97, 2004.

[14] – Turnbull A. de los Rios ER. Tait RB. Laurant C. Boabaid JS., "*Improving the fatigue resistance of wasp alloy by shot peening*", Fatigue Fract Eng Mater Struct; 21:1513–24, 1998.

[15] – H. Luong. M.R. Hill., "*The effects of laser peening and shot peening on high cycle fatigue in 7050–T7451 aluminum alloy*", Materials Science and Engineering A 527, 699–707, 2010.

[16] – B.X. Wu. S. Tao. S.T., "*Lei. Numerical modeling of laser shock peening with femtosecond laser pulses and comparisons to experiments*", Applied Surface Science 256, 4376–4382, 2010.

[17] – Y.K. Gao., "*Improvement of fatigue property in 7050–T7451 aluminum alloy by laser peening and shot peening*", Materials Science and Engineering A 528, 3823–3828, 2011.

[18] – A. Cherif. Y. Pyoun. B. Scholtes., "*Effects of ultrasonic nanocrystal surface modification (UNSM) on residual stress state and fatigue strength of AISI 304*"; Journal of Materials Engineering and Performance 19, 282–286, 2010.

[19] – Ramos R, Ferreira N, Ferreira JAM, Capela C. A.C. Batista AC., "*Improvement in fatigue life of Al 7475-T7351 alloy specimens by applying ultrasonic and microshot peening*", International Journal of Fatigue 92, 87–95, 2016.

[20] – Luo W. Noble B. Waterhouse RB., "*The effect of shot peening intensity on the fatigue and fretting behaviour of an aluminum alloy*", In: Niku-Lari A. editor. Advances in surface treatments. vol. 2. Oxford: Pregamon Press; p. 145–53, 1988.

[21] – Benedetti M, V. Fontanari. M. Bandini. E. Savio., "*High- and very high-cycle plain fatigue resistance of shot peened high-strength aluminum alloys: The role of surface morphology*", International Journal of Fatigue 70, 451–462, 2015.

[22] – DIN EN ISO 4288, "*Profile method: Rules and procedures for the assessment of surface texture*", 1996.

[23] – Li JK, Mei Y, Wang D, Wang R, "*An analysis of stress concentration caused by shot peening and its application in predicting fatigue strength*", Fatigue Fract. Eng.Mater Struct, vol. 152, p. 1271-1279, 1992.

[24] – Robertson GT, "*The Effect of shot size on the residual stresses resulting from shot peening*", The shot peener;11(3):46-48;1997.

[25] – Murakami Y, "*Metal fatigue: effects os small defects and nommetallic inclusions*", Elsevier Science; 2002.

[26] – Dong P, Liu Z, Zhai X, Yan Z, Wang W, Liaw PK., "*Incredible improvement in fatigue resistance of friction stir welded 7075-T651 aluminum alloy via surface mechanical rolling treatment*", International Journal of Fatigue 124, 15–25, 2019.

[27] – C. He, K. Yang, Y. Liu, Q. Wang, M. Cai., "*Improvement of very high cycle fatigue properties in an Al 7075 friction stir welded joint by ultrasonic peening treatment*", Fatigue Fract Engng Mater Struct, 40, 460–468, 2017.

CHAPTER 6 – Discussion, Main conclusions, Future Works

This investigation studied the behavior of aeronautical alloy Al 7475 with T7351 treatment, which is one of the most recent aluminum alloys used in the aeronautical industry, and specifically in parts of the KC390 aircraft, currently produced in Portugal, at OGMA – Indústria Aeronáutica de Portugal, S.A.

This study aimed to assess fatigue improvement of surface treatments on fatigue strength and crack propagation.

For the study of fatigue improvement of surface treatments, notched and flat specimens were used and also cylindrical specimens without notch.

For the study of crack propagation, CT specimens were used.

Tests were carried out on specimens subjected to shot peening, ultrasonic peening and microshot peening, and using two bead materials: steel and glass. As for bead materials, two different diameters were used.

After shot peening surface treatments, all specimens were subjected to tensile testing, microstructure analysis, hardness analysis, etc.

The study here carried out provides further conclusions, which will be shown after the discussion of each article.

6.1 Discussion

6.1.1 Article: Improvement in fatigue life of Al 7475-T7351 alloy specimens by apllying ultrassonic and microshot peening

This work aimed to evaluate the benefits on the mechanical properties of the Al 7475-T7351 alloy by applying three different peening processes: Ultrasonic Peening (USP) and

Microshot Peening, with two different bead sizes (MSP1 and MSP2), using notched flat specimens, with a thickness of 4 and 8mm.

The USP process allows for a better surface appearance compared to MSP.

All surface treatments increase material microhardness. The treatment that provides greater microhardness is MSP1, followed by MSP2, and finally by USP. A decrease in microhardness from the longitudinal surface to the notch surface is verified in all treatments, but the values are always higher than those of base material.

The highest residual surface stresses are achieved by USP, followed by MSP1, and then by MSP2. In the subsurface layer, USP reaches lower compressive stress values than MSP. USP also shows the lowest maximum compressive stress value at depth. However, it ranges between the MSPs regarding the change from compressive to tensile stresses. MSP2 achieves the highest and the deepest compressive stresses. It can be concluded that for MSP, smaller bead diameters provide higher and deeper residual stresses. A relationship is found between bead diameter and contact area, as a result of maximum stress depth. MSP2 smallest diameter beads produce the largest and deepest residual stresses. USP generates the highest residual surface stresses.

For both 4 and 8mm, USP improves fatigue life between 19.7 and 23.9% over the base material at R=0. It is also found that all treatments improve the fatigue life in comparison with the base material to R=-1, by about 33 and 34.2% for 200,000 cycles. MSP2 is the treatment that shows the best performance for short lives compared to USP and MSP1, 1.5% and 6.5% improvement, respectively. As for long lives, MSP1 shows the best performance, standing out at 11.9% of MSP2 and 6.7% of USP. The USP treatment has shown intermediate performances between MSPs. MSP1 better performance for long lives can be explained by the higher average values of microhardness and residual stresses in the subsurface zone. MSP2 better performance for short lives can be explained by the higher value of the residual stress whole area in the rolling direction.

In general, good correlations were obtained between the experimental results and the predictions of fatigue life according to the Glinka Method, taking into account the residual stresses determined by X-ray diffraction.

From the SEM analysis, it can be concluded that the specimens start their fracture on the surface, including the specimens with the best surface USP finish. Depending on the applied stress, there may or may not be formation of a micronucleation zone. It was not possible to detect

precipitates or second-phase particles, because they were too fine and dispersed for appropriate analysis conditions.

A very recent study [1] related to another aluminum alloy, compared the application of conventional shot peening (CSP) and micro-shot peening (MSP) processes to 6086-T6 aluminum alloy. This study reveals that on this aluminum alloy the results are similar for Al 7475-T7351 aluminum alloy, because the results for MSP are higher than for CSP for in regard to surface anti-fatigue strengthening of bare alloys, due to its inhibiting effect on crack initiation. This study brings about another interesting concept and process, the micro-arc oxidation coat (MAO), that when applied on these materials, with CSP and MSP, changes the tendency. For MAO coated alloys with strict requirements for the resistance to corrosion and abrasion, CSP is more effective for enhancing their fatigue properties, due to its inhibiting effect on crack propagation.

Shot peening treatment generally increases the fatigue strenght of aeronautical components by around 35% and the this study shows such improvement tendency.

6.1.2 Article: Effects of shot peening and stress ratio on fatigue crack propagation of Al 7475-T7351 specimens

The main purpose of this work was to analyze the effect of shot peening on fatigue crack propagation of the 7475 aluminum alloy, under both constant amplitude loading and periodic overload blocks.

In this particular study, notched flat compact tension (CT) specimens were used, with a thickness of 4 and 8mm, and with 0.05 and 0.4 stress ratios. Analysis of the shot-peened surface showed a small increase of micro-hardness values due to the plastic deformations caused by shot peening. The surface peening beneficial effect on fatigue crack growth is very limited; its main effect is more noticeable near the threshold. Specimen's thickness only has marginal influence on crack propagation, in opposition to stress ratio. Periodic overload blocks of 300 cycles reduce the fatigue crack growth rate for both intervals of 7,500 and 15,000 cycles.

As studied before, and as it could be expected, the physical parameters, namely thickness and geometry, also affect the plane strain values [2, 3].

Another study [4], observed that surface propagation occurs in transgranular mode. Therefore, the plane stress state inhibits time dependent crack propagation (intergranular). These results may explain the crack shapes on corner cracks. When the crack propagation mode is the same inside the specimen and near the surface, the crack adopts an almost quarter-circular shape because the fatigue crack growth rate (FCGR) is not greatly affected by stress state. However, when the crack propagation modes are different, a quarter-circular crack has a lower FCGR near the surface, and so a tunneling effect is observed. This agrees with findings of Tong et al. [5] in Waspaloy[3] at 650°C. In fact, a greater tunneling effect of the crack front (i.e. a higher influence of stress state) was observed when the interior crack growth was time-dependent.

A recent study in 7B50-T7751 aluminum alloy [6], shows that the shot peening coverage has a quite limited effect on the crack growth rate during the early stages of fatigue crack growth. However, when the shot peening coverage is 300%, this is the best for improving fatigue crack growth properties for the 7B50-T7751 alloy treated with 0.1–0.2mmA shot peening intensity. With the increase in shot peening coverage from 100% to 300%, the compressive resisual stress increased significantly.

Other study [7], using other process and other material, Laser Peening (LP), on the Ti-6Al-4V titanium alloy, shows that using different coverage rates, LP can decrease the fatigue crack growth rate, with results of 80% coverage rate, instead of 20% or 40%. So, this study shows that it be could be possible to improve the fatigue life on Al 7475 T7351, if the shot peening coverage is greater than 100%. This is a possibility for a future work.

Shot peening do not has an important effect on crack propagation and the author could not find a large number of studies regarding this subject. As for the thickness effect, the tunnel effect is also verified, as it is in other articles that are used as a reference.

---

3 Waspaloy is a precipitation hardening, nickel-based alloy which has been used in elevated temperature applications. The alloy has been used for gas turbine engine parts which require considerable strength and corrosion resistance at temperatures up to 1600°F (871°C).

6.1.3 Article: Effect of bead characteristics on the fatigue life of shot peened Al 7475-T7351 specimens

This work aimed to analyze the effect of shot peening processing parameters, material and size of beads on the fatigue behavior of aluminum alloy Al 7475-T7351.

This particular study used unnotched cylindrical specimens and two different bead materials: glass and steel. Additionally, two different diameters were also used in each material, glass and steel.

It was verified that SB170 and SB110 steel beads, which have a much higher mass than glass beads, produce a larger damaged area in comparison with glass beads. The SB110 and GB35 beads seam to have similar roughness, lower than that of SB170 series, and a few surface defects, with a significantly lower depth than the plastically deformed layer created by the shot peening treatment, which may cause the onset of fatigue cracking. GB8 beads reduced the plastic deformed layer and roughness significantly, in comparison with all the other shot peening beads.

Analysis of roughness values indicates that even the higher roughness caused by SB170 steel beads presents a smoother surface profile, with fewer localized notches, when compared to GB35 and SB110 beads. In all cases the layer treated by shot peening has a little depth, less than 100μm, affecting only a few surface grains.

Shot peening does not produce significant improvement of fatigue life of 3PB specimens, but the use of small glass beads is potentially beneficial. All tensile treated specimens present an improvement of fatigue life in comparison with the untreated specimens, particularly when the crack initiates internally.

From the analysis of the fracture surface, it seems that the internal cracks propagate generating a conical fracture surface until transition to mode I propagation.

The use of glass beads in surface treatment is generally more beneficial than the use of steel beads.

Other study [8] using ceramic beads, on Ti-6Al-4V titanium alloy, and wet shot peening instead of the usual dry shot peening, reveals that severe plastic deformation is induced on material surface by this process. Residual stress and depth of stress field also increased with

increased peening intensity and, at the same time, surface roughness resulting from wet shot peening is lower than that resulting from dry shot peening.

Therefore, where the application of wet shot peening, with glass beads, is practicable on Al 7475-T7351 aluminum alloy, the best results for improvement of fatigue life will probably be achieved.

According to literature studies, ceramic beads always provide better results in improvement of fatigue life. However, during the tests performed at OGMA – Indústria Aeronáutica de Portugal, such beads were not available. It is the author's intention to perform such tests in the future using ceramic beads.

6.2 Main Conclusions

These three articles provided important insights into the behavior of the Al 7475T7351 aluminum alloy when treated with different shot peening processes.

In general, it can be concluded that:

- USP provides better surface finish and lower roughness values than MSP. All three-surface peening processes slightly increased the surface hardness of Base Material, in ascending order: USP, MSP2 and MSP1. No significant hardening near surface, caused by shot peening, was observed;
- All three surface peening processes were capable of improving fatigue life. Micro nucleation was observed in general cases and particularly for low nominal stress;
- Analytic predictions according to the Molski-Glinka approach related well to the experimental results;
- As a result of its small influence depth, the beneficial effect of shot peening on $da/dN - \Delta K$ curves is negligible, particularly for R = 0,4. However, this effect seems to increase near the threshold condition;
- For both mechanically polished and shot-peened samples, a specimen's thickness has only marginal influence on the stable crack propagation regime;
- A significant effect of the mean stress was observed, particularly in near- threshold region;

- Periodic overload blocks provide a reduction of the fatigue crack growth rate. For MP specimens, the reduction reaches the maximum value of 7500 cycles, for the interval between blocks, while for SP specimens, the crack growth rate continues to decrease for intervals of 15,000 cycles;
- For 3PB specimens, surface roughness plays a role as much or even more important than the residual stresses resulting from shot peening and that produce surface crack initiation, while for tensile specimens, the combination of these factors and the uniform stress distribution in tensile loading leads to a predominant internal crack initiation. Internal cracks propagate generating a conical fracture surface up to transition to mode I propagation;
- Shot peening does not provide significant improvement of fatigue life of 3PB specimens, but the use of small glass beads is potentially beneficial. All tensile treated specimens present an improvement of fatigue life in comparison with untreated specimens, particularly when the crack initiates internally.

6.3 Future Works

From the exposition above, and in terms of future work, the author is in a position to state that several possibilities are presented to further knowledge on the advantages of using this technology. In literature, a large number of other technologies and/or parameters can be tested. For example:

- It is suggested that an optimization of MSP parameters be carried out, so that the beneficial effects of residual compressive stresses outweigh the harmful effects of required surface roughness, thus providing improvements of fatigue strength of the Al 7475-T7351 alloy;
- Also a similar analysis for laser peening treatments is proposed, in order to compare the potential of more recent treatments in relation to more traditional ones such as shot peening.

It is also suggested that shot peening tests be carried out with the new fully automatic equipment existing at OGMA – Indústria Aeronáutica de Portugal, S.A., in order to understand the impact of more stable parameter control. This new equipment will provide for the improvement of several aspects related to the shot peening process. Technical data of the new automatic shot peening equipment available at OGMA are indicated in Table 6.1. Process reliability increases substantially, as well as the typology and size of aeronautical components that can be subjected to surface treatment.

Table 6.1 – Technical data of the automatic shot peening equipment available at OGMA.

Equipment	**Automatic equipment**
Model	ROSLER SP 1500 LR G1
Application mode	Robotized
Shot changing process	Automatic
Sieving	Automatic
Flow control (kg/min)	Automatic
Process monitoring	Computerized
AMS 2432 standard compliance	Yes
AMS 2430 standard compliance	Total
Noise (db)	<80
Cabin capacity (m)	Parts up to 2.5

In addition, other studies suggest that still other types of materials can be used for shot peening, to assess whether better results can be obtained. As, in general, better results were obtained with glass beads, compared to the use of steel beads, the idea of using ceramic beads may be practicable to obtain better results in improving fatigue resistance. Ceramic beads are spheres known to provide the best surface finish and therefore better behavior in fatigue resistance.

Another opportunity arises in using a different process called cavitation peening (CP), because according to studies already carried out on the Al 7075 alloy, the use of this process

provided improvements of fatigue life compared to those of the shot peening process. Cavitation peening (CP), which does not use shots, has attracted attention as studies have shown that it can improve fatigue strength. CP is a process that causes plastic deformation of a surface layer of the treated substrate via impact of cavitation bubbles. CP introduces compressive residual stresses without increasing surface roughness significantly, as it does not involve contact between solids. [9]

Another idea that emerges as a future work is the application of shot peening to materials whose manufacturing process is the recent 3D printed technology. This part manufacturing process is carried out using 3D technology. Studies carried out on steels reveal a surface hardening of approximately 119% using steel and ceramic particles, thus allowing increased wear and corrosion resistance. [10]

6.4 References

[1] – K. Su, J. Zhang, H. Li, D. Ji, L. Hu; "*Anti-fatigue strengthening mechanism of conventional shot peening and micro-shot peening on bare and micro-arc oxidation coated 6082-T6 aluminum alloy*"; State Key Laboratory of Traction Power, Southwest Jiaoyong University; Chengdu; China; October; 2022.

[2] – Antunes, F.V.; Chegini, A.G.; Branco, R.; Camas, D.; "*A numerical study of plasticity induced crack closure under plane strain conditions*"; Int. J. Fatigue; 71, 75–86; 2015;

[3] – J. Tong; "*T-stress and its implications for crack growth*"; Eng Fract Mech, 69, pp. 1325-1337; 2002.

[4] – Antunes, F.V.; Ramalho, A.L.; Ferreira, J.A.M.; "*Identification of Fatigue Crack Propagation Modes with Roughness Measurements*", Int. J. Fatigue; 22, p. 781–788; 2000.

[5] – J. Tong, B. Vermeulen; "*The description of cyclic plasticity and viscoplasticity of waspaloy using unified constitutive equations*"; I. Journal of Fatigue; University of Portsmouth, UK, p. 413-420, 2003.

[6] – Z. Qin, B. Li, H. Zhang, T. Wilfried, T. Gao, H. Xue; "*Effects of shot peening with differente coverage on surface integrity and fatigue crack growth properties of 7B50-T7751*

aluminum alloy"; School of Mechanical Engineering, Northwestern Polytechnical University; Xian; China; December; 2021.

[7] – J. Zhou, S. Huang, L. Zuo, X. Meng, J. Sheng, Q. Tian, Y. Han, W. Zhu; "*Effects of laser peening onresidual stresses and fatigue crack growth properties of Ti-6Al-4V titanium alloy*"; School of Mechanical Engineering; Jiangsu University; Zhenjiang; China; January; 2014.

[8] – G. Chen, Y. Jiao, T. Tian, X. Zhang, Z. Qiang, W. Zhou; " *Effect of wet shot peening on Ti-6Al-4V alloy treated by ceramic beads*"; School of Materials Science and Engineering; Dalian University of Technology; Dalian; China; July; 2013.

[9] – T. Koji, O. Hiroko, S. Takaya, F. Shinsaku; "*Fatigue strenght improvement of na aluminum alloy with a crack-like surface defect using shot peening and cavitation peening*"; National University; Yokohama; Japan; February; 2018.

[10] – W. Mariusz, S. Miroslaw; "*Effect of shot peening on the surface properties,corrosion and wear performance of 17-4PH steel produced by DMLS additive manufacturing*"; Department of Mechanical Engineering, Universyti of Poland; Lublin; Poland; 2021.